TAMPEREEN TEKNILLINEN YLIOPISTO
TAMPERE UNIVERSITY OF TECHNOLOGY

Vladimír Dospěl

Elastodynamic Response of Thin Circular Cylindrical Shells to Grinding Loads

Julkaisu 1014 • Publication 1014

Tampere 2011

Tampereen teknillinen yliopisto. Julkaisu 1014
Tampere University of Technology. Publication 1014

Vladimír Dospěl

Elastodynamic Response of Thin Circular Cylindrical Shells to Grinding Loads

Thesis for the degree of Doctor of Science in Technology to be presented with due permission for public examination and criticism in Festia Building, Auditorium Pieni Sali 1, at Tampere University of Technology, on the 22nd of December 2011, at 12 noon.

Tampereen teknillinen yliopisto - Tampere University of Technology
Tampere 2011

ISBN 978-952-15-2723-4 (printed)
ISBN 978-952-15-2750-0 (PDF)
ISSN 1459-2045

Abstract

This thesis concentrates on mathematical modelling of a grinding system consisting of a grinding machine-tool and a thin-walled roll as a work piece. In this system the roll is subjected to process, grinding forces produced by the contact between the tool and the work piece. The model is presented in two versions. In the first the roll is modelled as a shell by utilizing Love's equations, in the other one the roll is modelled as an Euler-Bernoulli beam. The mathematical representation of the system is based on principles of mechanics of continuum and cutting mechanics, which is expressed by a set of delay differential equations. These governing equations are solved numerically and the response is analyzed in time domain. First, the response is studied in the contact area, then the response is investigated along the whole span of the roll. The analysis is extended by a case, where the roll is supported by an additional support. The dynamic behaviour of the system is evaluated and the models based on two different theories are compared. Finally, technical recommendations that should lead to an improved dynamic performance of the studied system are addressed to industry.

Preface

The work presented in this thesis was carried out at the Department of Mechanics and Design at the Tampere University of Technology during 2008 – 2011. The research was initiated by the Paper Manufacturing Graduate School and supported by the Graduate School of Concurrent Engineering funded by the Ministry of Education.

I would like to express my gratitude to my supervisor professor Erno Keskinen for his inspiration and guidance during this study. I especially appreciate that he made it possible for me to work in a flexible and productive research environment. I am thankful for his encouragement and support of this work. I wish to give my thanks to my colleague Dr. Kai Jokinen for his participation and effort as well as practical advice and comments during my research. I also thank professor Michel Cotsaftis for his critical and inspiring discussions that contributed to my work. In addition, I wish to thank the staff of the Department of Mechanics and Design for creating a pleasant and supportive working atmosphere.

I wish to express my gratitude also to the assessors of the manuscript, professor Wolfgang Seemann and professor Chandrasekhar Nataraj. They are kindly acknowledged for their highly valuable comments and language checking that helped to increase the quality of the manuscript. I also appreciate their great effort to carry out the review in a short time period.

I wish to express my warmest gratitude to my family, my father Vladimír and my mother Hana as well as to my sisters for their support and encouragement through my life.

Tampere, November 2011

Vladimír Dospěl

Table of contents

Nomenclature

Symbols of Latin alphabet

A, B, C, A_j, B_j, C_j	amplitudes of mode shapes ($j = 1 – 3$ for beam, $j = 1 – 6$ for shell)
A_1, A_2	fundamental form parameters, Lamé parameters
A_R	cross-sectional area of the roll
D	bending stiffness
E	Young's modulus of elasticity
E_1	amplitude of the surface error function of the roll
$E_2, E_3, E_4, \ldots$	amplitudes of the surface error function of the grindstone
E_S	strain energy of the stone subsystem
F_{Sup}	support point force
$F_{k,mn,C}$	modal force caused by the contact (grinding) forces corresponding to modes m, n and set k
$F_{k,mn,G}$	modal force caused by the gravity (self-weight) load of the roll corresponding to modes m, n and set k
$F_{k,mn,Sup}$	modal force caused by the support forces corresponding to modes m, n and set k
$F_{k,mn,p}$	modal force caused by the uniform distributed load p_0 corresponding to modes m, n and set k
$F_{m,G}$	modal force caused by the gravity (self-weight) load of the roll corresponding to mode m
$F_{m,Q}$	modal force related to tangential grinding force Q corresponding to mode m
$F_{m,N}$	modal force related to normal grinding force N corresponding to mode m
G	distributed gravity load
I	second moment of area
I_x	second moment of area about y axis
I_y	second moment of area about x axis
I_z	second moment of area about z axis
J_d	the mass moment of inertia of the stone drive
J_s	the mass moment of inertia of the grindstone
K	membrane stiffness
K_D^r	gain of speed error for the roll

K_D^s	gain of speed error for the grindstone
K_P^r	gain of position error for the roll
K_P^s	gain of position error for the grindstone
K_S	kinetic energy of the stone subsystem
L	length of the roll
$M_{\lambda\chi}$	bending moment in the λ-χ direction (λ, χ = *1, 2* or λ, χ = *z*, φ)
M_μ	bearing friction torque
N	normal grinding force
$N_{k,mn}$	coefficient in the modal force expression corresponding to modes *m*, *n* and set *k*
N_m	coefficient in the modal force expression corresponding to mode *m*
$N_{\lambda\chi}$	membrane force in the λ-χ direction (λ, χ = *1, 2* or λ, χ = z, φ)
N_{z0}^i	initial tension in *z* direction
$N_{\varphi 0}^i$	initial tension in φ direction
P_S	power of the stone subsystem
Q	tangential grinding force
$Q_{\lambda 3}$	transverse shear force in the λ-*3* direction (λ = *1, 2* or λ = *z*, φ)
R	radius of the roll
R_1	radii of curvature in α_1 direction
R_2	radii of curvature in α_2 direction
R_z	radii of curvature in *z* direction
R_φ	radii of curvature in φ direction
T_r	driving torque of the roll
T_S	torque of the stone drive
$\boldsymbol{S}(t)$	vector of history in delay differential equations
U	displacement of the centerline in *X* direction
$U_{3,kmn}$	radial (transverse) mode shape corresponding to modes *m*, *n* and set *k*
U_m	transverse mode shape corresponding to mode *m*
$U_{z,kmn}$	longitudinal mode shape corresponding to modes *m*, *n* and set *k*
$U_{\varphi,kmn}$	tangential mode shape corresponding to modes *m*, *n* and set *k*
V	displacement of the centerline in *Y* direction
V_{stat}	static displacement in *Y* direction
$\dot{V}$	velocity of the centerline in *Y* direction

XYZ	non-rotating coordinate frame
a	mean radius of the roll
	left limit of integrating interval in differential equations
a_1 - a_5	coefficients of characteristic equation of the shell
b	beam width
	right limit of integrating interval in differential equations
c_e	specific energy consumption factor
c_{eq}	the equivalent damping
$c_{k,mn}$	modal damping corresponding to modes m, n and set k
c_m	modal damping corresponding to mode m
d	diameter of the roll ending shaft
$f(\cdot)$	function
$\boldsymbol{f}(\cdot)$	vector function
g	gravitational acceleration on Earth on the sea level
g_3	gravitational loading pressure in radial direction
g_φ	gravitational loading pressure in tangential direction
h	shell thickness
	integration step
i	step in numerical integration
j	index of natural frequency ($j = 1 – 3$ for beam, $j = 1 – 6$ for shell)
k	index of orthogonal set ($k = 1, 2$)
	iteration step in Trapezoidal rule
k_{11} *to* k_{33}	members of matrix of the homogeneous equation
k_N	contact stiffness
k_{Sup}	support stiffness
k_b	the stiffness of the transmission belt
k_{eq}	the equivalent stiffness
$k_{k,mn}$	modal stiffness corresponding to modes m, n and set k
k_m	modal stiffness corresponding to mode m
$k_{\lambda\chi}$	bending strain in the λ-χ direction ($\lambda, \chi = z, \varphi$)
k_w	wear factor
m	number of beam eigenmodes
m_{eq}	the equivalent mass
$m_{k,mn}$	modal mass corresponding to modes m, n and set k

m_m	modal mass corresponding to mode *m*
n	number of ring eigenmodes
p_0	uniform distributed load caused by pressure
q_1	external loading pressure in α_1 direction
q_2,	external loading pressure in α_2 direction
q_3	external loading pressure in α_3 direction
$q_3^{'}$	force per unit length in radial (transverse) direction
$q_x^{'}$	force per unit length in *x* direction
$q_y^{'}$	force per unit length in *y* direction
$q_z^{'}$	force per unit length in longitudinal direction
r	radius of the grindstone
r_s	radius of the grindstone sheave
t	time
t_0	starting time in time integration
u	displacement of the centerline in *x* direction
u_1	displacement in α_1 direction
u_2	displacement in α_2 direction
u_3	displacement in α_3 direction
	displacement in radial direction
$u_{3,Cont}$	displacement of the contact point in radial direction in the non-rotating frame
$u_{3,stationar}$	displacement in radial direction in the non-rotating frame
$u_{3,stat}$	static displacement in radial direction
u_{stat}	static displacement in *x* direction
u_z	displacement in longitudinal direction
u_φ	displacement in tangential direction
$u_{\varphi,Cont}$	displacement of the contact point in tangential direction in the non-rotating frame
$u_{\varphi,stationar}$	displacement in tangential direction in the non-rotating frame
$u_{\varphi,stat}$	static displacement in tangential direction
$\dot{u}$	velocity of the centerline in *x* direction
$\dot{u}_3$	velocity in radial direction
$\dot{u}_z$	velocity in longitudinal direction

$\dot{u}_{\varphi}$	velocity in tangential direction
v	displacement of the centreline in y direction
v_{stat}	static displacement in y direction
$\dot{v}$	velocity of the centerline in y direction
w	width of the grindstone
xyz	rotating coordinate frame
x	independent variable in differential equations
x_s	nominal depth of cut
$y(\cdot)$	dependent variable in differential equations
$\boldsymbol{y}(\cdot)$	vector of dependent variables in differential equations
$\boldsymbol{y_a}$	vector of initial values
z	longitudinal coordinate of the roll
z_s	position of the grindstone
$\dot{z}_s$	axial feeding speed
z^*	position of the acting force in the longitudinal direction

Symbols of Greek alphabet

ΔR	surface error function of the roll
Δr	surface error function of the grindstone
$\Delta\sigma$	deviation in the angular position of the stone
Δ^E	displacement of the contact point on the roll in terms of Euler-Bernoulli theory
Δ^L	displacement of the contact point on the roll in terms of Love's equations
$\dot{\Delta\sigma}$	change of the deviation in the angular position of the stone
$\dot{\Delta}^{\mathrm{E}}$	velocity of the contact point on the roll in terms of Euler-Bernoulli theory
$\dot{\Delta}^{\mathrm{L}}$	velocity of the contact point on the roll in terms of Love's equations
α	over-lapping constant
$\alpha_1, \alpha_2, \alpha_3$	three-dimensional curvilinear surface coordinates
β	recovering constant or reduction parameter
β_λ	angle of deformed element in the λ direction ($\lambda = z, \varphi$)
δ	displacement of the contact point on the grinding stone
γ	coefficient in the solution of characteristic equation of the shell

ε	depth of penetration
$\varepsilon_{\lambda 3}$	shear strain in the λ-*3* direction (λ =*1, 2*)
ε^{L}	total penetration in terms of Love's equations
ε^{E}	total penetration in terms of Euler-Bernoulli theory
$\overset{\circ}{\varepsilon}_{\lambda\chi}$	membrane strain in the λ-χ direction (λ, χ = *z*, φ)
ζ	viscous damping ratio
$\eta_{k,mn}$	participation factor corresponding to modes *m*, *n* and set *k*
η_m^u	participation factor for *x* direction corresponding to mode *m*
η_m^v	participation factor for *y* direction corresponding to mode *m*
$\dot{\eta}_{k,mn}$	time derivative of the participation factor corresponding to modes *m*, *n*
$\dot{\eta}_m^u$	time derivative of the participation factor for *x* direction corresponding to mode *m*
$\dot{\eta}_m^v$	time derivative of the participation factor for *y* direction corresponding to mode *m*
$\ddot{\eta}_{k,mn}$	second time derivative of the participation factor corresponding to modes *m*, *n* and set *k*
$\ddot{\eta}_m^v$	second time derivative for *y* direction of the participation factor corresponding to mode *m*
$\ddot{\eta}_m^u$	second time derivative for *x* direction of the participation factor corresponding to mode *m*
μ	Poisson's ratio
μ_{fr}	friction coefficient
θ	angular position of the roll
$\dot{\theta}$	rotational frequency of the roll drive
$\dot{\theta}_d$	desired value of the roll speed
ι	number of waves on the surface of the roll
κ	transmission ratio
$\kappa_1 - \kappa_4$	coefficients in integration methods
ρ	mass density
σ	angular position of the stone drive
$\dot{\sigma}$	rotational frequency of the grinding stone drive
$\dot{\sigma}_d$	desired value of speed of the grindstone drive
τ	time delay

$\dot{\tau}$	relative cutting speed
$\dot{\tau}_d$	desired tangential speed in grinding zone
$\dot{\tau}_{\mathrm{r}}^{\mathrm{E}}$	tangential velocity of the contact point on the roll in terms of Euler-Bernoulli theory
$\dot{\tau}_{\mathrm{r}}^{\mathrm{L}}$	tangential velocity of the contact point on the roll in terms of Love's equations
$\dot{\tau}_{\mathrm{s}}$	tangential velocity of the contact point on the grindstone
φ	circumferential coordinate of the roll
ϕ	arbitrary phase angle in the ring eigenmode
φ^*	position of the acting force in the tangential direction
ψ	circumferential coordinate of the grindstone
ω	natural frequency
ω_{-1mn}	transverse negative natural frequency for m^{th}, n^{th} modes
ω_{+1mn}	transverse positive natural frequency for m^{th}, n^{th} modes
ω_{SDF}	natural frequency of a single-degree-of -freedom system
ω_m	natural frequency for m^{th} mode
ω_n	natural frequency
ω_{mn}	natural frequency for m^{th}, n^{th} modes

1. Introduction

Manufacturing engineering with its machining systems represents a powerful tool across the industrial spectrum. The level of quality output of all industrial branches is among others strongly dependent on the manufacturing quality. Nowadays, on the one hand high quality and precision requirements are demanded by needs for further development of high technology and applied sciences; on the other hand needs of market economy call for higher performance and better efficiency in production leading to lower production costs. These, in general, contradictory requirements are setting a challenging task for manufacturing engineers and researchers. To succeed in improving of performance of any kind of system it is essential to understand the relations, interactions and behaviour of all elements inside the system. Analytical methods enable us to go deep inside the problem and are able to extract the valuable information. With this knowledge one can adjust, tune, optimise or even change the given system in order to improve the performance of the system.

Machining systems are usually represented by a pair “work piece – machine-tool”, where the work piece is typically a simple unit while a machine-tool represents a mechatronic subsystem, i.e. it contains mechanical, electrical, hydraulic, control and other elements. When analysing dynamic behaviour of such a system methods of multi-body dynamics are often used. In machining the main goal is to change the shape of the work piece according to given requirements and to guarantee that the geometry and surface quality lie in a required tolerance. Therefore, for the product quality the interaction between the machine-tool and the work piece is essential in the machining processes and therefore it is a crucial part in the dynamic analysis of such a system.

In general, it has been observed that due to existing compliance of the machine-tool structure as well as of the work piece a relative movement or vibration between the tool and the piece is present during a cutting process. These vibrations are usually excited by certain periodic forces such as cutting forces, forces caused by imbalances of rotating parts, etc. However, the process under these conditions remains stable. Nonetheless, in cutting and grinding operations another type of vibrations, so called self-excited vibrations, are present and these, in contrast to forced vibrations cause loss of stability very often. As a consequence, the surface error becomes unacceptable and there is a real possibility of damage of the tool or other parts of the machine-tool or the work piece or even a danger of injury of the operator. These undesirable or even catastrophic situations can be avoided.

Grinding of rolls for paper manufacturing industry is one of the machining operations that require high precision finishing in order to produce high geometrical accuracy and surface quality. Also in this branch of industry the market competition pushes the production efficiency to its upper limits. That was the reason why the leading Finnish paper manufactures in collaboration with university researchers started to deeply investigate the process of grinding paper machine rolls. One of the first mathematical models of this particular problem was presented in [Keskinen 1999]. This model described a grinding process of a solid paper machine roll that included the basic delay differential equations, where the roll was modelled as an Euler-Bernoulli beam. This topic was further developed with focus on the delay phenomenon in [Yuan 2002]. Promising results of these studies encouraged the industry to set the research goals even further: analysis of grinding thin-walled rolls.

A top-level paper machine consists of approximately *100* rolls of various types and functions: lead rolls, suction and forming rolls, deflection-compensated rolls, centre rolls, grooved and press rolls and calendar rolls [Paulapuro 2000]. These rolls, as their names indicate, lead, support, form or otherwise act on the paper web. Among others, knowledge of the tension in the paper web is important information in paper making technology. Several designs to carry out the measurement have been developed. One of the latest ones is to use an extremely thin-walled roll, which would possess significantly low mass that would enable high measurement accuracy. For economic reasons, the roll material should be steel. In addition, the surface quality is required to be as high as in case of the other rolls in order to assure high quality of produced paper web. Since certain unstable and unpredictable behaviour during the grinding process was expected, it has been decided to carry out an analysis of dynamic behaviour of thin-walled rolls under grinding conditions. This is the topic of the presented doctoral dissertation.

Table 1.1: Tasks in question

	Love	**Euler-Bernoulli**
Governing equations	x	x
Analysis of the original system	x	x
Analysis of the system with additional support	x	x
Technical solution – recommendations	x	–

In this work two models are presented; one, whose roll model is based on the shell theory utilizing Love's equations, and the other, whose roll model is based on Euler-Bernoulli theory. The former is the original model, the latter is based on [Yuan 2002] and is used for comparison, since there are no available measurement data of the analyzed system. Both models include the delay phenomenon that characterizes the chatter vibrations. Three case studies are carried out for both models studying the behaviour of three different wall thicknesses of the roll: *10 mm*, *5 mm* and *2.5 mm* (see Table 1.1).

The main goals of this work are:

i. To select a suitable method for modelling a thin-walled roll
ii. To analyze the dynamic behaviour of the grinding system
iii. To analyze the dynamic behaviour of the grinding system with an additional roll support
iv. To suggest technical solutions to improve the performance of the system

In this thesis, first the studied problem is introduced. The analyzed system consisting of the pair "grinding machine-tool – thin-walled cylindrical work piece" is defined. The system and process parameters are specified and the main problems are stated.

Next, the state of the art in the studied area is presented. Due to the fact that the problem crosses various scientific disciplines, this section is divided into three parts. First part deals with mechanics of cutting and grinding. Second part follows with a typical problem related to cutting and grinding operations, which is known as chatter vibration, and it also deals with methods for modelling of this phenomenon. The third part of the review provides an overview of developed theories and used methods in mechanics of continuum concentrating on beam and shell structures. All parts are aiming to monitor the state of the art from the first historical discoveries up to the latest modern studies.

Then, the mathematical description of the system is carried out. First, the system is divided into subsystems and certain assumptions and simplifications, necessary for the modelling, are adopted. Then the model exploiting Love's equations is created and the governing equations are presented. The effect of centrifugal and Coriolis' forces are neglected due to the low rotational speed of the roll; the decision is based on eigenfrequency analysis. The forced response is obtained in terms of eigenfunctions expansion. The model exploiting Euler-Bernoulli beam theory is derived by reduction from the shell model and the governing equations for this beam model turn out to be of

the same form as in [Keskinen 1999]. The equations describing the grinding wheel subsystem are derived by method of power equilibrium. The grinding forces are obtained in correspondence with a classical wear theory, bringing the delay term. Finally, the linear drive models are introduced.

Following chapter is devoted to a numerical solution of the governing equations. It compares several numerical methods for solving second order differential equations that can be also applied for solving delay differential equations. Based on the numerical testing, the Euler's first improved method is selected and used in this work.

The next section provides the major part of the presented results. First, it studies the effect of the gravity load on the thin-walled roll. Next, the generation of the surface waviness as well as its relation to the natural frequency of the system is analyzed and discussed. Then, 3 case studies are presented. The cases defer only in the parameter of the wall thickness of the roll. The wall thickness values are *10 mm*, *5 mm* and *2.5 mm*. Each case presents its responses in time domain of both models. In addition, a closer look is taken at the cross-sectional deformation of the roll in various positions of the roll. The suitability of both applied theories is discussed.

The change of the performance of the system by applying an additional roll support is studied too. The support is modelled as a spring force that acts only if the spring is compressed. These results are compared with the results of the original system.

Finally, recommendations addressed to industry, leading to improvement in the performance of the system, are proposed.

The following original contributions were developed in the course of this work:

1. Mathematical model describing a complete manufacturing system with a complex two-way interaction of a controlled machine tool and an elastic work body.
2. Feasibility analysis and validity domain determination of shell and beam models for tubular work bodies under the effect of moving machining load.
3. A proposal for a technical solution improving the performance of the manufacturing system.

2. Problem description

Finishing operations of paper machine rolls are carried out on various types of roll grinders. A commonly used roll grinder Herkules is depicted in Figure 2.1. In this work, exactly this type of machine-tool is included in the analysis. Nevertheless, other types of grinders could be easily used as well.

The grinding system consists of a grinding machine-tool and the work piece. The work piece – the roll – is held in a chuck, which is fixed to the spindle on the spindle side, and supported by a tail stock on the other side (see Figure 2.1). The tool – the grinding stone – is attached to a carriage, which has motions along the axis between the spindle and tail stock centres, and is perpendicular to this axis. Its axial movement is carried out by a lead screw – nut transmission, driven by a feed drive, and guided via lubricated slide ways. The spindle has its own electric motor and they are connected directly. The grinding stone is driven by a DC motor via transmission belts and it is controlled by a PD controller.

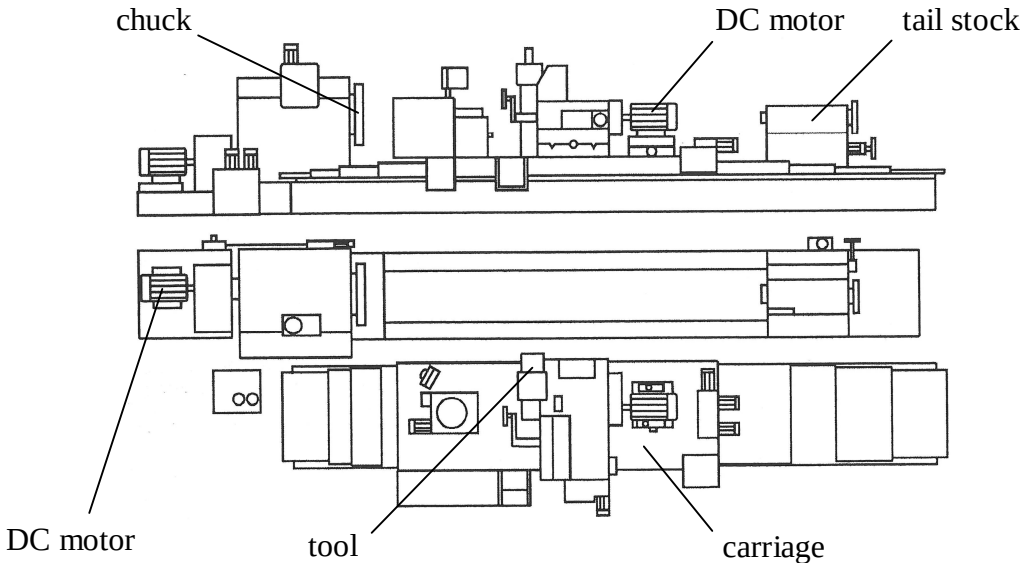

Figure 2.1: Top and front projections of a typical roll grinder

Grinding the roll surface is executed by entering the roll surface at one end of the roll by the tool in the radial direction. When the nominal depth of cut, x_s, is reached, the tool starts to move with a constant speed, $\dot{z}_s$, in the axial direction of the roll, grinding off a thin layer of the roll material. When the tool reaches the other end of the roll, one pass of the grinding operation has been

completed. For completing the whole operation, several passes in two grinding configurations are needed. First is called roughing, for which the typical values of x_s are *0.1 – 0.01 mm*, the second is called finishing, for which x_s is usually *0.01 – 0.001 mm*. The rotational frequency of the spindle, $\dot{\theta}$, is *0.1 – 0.2 Hz* and the rotational frequency of the grinding stone drive, $\dot{\sigma}$, is *10 Hz*. Axial feeding speed, $\dot{z_s}$, is about *0.01 m/s*.

In common practice when grinding standard paper machine rolls, it has been observed that for a certain configuration of system parameters the lateral vibration of the roll starts to grow exponentially and the process becomes unstable. In that case, the process must be interrupted immediately; otherwise serious damage of the work piece surface or the tool occurs. The instability is caused by self-excited vibrations or chatter vibrations that are closely related to the first natural frequency of the system. Even in a stable situation the tool and the piece experience relative vibration that creates marks on the work piece surface as well as on the stone surface. This means that the surface of the roll is no longer purely round but contains sinusoidal waves, related to the natural frequency of the system and the rotational speed of the work piece. This has been measured in [Järvinen 1998] and Figure 2.2 shows a measured surface profile at an arbitrary cross-section of a testing roll after grinding. It should be noted that a similar mechanism applies also for the grinding stone, although the process of waviness forming is much slower.

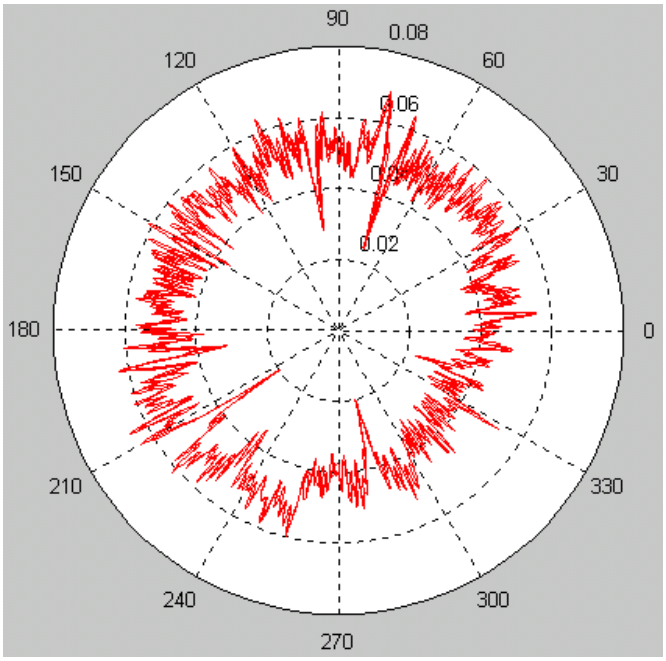

Figure 2.2: Measured surface profile of a testing roll

In this work, grinding a thin-walled roll is investigated. This brings additional expected features to the previous system that must be included in the analysis. Namely, local deformations caused by lower stiffness of the roll (compared to a standard roll), next, due to expected higher amplitudes of lateral vibrations a loss of contact between the work piece and the tool is present and last but not least, the presence of tangential vibrations of the roll. It turns out that for this case, a utilization of beam theories is not sufficient and employment of higher level theories of elasticity of continuum mechanics is necessary. In this work, a shell theory for deep shell structures expressed by Love's equations is used.

3. State of the art

The problem studied in this work represents a multidisciplinary task. In order to describe such a system mathematically, one has to utilize knowledge of (1) cutting mechanics for determination of cutting forces, leading in cutting and grinding to (2) delay differential equations (DDE). Then, for description of vibration behaviour of work pieces like rolls, (3) theory of elasticity of continuum mechanics in different forms is needed. These are always expressed in terms of (4) partial differential equations (PDE) that are usually convertible to a set of ordinary differential equations (ODE) with constant coefficients. Finally, for describing the whole system with all its interacting components, principles of (5) multi-body dynamics are used.

A lot of research work in these areas of science has been done during the last decades, in some cases during the last centuries. The following sections summarize the most important discoveries in these areas in a chronological order.

3.1 Mechanics of metal cutting and grinding

The history of metal cutting is rather long. Some authors dealing with this subject date the beginning of metal cutting to the prehistoric or ancient times. Nevertheless, first attempts to describe the chip formation mathematically fall to the end of 19^{th} century and they are related to names Time and Tresca [Black 1961]. Time reported that the chip is formed by the shear of the metal. Tresca stated that the cutting process was one of compression of the metal ahead of the tool. Time later developed a single shear-plane model for two-dimensional orthogonal cutting that assumes that in metal cutting the state of plane strain exists when the width of cut is considerably greater than the thickness of the layer to be removed. Much later, Merchant further developed this model and the main assumption was that the shear zone is a thin plane [Merchant 1945a, Merchant 1945b]. Other models were presented by Lee and Shaffer and Palmer and Oxley [Palmer 1959] who based their analysis on a thick shear deformation zone. The shear stress and shear angle can be determined from the orthogonal cutting tests [Altintas 2000]. There were attempts to predict the shear angle theoretically too. Krystof proposed a shear angle relation based on the maximum shear stress principle, i.e., shear occurs in the direction of maximum shear stress. On the other hand, Merchant proposed applying the minimum energy principle [Merchant 1945b]. Both these principles can be extended to the domain of three-dimensional oblique cutting [Altintas 2000]. Empirical approach in oblique cutting is used by Stabler who assumes that the shear velocity is

collinear with the shear force [Stabler 1951] and by Armagero who adds additional assumption that the chip length ratio in oblique cutting is the same as in the orthogonal cutting. Another empirical approach is presented in [Lin 1982]. Other metal cutting models can be found, e.g. in textbooks [Sharma 1986, Trent 1977 and Shaw 1984]. A very detailed survey of the historical development in metal cutting with personal opinions of the author is presented in [Ashtakhov 2002].

3.2 Chatter vibrations in metal cutting and grinding

In general, there are two types of mechanical vibration in cutting and grinding processes: forced vibration and self-excited vibration (see Figure 3.1). Internal forced vibration comes from the imbalance and eccentricity of rotating parts and from other sources, e.g., hydraulic motors. External forced vibration is caused by remote sources transmitted typically via floor. These vibrations are rather easy to model in dynamic analyses in contrast to the self-excited or chatter vibrations.

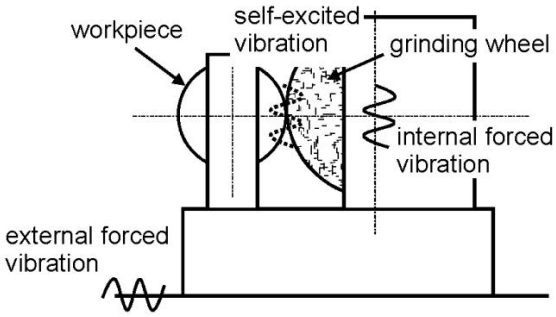

Figure 3.1: Chatter vibrations in grinding process [Inasaki 2001]

The problem of chatter in metal cutting was first time recognized by Taylor in 1907. He realized the process limitations imposed by chatter and the difficulty with modelling its source and he stated that chatter is the “most obscure and delicate of all problems facing the machinist” [Taylor 1907]. Later studies by Arnold defined the negative damping as a source of chatter [Arnold 1946], while research by Tlustý and Tobias led to a fundamental understanding of regeneration of waviness, or the overcutting of a machined surface by a vibrating cutter, as a primary feedback mechanism for the growth of self-excited vibrations (or chatter) due to the modulation of the instantaneous chip thickness, cutting force variation, and subsequent tool vibration [Tobias 1958, Tlustý 1963, Tlustý 1980]. Tlustý and Tobias also described the mode coupling effect as a second chatter mechanism.

Merritt [Merritt 1965] first time defined chatter as self-excited vibration and published stability charts, where the control parameters were depth of cut and spindle speed.

These studies were mainly dealing with milling and turning cutting processes. First studies on chatter in grinding appeared in 1960s. A characteristic problem of chatter in grinding is that the regenerative effect is present in both the work piece and the tool. This has been studied carefully in [Gurney 1965, Snoeys 1969, Inasaki 1977, Thompson 1986, Chen 1998, Salisbury 2001a and Salisbury 2001b]. It is apparent that the waves generated on the work piece surface grow rather fast. This is depicted in Figure 3.2 [Inasaki 2001].

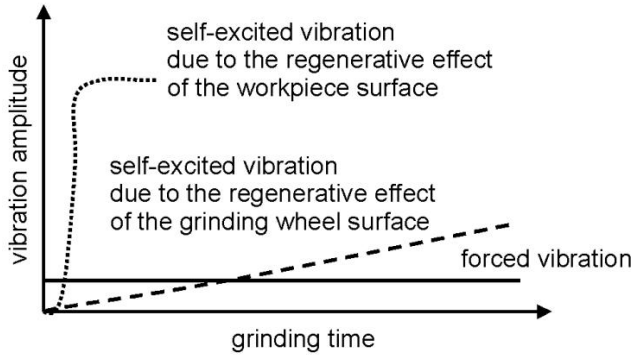

Figure 3.2: Vibration phenomena in grinding [Inasaki 2001]

When modelling a dynamic grinding process one should take into account grinding stiffness, grinding damping, contact stiffness, wear stiffness and geometrical constraints. Very often, the development of grinding wheel regeneration is much slower that the work piece regeneration; in that case the regeneration effect of the wheel can be ignored. An analysis of the rigidity of the grinding wheel – work piece – grinding machine system has been carried out in [Kaliszer 1966]. An analysis of the dynamic behaviour in plunge grinding is presented in [Biera 1997] and a simplified methodology to determine the cutting stiffness and the contact stiffness in the plunge grinding process was proposed in [Ramos 2001]. A detailed description of modelling dynamic behaviour of centreless grinding machines is introduced in [Giménes 1995]. Li and Shin present a time-domain dynamic model for chatter prediction of cylindrical plunge grinding process [Li 2006], which is further developed in [Li 2007]. An effect of torsional stiffness of both the work piece and the tool on the chatter phenomenon is studied in [Mannan 2000].

A multi-body dynamics approach was used by Keskinen et al. [Keskinen 1999] to develop a mathematical model of grinding standard paper machine rolls. The model included a roll, modelled as an Euler-Bernoulli beam, grinding stone, modelled as a rigid rotor, and two electric motors, driving the work piece and the tool. The grinding forces were described in terms of the relative tangential speed and the instantaneous chip thickness containing the time delay term. Detailed analysis of the time delay phenomenon of this system was carried out in [Yuan 2002a], while [Yuan 2002b] focuses on the speed control and its effect on the system performance. An analogous problem of delay phenomenon, a paper machine roll contact with regenerative out-of-roundness excitation, is handled numerically in [Järvenpää 2007]. Dospěl concentrates in his work [Dospěl 2010] on grinding thin-walled paper machine rolls and following conclusions of Saito [Saito 1986] he uses the Timoshenko beam theory to describe the roll vibrations.

[Yuan 2005] deals with the stability analysis of the roll grinding system with double time delay effects. Here is first used the classical stability analysis of metal cutting processes, then a non-linear limit cycle analysis is employed and finally the Lyapunov method for the full multi degree of freedom grinding system is utilized. A similar analysis is done by another research group in [Liu 2007]. Here for the exactly same mechanical model by referring to [Yuan 2005], Liu et al. proposes a practical algorithm for the stability analysis of the system. A direct application of non-linear dynamics and chaos theory to machining, grinding, and rolling processes and investigation of the problem of chatter dynamics in cutting processes can be found in [Moon 1998]. En extensive overview on chatter in grinding can be found in [Inasaki 2001] and a detailed survey on chatter stability of metal cutting and grinding is presented by Altintas and Weck in [Altintas 2001].

3.3 Theory of elasticity for continuous structures

The first investigations of mechanical vibrations date to the 16th century when Galilei found, by using geometrical relations, dependence of the natural frequency of a simple pendulum on its length. He was followed by Mersene and Sauveur who devoted their studies to free vibrations of strings. Sauveur implemented a term “node” for zero displacement points on a freely vibrating string.

Remarkable progress in continuum mechanics brought in 17th century Hook’s basic law of elasticity, Newton’s second law of motion and differential calculus founded by Leibnitz. Following principles of differential calculus, d’Alembert derived in 1747 the partial differential equation that is also known as the wave equation. His contemporary Bernoulli published the principle of

superposition of modes in 1747, which was proven by Euler in 1753. In 1822 Fourier used this method in theory of heat and presented his Fourier series, which is a special case of method of eigenfunction expansion. The first equation of motion for lateral vibration of a slender beam was derived by Bernoulli in 1735. Solutions of this equation for simply supported, clamped and free boundary conditions were published by Euler in 1744.

In parallel, investigations of circular and rectangular membranes were carried out by Euler, Poisson, Pagani and Lamé. Chladni's experiment with vibrating plates resulting in visualizing of nodal lines [Chladni 1787] encouraged other scientists in putting further effort in area of plate vibrations. Work of German, Todhunter [Todhunter 1886] and Lagrange led to equations of motion for plates. Consistent boundary conditions were derived by Kirchhoff [Kirchhoff 1850]. The first attempt do derive the equations of motion for vibrating shells was done by German and dates back to 1821. Aron derived a set of equations for which it was possible to reduce to plate equations by setting the curvatures to zero. In 1888 Love introduced his simplifications [Love 1927] for both the transverse and in-plane motion. The historical overview of development in vibrations of continuous elastic structures can be found in [Soedel 1981, Todhunter 1886].

The modern part of historical development in beam theories starts with further development of Euler-Bernoulli beam theory that includes strain energy due to bending and kinetic energy due to lateral displacement. In 1877 Rayleigh theory that includes the effect of rotation of the cross section [Strutt 1877] was published. Next improvement of the Euler-Bernoulli model came with the shear model that adds shear distortion. And finally, in 1921 the Timoshenko beam theory was released that adds to the Euler-Bernoulli model both the shear distortion and the effect of rotation of the cross-section and it is suitable for both slender and non-slender beams [Timoshenko 1921, Timoshenko 1922].

On the other hand, Love's equations experienced a number of further simplifications proposed by his followers. For shells and arches where stretching of the neutral surface is dominating, the membrane or the extensional approximation can be used. It is derived from Love's equations by neglecting the bending stiffness. On the contrary, the bending or inextensional approximation is applicable for shells whose transverse modes dominate. Analogously, here the simplification comes from Love's equations by neglecting the membrane stiffness. Both of the approximations were first employed by Lord Rayleigh [Strutt 1877]. Another widely used simplification that neither neglects bending nor membrane effects was derived independently by Donnell [Donnell 1976] and Mushtari [Mushtari 1961] for a circular cylindrical shell and was generalized for any geometry by Vlasov [Vlasov 1964]. The main assumptions are that the contributions of in-plane deflections can be

neglected in the bending strain expressions but not in the membrane strain expressions and that the inertia in the in-plane direction and the shear terms can be neglected. From this definition it is apparent that this theory is applicable only for loadings normal to the surface. Other simplifications were presented by Novozhilov [Novozhilov 1964] and Flügge [Flügge 1960, Flügge 1962]. Different representations of other simplifications can be found also in [Kraus 1967, Calladine 1983, Blevin 1976, Leissa 1973].

In the literature one can find a number of studies that either carry out interesting comparisons of those above introduced theories or use these theories for various applications. For example Han carefully compares in [Han 1999] Euler-Bernoulli, Shear, Rayleigh and Timoshenko beam theories applied on a beam of different boundary conditions subjected to a simple harmonic excitation. An influence of distributed rotary inertia and shear deformation on the motion of a mass-loaded cantilever beam was studied by Horr and Schmidt [Horr 1995], where a closed-form solution was obtained. Wang in his work [Wang 1997] utilises a Timoshenko beam B-spline Rayleigh-Ritz method for vibration analysis of beams. A discrete singular convolution method was used in [Civalek 2009] for free vibration analysis of Timoshenko beam of uniform cross-section and a method of differential quadrature was presented in [Laura 1993] for free vibration analysis of Timoshenko beam of non-uniform cross-section. Similar studies can be found in the field of vibration of shells. Miller studied free vibrations of a stiffened cylindrical shell in [Miller 1960]. [Ong 1996] presents an analysis of a cylindrical shell filled with liquid and supported by two longitudinal beams.

Certain research has been done also in the field of rotating beams. [Al-Asnary 1998 and Lin 2001] study the flexural and free vibration of a rotating Timoshenko beam and [Ouyang 2007] presents a model of a rotating Timoshenko beam subjected to axially moving forces.

Remarkable contribution in the field of shells and plates has been presented in a large number of publications by Soedel and Huang [Soedel 1981]. For example in [Huang 1987], a method for obtaining response to a harmonic excitation of rotating rings has been proposed and in [Huang 1988] the method was extended to rotating shells. In the problem of rotating structures the phenomenon of travelling modes always appears. This makes, especially in case of rotating shells, the solution of forced vibration more complicated. Doyle devotes a chapter to this problem in his textbook on wave propagation in structures [Doyle 1997]. To Soedel's and Huang's work refers, e.g. [Kim 2004] where the effects of rotation on the dynamics of a circular cylindrical shell with application to tire vibration has been investigated as well as in [Ng 1999] where the vibration and critical speed of a rotating cylindrical shell subjected to axial loading was under analysis. An

interesting analysis is carried out in [Saito 1986] where a rotating cylindrical shell is compared with a solution of a rotating Timoshenko beam with a conclusion that in case of transverse vibration, it is possible to treat a circular cylindrical shell as a beam.

3.4 Challenges

The purpose of the previous sections was to monitor the state of the art of relevant research fields with respect to the topic of this work from the beginning to the latest discoveries in these areas. According to opinion of the author, the fundamental and most important theories and studies in the area of metal cutting, modelling of grinding systems, chatter vibrations and vibration behaviour of continuous structures have been selected and briefly introduced. A review of the state of art in differential calculus, methods of solving ODEs, PDEs and DDEs with constant and variable delays has not been carried out since it does not belong to the main objectives of this work. Nevertheless, useful information on this subject can be found in a large number of textbooks, e.g. in [Hirsch 2004, Shampine 2003, Larsson 2003, Elden 2004, Kopchenova 1981].

Based on the literature review, it can be said that a lot of work in all above mentioned research areas has been done. Nevertheless, no comprehensive and scientifically recognised study dealing with vibration behaviour of rotating thin walled tubes subjected to grinding loads and taking into account delay phenomena has so far been published. Therefore, due to this fact in combination with the interest of industry, this topic has been chosen as the main subject of this work.

4. Mathematical description of the grinding system

4.1 Introduction

The whole grinding system and its basic process parameters were described in chapter 2. As mentioned earlier the real system is rather complicated.

The machine tool consists of stationary mechanical parts as beds, columns, gear box housings as well as of moving mechanical parts as slides and guideways, spindles, gears, bearings and carriages. Crucial parts are the spindle and the feed drives, supplying the system with sufficient angular speed, torque and power. Then, necessary are also the elements of power transmission as V-belts, clutches and nut – lead screw units. And finally, measuring systems, relays, limit and control switches, gauging, software and operating interface are present as well.

The work piece, the real roll, is assembled from the middle part, a thin walled tube, whose ends are closed by solid steel disks and connected to roll shafts. The contact between the grinding stone and the work piece physically experiences a plane, 3D contact, producing, apart from the grinding forces, also a heat loading.

Therefore, in order to gain a feasible and reliable mathematical model of vibration behaviour of a roll, assuring sufficiently accurate outputs, certain simplifying assumptions need to be adopted. The assumptions are as follows:

a) friction forces in the carriage slide ways and lead screw – nut system and their masses are neglected, friction in bearings and gears is not taken into account either;
b) the machine frame and bearings are infinitely stiff;
c) the effect of the roll shafts and endings is not taken into account;
d) the grinding contact is modelled by means of contact point forces;
e) the contact force in axial direction is neglected;
f) the thermal effects are not taken into consideration.

The whole system, in terms of analysis, can be divided into two subsystems: the roll subsystem and the stone subsystem. A scheme of the simplified system is shown in Figure 4.1.

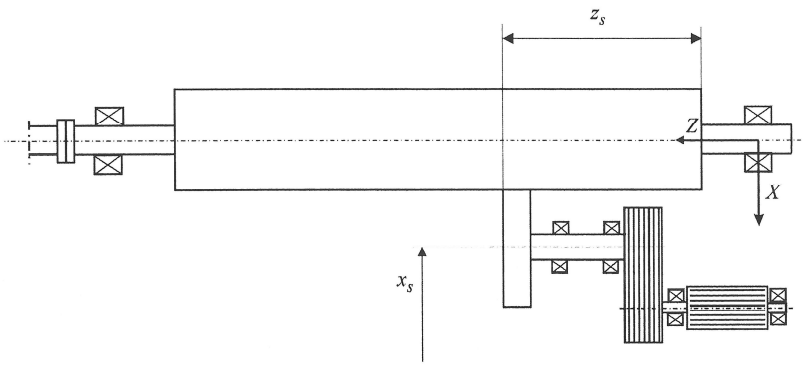

Figure 4.1: Scheme of the analyzed grinding system

Based on the literature review (chapter 3) and on investigations of the author, e.g. [Dospěl 2010, Dospěl 2011], the roll is modelled as a circular cylindrical shell, utilizing Love's equations. A beam model of the roll, exploiting the Euler-Bernoulli beam theory, is used as a reference.

4.2 Shell model

4.2.1 Love's equations

An English mathematician, A. E. H. Love, derived in the second half of 19th century a set of equations of motion for a general shell structure [Love 1927, Soedel 1981]. These equations were derived based first on definition of the infinitesimal distances in a shell structure and then defining the stress-strain and strain-displacement relationship followed by deriving the membrane forces and bending moments. After so called Love simplifications and using Hamilton`s principle (based on determination of potential and kinetic energies, variation of the boundary energy and the energy due to the load) following Love's equations can be obtained:

$$-\frac{\partial(N_{11}A_2)}{\partial\alpha_1}-\frac{\partial(N_{21}A_1)}{\partial\alpha_2}-N_{12}\frac{\partial A_1}{\partial\alpha_2}+N_{22}\frac{\partial A_2}{\partial\alpha_1}-A_1A_2\frac{Q_{13}}{R_1}+A_1A_2\rho h\frac{\partial^2u_1}{\partial t^2}=A_1A_2q_1 \tag{4.1}$$

$$-\frac{\partial(N_{12}A_2)}{\partial\alpha_1}-\frac{\partial(N_{22}A_1)}{\partial\alpha_2}-N_{21}\frac{\partial A_2}{\partial\alpha_1}+N_{11}\frac{\partial A_1}{\partial\alpha_2}-A_1A_2\frac{Q_{23}}{R_2}+A_1A_2\rho h\frac{\partial^2u_2}{\partial t^2}=A_1A_2q_2 \tag{4.2}$$

$$-\frac{\partial(Q_{13}A_2)}{\partial\alpha_1}-\frac{\partial(Q_{23}A_1)}{\partial\alpha_2}+A_1A_2\left(\frac{N_{11}}{R_1}+\frac{N_{22}}{R_2}\right)+A_1A_2\rho h\frac{\partial^2u_3}{\partial t^2}=A_1A_2q_3 \tag{4.3}$$

where Q_{13} and Q_{23} are defined by

$$\frac{\partial(M_{11}A_2)}{\partial\alpha_1}+\frac{\partial(M_{21}A_1)}{\partial\alpha_2}+M_{12}\frac{\partial A_1}{\partial\alpha_2}-M_{22}\frac{\partial A_2}{\partial\alpha_1}-Q_{13}A_1A_2=0 \tag{4.4}$$

$$\frac{\partial(M_{12}A_2)}{\partial\alpha_1}+\frac{\partial(M_{22}A_1)}{\partial\alpha_2}+M_{21}\frac{\partial A_2}{\partial\alpha_1}-M_{11}\frac{\partial A_1}{\partial\alpha_2}-Q_{23}A_1A_2=0 \tag{4.5}$$

A_1 and A_2 are fundamental form parameters, related to the geometry of the shell, α_1, α_2 and α_3 are the three-dimensional curvilinear surface coordinates, u_1, u_2, u_3 are the displacements in α_1, α_2, and α_3 directions, respectively, N is a normal force, Q is a shear force, M is a moment, R_1 and R_2 are the radii of curvature, ρ is the mass density and h is the shell thickness. Coordinates and directions of displacements of a general circular shell of revolution are shown in Figure 4.2 on an example of a sphere.

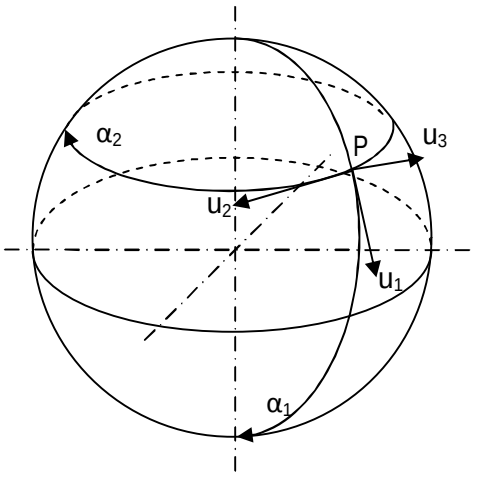

Figure 4.2: Spherical shell of revolution

One can notice that the contribution of the transverse shear deflection ($\varepsilon_{13} = \varepsilon_{23} = 0$) is neglected. This assumption is justified by the definition that for shells where the thickness is small as compared to overall dimensions the shear deformation can be set to *0*. This statement is supported by a study [Dospěl 2010] that compares dynamical behaviour of an Euler-Bernoulli and a Timoshenko beam.

4.2.2 Equations of motion of a rotating circular cylindrical shell

Equations of motion for a circular cylindrical shell can be derived from the general Love's equations by reduction to the simpler geometry [Soedel 1981]. Thus, for a circular cylindrical shell: $\alpha_1 = z$, $\alpha_2 = \varphi$, $u_1 = u_z$, $u_2 = u_\varphi$, $A_1 = 1$, $A_2 = a$, $R_1 = R_z = \infty$ and $R_2 = R_\varphi = a$ (see Figure 4.3). By taking into account the angular speed $\dot{\theta}$ that rotates the shell the inertia expressions in the Love's equations for a circular cylindrical shell gain additional terms. Also terms $N^i_{\varphi 0}$ appear on the left side of the equations that introduce an additional tension in φ direction.

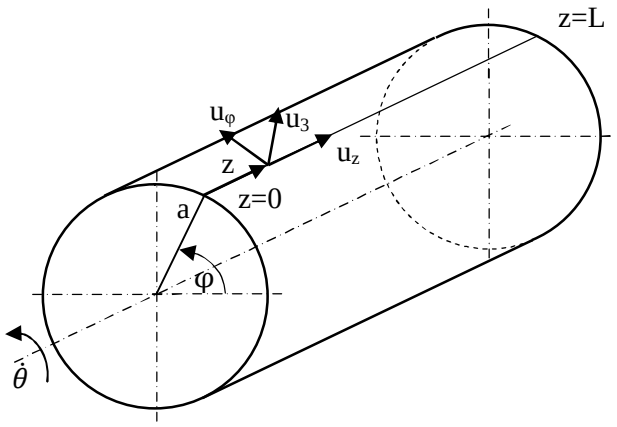

Figure 4.3: Circular cylindrical shell

Thus, Love's equations for a rotating circular cylindrical shell can be written as

$$\frac{\partial N_{zz}}{\partial z} + \frac{1}{a}\frac{\partial N_{\varphi z}}{\partial \varphi} + \frac{N^i_{\varphi 0}}{a^2}\frac{\partial^2 u_z}{\partial \varphi^2} + q_z = \rho h \frac{\partial^2 u_z}{\partial t^2} \tag{4.6}$$

$$\begin{aligned}\frac{\partial N_{z\varphi}}{\partial z} + \frac{1}{a}\frac{\partial N_{\varphi\varphi}}{\partial \varphi} + \frac{Q_{\varphi 3}}{a} + \frac{N^i_{\varphi 0}}{a^2}\left(2\frac{\partial u_3}{\partial \varphi} + \frac{\partial^2 u_\varphi}{\partial \varphi^2} - u_\varphi\right) + q_\varphi \\ = \rho h\left(\frac{\partial^2 u_\varphi}{\partial t^2} + 2\dot{\theta}\frac{\partial u_3}{\partial t} - \dot{\theta}^2 u_\varphi\right)\end{aligned} \tag{4.7}$$

$$\begin{aligned}\frac{\partial Q_{z3}}{\partial z} + \frac{1}{a}\frac{\partial Q_{\varphi 3}}{\partial \varphi} - \frac{N_{\varphi\varphi}}{a} + \frac{N^i_{\varphi 0}}{a^2}\left(-2\frac{\partial u_\varphi}{\partial \varphi} + \frac{\partial^2 u_3}{\partial \varphi^2} - u_3\right) + q_3 \\ = \rho h\left(\frac{\partial^2 u_3}{\partial t^2} - 2\dot{\theta}\frac{\partial u_\varphi}{\partial t} - \dot{\theta}^2 u_3\right)\end{aligned} \tag{4.8}$$

where Q_{z3} and $Q_{\varphi 3}$ are defined by

$$Q_{z3} = \frac{\partial M_{zz}}{\partial z} + \frac{1}{a}\frac{\partial M_{\varphi z}}{\partial \varphi} \tag{4.9}$$

$$Q_{\varphi 3} = \frac{\partial M_{z\varphi}}{\partial z} + \frac{1}{a}\frac{\partial M_{\varphi\varphi}}{\partial \varphi} \tag{4.10}$$

and

$$N_{\varphi 0}^{i} = \rho h a^2 \dot{\theta}^2 \tag{4.11}$$

$$N_{zz} = K\left(\varepsilon_{zz}^{\circ} + \mu\varepsilon_{\varphi\varphi}^{\circ}\right) \tag{4.12}$$

$$N_{\varphi\varphi} = K\left(\varepsilon_{\varphi\varphi}^{\circ} + \mu\varepsilon_{zz}^{\circ}\right) \tag{4.13}$$

$$N_{z\varphi} = \frac{K(1-\mu)}{2}\varepsilon_{z\varphi}^{\circ} \tag{4.14}$$

$$M_{zz} = D\left(k_{zz} + \mu k_{\varphi\varphi}\right) \tag{4.15}$$

$$M_{\varphi\varphi} = D\left(k_{\varphi\varphi} + \mu k_{zz}\right) \tag{4.16}$$

$$M_{z\varphi} = \frac{D(1-\mu)}{2}k_{z\varphi} \tag{4.17}$$

$$\varepsilon_{zz}^{\circ} = \frac{\partial u_z}{\partial z} \tag{4.18}$$

$$\varepsilon_{\varphi\varphi}^{\circ} = \frac{1}{a}\frac{\partial u_\varphi}{\partial \varphi} + \frac{u_3}{a} \tag{4.19}$$

$$\varepsilon_{z\varphi}^{\circ} = \frac{\partial u_\varphi}{\partial z} + \frac{1}{a}\frac{\partial u_z}{\partial \varphi} \tag{4.20}$$

$$k_{zz} = \frac{\partial \beta_z}{\partial z} \tag{4.21}$$

$$k_{\varphi\varphi} = \frac{1}{a}\frac{\partial \beta_\varphi}{\partial \varphi} \tag{4.22}$$

$$k_{z\varphi} = \frac{\partial \beta_\varphi}{\partial z} + \frac{1}{a}\frac{\partial \beta_z}{\partial \varphi} \tag{4.23}$$

$$\beta_z = -\frac{\partial u_3}{\partial z} \tag{4.24}$$

$$\beta_\varphi = \frac{u_\varphi}{a} - \frac{1}{a}\frac{\partial u_3}{\partial \varphi} \tag{4.25}$$

K is called membrane stiffness and it is defined as:

$$K = \frac{Eh}{1-\mu^2} \tag{4.26}$$

where *E* is Young's modulus of elasticity and μ is Poisson's ratio. *D* is called bending stiffness and it is defined as:

$$D = \frac{Eh^3}{12(1-\mu^2)} \tag{4.27}$$

4.2.3 Natural frequencies and modes of a non-rotating circular cylindrical shell

Setting $\dot{\theta}$, q_z, q_φ, $q_3 = 0$ in eqs. (4.6) to (4.8) and recognizing that at a natural frequency every point in the elastic system moves harmonically, it may be assumed that

$$u_z(z,\varphi,t) = U_z(z,\varphi)e^{j\omega t} \tag{4.28}$$

$$u_\varphi(z,\varphi,t) = U_\varphi(z,\varphi)e^{j\omega t} \tag{4.29}$$

$$u_3(z,\varphi,t) = U_3(z,\varphi)e^{j\omega t} \tag{4.30}$$

And after substituting this into (4.6) through (4.8) and factoring out $e^{j\omega t}$ it yields

$$\frac{\partial N_{zz}^{'}}{\partial z} + \frac{1}{a}\frac{\partial N_{\varphi z}^{'}}{\partial \varphi} + \rho h\omega^2 U_z = 0 \tag{4.31}$$

$$\frac{\partial N_{z\varphi}^{'}}{\partial z} + \frac{1}{a}\frac{\partial N_{\varphi\varphi}^{'}}{\partial \varphi} + \frac{Q_{\varphi 3}^{'}}{a} + \rho h\omega^2 U_\varphi = 0 \tag{4.32}$$

$$\frac{\partial Q_{z3}^{'}}{\partial z} + \frac{1}{a}\frac{\partial Q_{\varphi 3}^{'}}{\partial \varphi} - \frac{N_{\varphi\varphi}^{'}}{a} + \rho h\omega^2 U_3 = 0 \tag{4.33}$$

The boundary conditions for a simply supported shell are defined for both ends of the shell:

$$u_3(0, \varphi, t) = 0 \tag{4.34}$$

$$u_\varphi(0, \varphi, t) = 0 \tag{4.35}$$

$$M_{zz}(0, \varphi, t) = 0 \tag{4.36}$$

$$N_{zz}(0, \varphi, t) = 0 \tag{4.37}$$

$$u_3(L, \varphi, t) = 0 \tag{4.38}$$

$$u_\varphi(L, \varphi, t) = 0 \tag{4.39}$$

$$M_{zz}(L, \varphi, t) = 0 \tag{4.40}$$

$$N_{zz}(L, \varphi, t) = 0 \tag{4.41}$$

It says that at the boundaries there is zero deflection in the radial and tangential directions and the resultant bending moment as well as the resultant force in the axial direction is zero. One can also find the solution for eqs. (4.31) to (4.33) that satisfies the boundary conditions:

$$U_z(z, \varphi) = A \cos\frac{m\pi z}{L} \cos[n(\varphi - \phi)] \tag{4.42}$$

$$U_\varphi(z, \varphi) = B \sin\frac{m\pi z}{L} \sin[n(\varphi - \phi)] \tag{4.43}$$

$$U_3(z, \varphi) = C \sin\frac{m\pi z}{L} \cos[n(\varphi - \phi)] \tag{4.44}$$

where m and n are integers and stand for number of eigenmodes in the longitudinal and circumferential direction, respectively, ϕ denotes any arbitrary phase angle. These solutions are now substituted into the equations above. And one obtains

$$\beta_\varphi' = \frac{1}{a}(B + nC) \sin\frac{m\pi z}{L} \sin[n(\varphi - \phi)] \tag{4.45}$$

$$\beta_z' = -\frac{m\pi}{L} C \cos\frac{m\pi z}{L} \cos[n(\varphi - \phi)] \tag{4.46}$$

$$k_{z\varphi}' = \frac{m\pi}{La}(B + 2nC) \cos\frac{m\pi z}{L} \sin[n(\varphi - \phi)] \tag{4.47}$$

$$k'_{\varphi\varphi} = \frac{n}{a^2}(B + nC)\sin\frac{m\pi z}{L}\cos[n(\varphi - \phi)] \tag{4.48}$$

$$k'_{zz} = \left(\frac{m\pi}{L}\right)^2 C\sin\frac{m\pi z}{L}\cos[n(\varphi - \phi)] \tag{4.49}$$

$$\varepsilon'^{\circ}_{z\varphi} = \left(\frac{m\pi}{L}B - \frac{n}{a}A\right)\cos\frac{m\pi z}{L}\sin[n(\varphi - \phi)] \tag{4.50}$$

$$\varepsilon'^{\circ}_{\varphi\varphi} = \frac{1}{a}(Bn + C)\sin\frac{m\pi z}{L}\cos[n(\varphi - \phi)] \tag{4.51}$$

$$\varepsilon'^{\circ}_{zz} = -A\frac{m\pi}{L}\sin\frac{m\pi z}{L}\cos[n(\varphi - \phi)] \tag{4.52}$$

$$M'_{z\varphi} = \frac{D(1-\mu)}{2}\frac{m\pi}{La}(B + 2nC)\cos\frac{m\pi z}{L}\sin[n(\varphi - \phi)] \tag{4.53}$$

$$M'_{\varphi\varphi} = D\left\{\frac{n}{a^2}B + \left[\frac{n^2}{a^2} + \mu\left(\frac{m\pi}{L}\right)^2\right]C\right\}\sin\frac{m\pi z}{L}\cos[n(\varphi - \phi)] \tag{4.54}$$

$$M'_{zz} = D\left\{\frac{\mu n}{a^2}B + \left[\mu\frac{n^2}{a^2} + \left(\frac{m\pi}{L}\right)^2\right]C\right\}\sin\frac{m\pi z}{L}\cos[n(\varphi - \phi)] \tag{4.55}$$

$$N'_{z\varphi} = \frac{K(1-\mu)}{2}\left(\frac{m\pi}{a}B - \frac{n}{a}A\right)\cos\frac{m\pi z}{L}\sin[n(\varphi - \phi)] \tag{4.56}$$

$$N'_{\varphi\varphi} = K\left(\frac{n}{a}B + \frac{1}{a}C - \mu\frac{m\pi}{L}A\right)\sin\frac{m\pi z}{L}\cos[n(\varphi - \phi)] \tag{4.57}$$

$$N'_{zz} = K\left(\frac{\mu n}{a}B + \frac{\mu}{a}C - \frac{m\pi}{L}A\right)\sin\frac{m\pi z}{L}\cos[n(\varphi - \phi)] \tag{4.58}$$

$$Q'_{z3} = D\frac{m\pi}{L}\left\{\frac{n}{a^2}\frac{1+\mu}{2}B + \left[\frac{n^2}{a^2} + \left(\frac{m\pi}{L}\right)^2\right]C\right\}\cos\frac{m\pi z}{L}\cos[n(\varphi - \phi)] \tag{4.59}$$

$$Q'_{\varphi 3} = -\frac{D}{a}\left\{\left[\frac{1-\mu}{2}\left(\frac{m\pi}{L}\right)^2 + \frac{n^2}{a^2}\right]B + n\left[\frac{n^2}{a^2} + \left(\frac{m\pi}{L}\right)^2\right]C\right\}\sin\frac{m\pi z}{L}\sin[n(\varphi - \phi) \tag{4.60}$$

Thus, equations (4.31, 4.32, and 4.33) become

$$\begin{bmatrix} \rho h\omega^2 - k_{11} & k_{12} & k_{13} \\ k_{21} & \rho h\omega^2 - k_{22} & k_{23} \\ k_{31} & k_{32} & \rho h\omega^2 - k_{33} \end{bmatrix}\begin{Bmatrix} A \\ B \\ C \end{Bmatrix} = 0 \tag{4.61}$$

where

$$k_{11} = K\left[\left(\frac{m\pi}{L}\right)^2 + \frac{1-\mu}{2}\left(\frac{n}{a}\right)^2\right] \tag{4.62}$$

$$k_{12} = k_{21} = K\frac{1+\mu}{2}\frac{m\pi}{L}\frac{n}{a} \tag{4.63}$$

$$k_{13} = k_{31} = \frac{\mu K}{a}\frac{m\pi}{L} \tag{4.64}$$

$$k_{22} = \left(K + \frac{D}{a^2}\right)\left[\frac{1-\mu}{2}\left(\frac{m\pi}{L}\right)^2 + \left(\frac{n}{a}\right)^2\right] \tag{4.65}$$

$$k_{23} = k_{32} = -\frac{K}{a}\frac{n}{a} - \frac{D}{a}\frac{n}{a}\left[\left(\frac{m\pi}{L}\right)^2 + \left(\frac{n}{a}\right)^2\right] \tag{4.66}$$

$$k_{33} = D\left[\left(\frac{m\pi}{L}\right)^2 + \left(\frac{n}{a}\right)^2\right]^2 + \frac{K}{a^2} \tag{4.67}$$

For a nontrivial solution, the determinant of eq. (4.61) has to be zero. Expanding the determinant gives

$$\omega^6 + a_1\omega^4 + a_2\omega^2 + a_3 = 0 \tag{4.68}$$

where

$$a_1 = -\frac{1}{\rho h}(k_{11} + k_{22} + k_{33}) \tag{4.69}$$

$$a_2 = \frac{1}{(\rho h)^2}\left(k_{11}k_{33} + k_{22}k_{33} + k_{11}k_{22} - {k_{23}}^2 - {k_{12}}^2 - {k_{13}}^2\right) \tag{4.70}$$

$$a_3 = \frac{1}{(\rho h)^3}\left(k_{11}{k_{23}}^2 + k_{22}{k_{13}}^2 + k_{33}{k_{12}}^2 + 2k_{12}k_{23}k_{13} - k_{11}k_{22}k_{33}\right) \tag{4.71}$$

The solutions of this equation are

$${\omega_{1mn}}^2 = -\frac{2}{3}\sqrt{{a_1}^2 + 3a_2}\,cos\frac{\gamma}{3} - \frac{a_1}{3} \tag{4.72}$$

$$\omega_{2mn}{}^2 = -\frac{2}{3}\sqrt{a_1{}^2 + 3a_2}\,cos\frac{\gamma + 2\pi}{3} - \frac{a_1}{3} \tag{4.73}$$

$$\omega_{3mn}{}^2 = -\frac{2}{3}\sqrt{a_1{}^2 + 3a_2}\,cos\frac{\gamma + 4\pi}{3} - \frac{a_1}{3} \tag{4.74}$$

where

$$\gamma = cos^{-1}\left(\frac{27a_3 + 2a_1{}^3 - 9a_1a_2}{2\sqrt{(a_1{}^2 - 3a_2)^3}}\right) \tag{4.75}$$

The ratio between coefficients *A*, *B* and *C* can be determined as

$$\frac{A_j}{C_i} = -\frac{k_{13}\left(\rho h\omega_{jmn}{}^2 - k_{22}\right) - k_{12}k_{23}}{\left(\rho h\omega_{jmn}{}^2 - k_{11}\right)\left(\rho h\omega_{jmn}{}^2 - k_{22}\right) - k_{12}{}^2} \tag{4.76}$$

$$\frac{B_j}{C_j} = -\frac{k_{23}\left(\rho h\omega_{jmn}{}^2 - k_{11}\right) - k_{21}k_{13}}{\left(\rho h\omega_{jmn}{}^2 - k_{11}\right)\left(\rho h\omega_{jmn}{}^2 - k_{22}\right) - k_{12}{}^2} \tag{4.77}$$

Where $j = 1, 2, 3$. And finally, three modes related to three natural frequencies ω_{jmn} for each *m*, *n* combination can be obtained

$$U_{zj} = A_j\,cos\frac{m\pi z}{L}cos[n(\varphi - \phi)] \tag{4.78}$$

$$U_{\varphi j} = B_j\,sin\frac{m\pi z}{L}sin[n(\varphi - \phi)] \tag{4.79}$$

$$U_{3j} = C_j sin\frac{m\pi z}{L}cos[n(\varphi - \phi)] \tag{4.80}$$

where the C_j are arbitrary constants.

4.2.4 Natural frequencies and modes of a rotating circular cylindrical shell

In case of a rotating circular cylindrical shell, one can notice that eqs. (4.6) to (4.8) contain additional terms $N^i_{\varphi 0}$ that represent an additional tension in φ direction, which causes an additional stiffening effect. This is a consequence of the rotating movement and can be viewed as an effect of centrifugal force. Theoretically, an additional tension in *z* direction N^i_{z0} can be present. However, it

is assumed that the shell can expand in the radial direction but not in the axial direction [Huang 1988]. Therefore,

$$N_{z0}^{i} = 0 \tag{4.81}$$

and

$$N_{\varphi 0}^{i} = \rho h a^2 \dot{\theta}^2 \tag{4.82}$$

Then, eqs. (4.6) to (4.8) can be used in the full form. Now, for solving the eigenvalue problem, q_z, q_φ, q_3 is set to zero and for the same boundary conditions, eqs. (4.34) to (4.41), one can find a solution of a form

$$u_z(z,\varphi,t) = A\cos\frac{m\pi z}{L}\cos(n\varphi + \omega t) \tag{4.83}$$

$$u_\varphi(z,\varphi,t) = B\sin\frac{m\pi z}{L}\sin(n\varphi + \omega t) \tag{4.84}$$

$$u_3(z,\varphi,t) = C\sin\frac{m\pi z}{L}\cos(n\varphi + \omega t) \tag{4.85}$$

After substituting these solutions into eqs. (4.9) through (4.27) and then into eqs. (4.6) to (4.8), similarly as in the previous section, one obtains

$$\begin{bmatrix} \rho h\omega^2 - k_{11} & k_{12} & k_{13} \\ k_{21} & \rho h\omega^2 - k_{22} & 2\rho h\omega\dot{\theta} - k_{23} \\ k_{31} & 2\rho h\omega\dot{\theta} - k_{32} & \rho h\omega^2 - k_{33} \end{bmatrix} \begin{Bmatrix} A \\ B \\ C \end{Bmatrix} = 0 \tag{4.86}$$

where

$$k_{11} = K\left[\left(\frac{m\pi}{L}\right)^2 + \frac{1-\mu}{2}\left(\frac{n}{a}\right)^2\right] + N_{\varphi 0}^{i}\left(\frac{n}{a}\right)^2 \tag{4.87}$$

$$k_{12} = k_{21} = K\frac{1+\mu}{2}\frac{m\pi}{L}\frac{n}{a} \tag{4.88}$$

$$k_{13} = k_{31} = \frac{\mu K}{a}\frac{m\pi}{L} \tag{4.89}$$

$$k_{22} = \left(K + \frac{D}{a^2}\right)\left[\frac{1-\mu}{2}\left(\frac{m\pi}{L}\right)^2 + \left(\frac{n}{a}\right)^2\right] + \frac{N_{\varphi 0}^{i}}{a^2}(1+n^2) - \rho h\dot{\theta}^2 \tag{4.90}$$

$$k_{23} = k_{32} = -\frac{K}{a}\frac{n}{a} - \frac{D}{a}\frac{n}{a}\left[\left(\frac{m\pi}{L}\right)^2 + \left(\frac{n}{a}\right)^2\right] + 2n\frac{N_{\varphi 0}^i}{a^2} \tag{4.91}$$

$$k_{33} = D\left[\left(\frac{m\pi}{L}\right)^2 + \left(\frac{n}{a}\right)^2\right]^2 + \frac{K}{a^2} + \frac{N_{\varphi 0}^i}{a^2}(1 + n^2) - \rho h\dot{\theta}^2 \tag{4.92}$$

For a nontrivial solution, the determinant of a matrix in eq. (4.86) has to be zero. Expanding the determinant gives

$$\omega^6 + a_1\omega^4 + a_2\omega^3 + a_3\omega^2 + a_4\omega + a_5 = 0 \tag{4.93}$$

where

$$a_1 = -\frac{1}{\rho h}(k_{11} + k_{22} + k_{33}) \tag{4.94}$$

$$a_2 = \frac{4\dot{\theta}}{\rho h}k_{23} \tag{4.95}$$

$$a_3 = \frac{1}{(\rho h)^2}\left(k_{11}k_{33} + k_{22}k_{33} + k_{11}k_{22} - {k_{23}}^2 - {k_{12}}^2 - {k_{13}}^2\right) \tag{4.96}$$

$$a_4 = -\frac{4\dot{\theta}}{(\rho h)^2}(k_{11}k_{23} - k_{12}k_{13}) \tag{4.97}$$

$$a_5 = \frac{1}{(\rho h)^3}\left(k_{11}{k_{23}}^2 + k_{22}{k_{13}}^2 + k_{33}{k_{12}}^2 + 2k_{12}k_{23}k_{13} - k_{11}k_{22}k_{33}\right) \tag{4.98}$$

The polynomial in eq. (4.93) is still of even-order, but the function is no longer symmetric about the *y* axis due to the rotation effect and therefore, *6* distinct natural frequencies related to *m, n* modes are obtained, in contrast to the non-rotating situation where only *3* pairs of distinct natural frequencies related to *m, n* modes are present.

The ratio between coefficients *A, B* and *C* can be determined as

$$\frac{A_j}{C_j} = -\frac{k_{13}\left(\rho h{\omega_{jmn}}^2 - k_{22}\right) - k_{12}\left(2\rho h\omega_{jmn}\dot{\theta} - k_{23}\right)}{\left(\rho h{\omega_{jmn}}^2 - k_{11}\right)\left(\rho h{\omega_{jmn}}^2 - k_{22}\right) - {k_{12}}^2} \tag{4.99}$$

$$\frac{B_j}{C_j} = -\frac{(2\rho h\omega_{jmn}\dot{\theta} - k_{23})(\rho h{\omega_{jmn}}^2 - k_{11}) - k_{21}k_{13}}{(\rho h{\omega_{jmn}}^2 - k_{11})(\rho h{\omega_{jmn}}^2 - k_{22}) - {k_{12}}^2} \tag{4.100}$$

where $j = 1, 2, ..., 6$. And finally, six modes related to six distinct natural frequencies ω_{jmn} for each m, n combination are obtained

$$u_{zj} = A_j \cos\frac{m\pi z}{L}\cos(n\varphi + \omega_{jmn}t) \tag{4.101}$$

$$u_{\varphi j} = B_j \sin\frac{m\pi z}{L}\sin(n\varphi + \omega_{jmn}t) \tag{4.102}$$

$$u_{3j} = C_j \sin\frac{m\pi z}{L}\cos(n\varphi + \omega_{jmn}t) \tag{4.103}$$

where the C_j are arbitrary constants. These modes are called travelling modes and are characteristic for rotating shells.

4.2.5 Comparison of natural frequencies and reduction to non-rotating situation

The reason why for a rotating circular cylindrical shell one gets *6* distinct eigenvalues instead of *3* is the shape of the polynomial function that is dependent on the rotational speed $\dot{\theta}$. Figure 4.4 a) shows the left hand side of eq. (4.68) and Figure 4.4 b) the left hand side of eq. (4.93) with $\dot{\theta}$ = *4000 rad/s*. In both figures, the zeros are the solutions of the eigenvalue problem and they represent the natural frequencies for *m = 1, n = 1*, in this case.

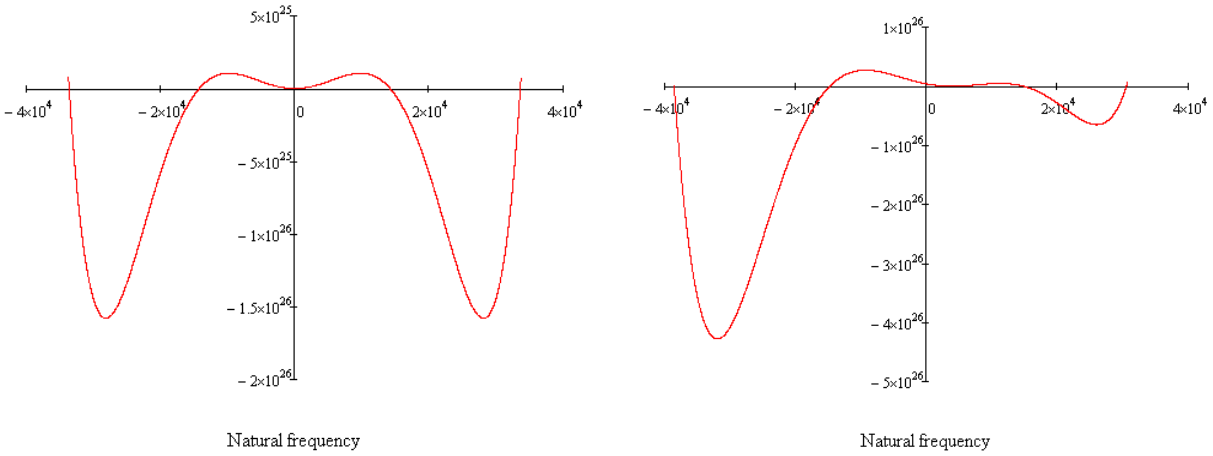

a) m = 1, n =1, $\dot{\theta}$ = 0 *b) m = 1, n =1, $\dot{\theta}$ = 4000 rad/s*

Figure 4.4: Polynomials for a rotating and non-rotating shell, *m = 1, n = 1*

If one substitutes, e.g., two distinct natural frequencies (rotating situation) related to the lowest mode, into one of the mode expressions, say into eq. (4.102), one gets two travelling waves:

$$u_{\varphi,+1} = B_j \sin\frac{m\pi z}{L}\sin(n\varphi + \omega_{+1mn}t) \tag{4.104}$$

$$u_{\varphi,-1} = B_j \sin\frac{m\pi z}{L}\sin(n\varphi + \omega_{-1mn}t) \tag{4.105}$$

where usually $\omega_{+1mn} > 0$ and $\omega_{-1mn} < 0$, for lower speeds, which means that the two waves travel in opposite direction with different speeds. If two natural frequencies (stationary situation) related to the lowest mode are now substituted into the same eq. (4.102), one gets two travelling waves that travel also in the opposite direction, but this time with the same speed, because $\omega_{+1mn} = -\omega_{-1mn}$. These two waves form a standing wave, which can be proven by addition of eqs. (4.104) and (4.105) that yields the same form of a mode shape as given in eq. (4.79), where the ϕ is only an arbitrary phase angle.

Figure 4.5 shows the bifurcation of flexural (related to the modes where the transverse component dominates) natural frequencies for *m = 1, n = 1, 2, 3, 4* as a function of the rotational speed. The rotational speed and the absolute values of the natural frequencies are normalized with respect to the stationary natural frequency.

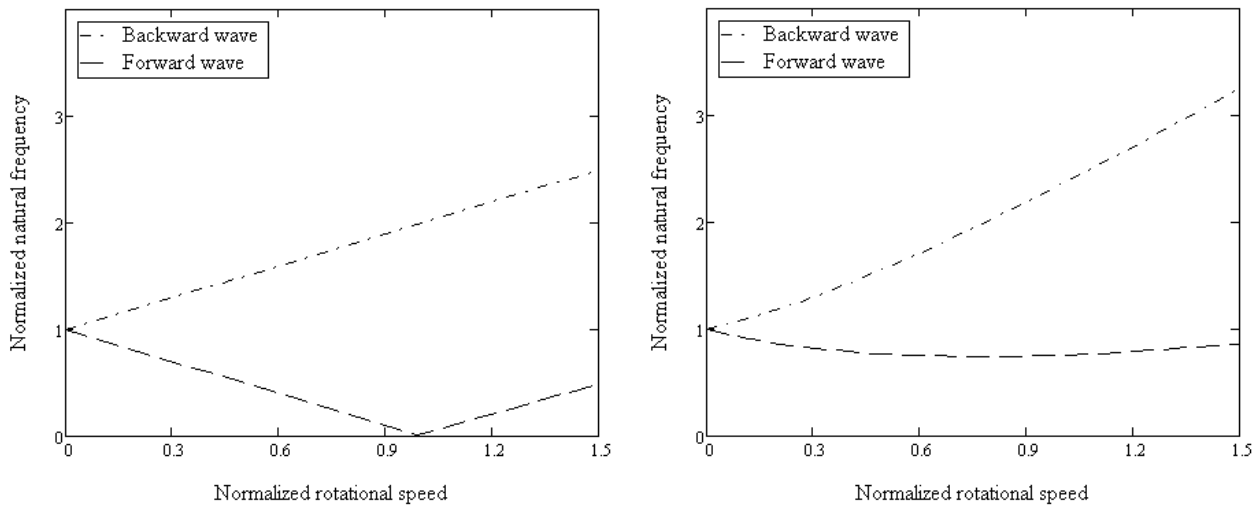

a) m = 1, n = 1 *b) m = 1, n = 2*

Figure 4.5: Bifurcation of flexural natural frequencies for *m = 1, n = 1, 2, 3, 4*

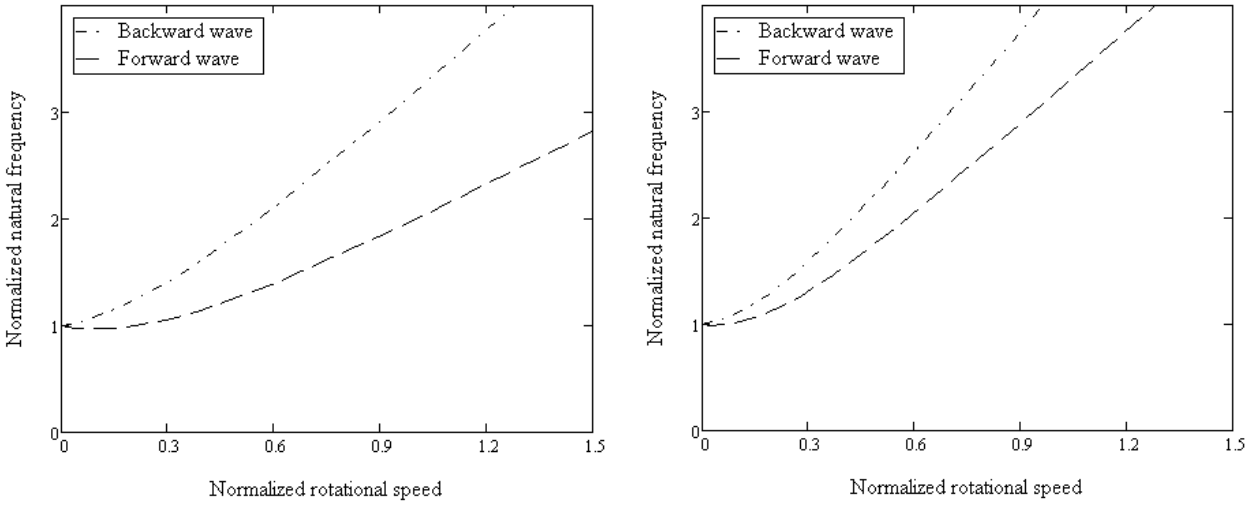

c) m = 1, n = 3 *d) m = 1, n = 4*

Figure 4.5: Bifurcation of flexural natural frequencies for *m = 1, n = 1, 2, 3, 4*

From Figure 4.5 a), it is apparent that when the speed of the forward wave equals the rotational speed, the wave does not move while the backward wave moves two times faster with respect to the rotating coordinates.

However, the bifurcation takes on gravity with higher rotational speeds. In the studied case, the rotational speed is $\dot{\theta} = -1.05$ *rad/s*. Now, let us examine the effect of rotation on the natural frequencies by comparing the rotating and non-rotating natural frequencies for a roll, whose dimensions are given in Table 4.1.

Table 4.1: Roll parameters

Roll	
Length	$L = 7.15$ *m*
Mean radius	$a = 0.2225$ *m*
Wall thickness	$h = 0.002$ *m*
Young's modulus	$E = 200$ *GPa*
Density	$\rho = 7874$ *kg/m*^{3}
Angular velocity	$\dot{\theta} = -1.05$ *rad/s*

The comparison is expressed in percentage (%) for *m, n* combinations and is tabulated in Table 4.2. The left hand side denotes the comparison of ω_{-1mn} and ω_{1mn} and the right hand side denotes the comparison of ω_{+1mn} and ω_{1mn}.

Table 4.2: Effect of rotation on natural frequencies (in %)

m/n	**1**	**2**	**3**	**4**
1	0.692 / 0.692	0.484 / 0.489	0.133 / 0.136	0.054 / 0.056
2	0.177 / 0.177	0.329 / 0.332	0.130 / 0.133	0.054 / 0.056

The effect of the centrifugal force on the natural frequencies can be obtained by setting $\dot{\theta} = 0$ in eq. (4.6) to (4.8) except for the term $N_{\varphi 0}^{i}$. The results are tabulated in Table 4.3.

Table 4.3: Effect of the centrifugal force on natural frequencies (in %)

m/n	**1**	**2**	**3**	**4**
1	$0.011 \cdot 10^{-3}$	$3.328 \cdot 10^{-3}$	$1.606 \cdot 10^{-3}$	$0.906 \cdot 10^{-3}$
2	$0.003 \cdot 10^{-3}$	$1.535 \cdot 10^{-3}$	$1.541 \cdot 10^{-3}$	$0.900 \cdot 10^{-3}$

From these results one can state that for the given rotational speed the effect of the centrifugal force is negligible. The effect of Coriolis forces is in general more pronounced and it can be seen also in this case. Since the effect of the centrifugal force is negligible, the effect of the rotation is practically entirely represented by the Coriolis effect (see Table 4.2). Nevertheless, for a given rotational speed the effect on the natural frequencies is less than one percent in all lower modes (*m = 1, 2; n = 1, 2, 3, 4*). In addition, the effect will be even lower with increasing wall thickness of the roll.

Therefore, based on this eigenvalue analysis it has been decided that the forced response can be obtained by using stationary eigenmodes and eigenfrequencies. For higher rotational speeds, the use of travelling modes and six distinct eigenvalues would be necessary. For the latter case, Huang and Soedel propose a method for solving this problem in [Huang 1988].

4.2.6 Forced response

In the grinding procedure, the contact forces in the axial direction are neglected. Thus, only the displacements u_φ and u_3 are to be solved. However, the contribution of the longitudinal mode is present, too. In order to express any shape in the φ direction, two orthogonal components are needed. These are obtained if one time $n\phi = 0$ and the other $n\phi = \pi/2$ [Soedel 1981]. This gives two sets of modes:

$$U_{z,1mnj}(\varphi, z) = A_{mnj}\, cos\frac{m\pi z}{L} cos(n\varphi) \tag{4.106}$$

$$U_{\varphi,1mnj}(\varphi, z) = B_{mnj}\, sin\frac{m\pi z}{L} sin(n\varphi) \tag{4.107}$$

$$U_{3,1mnj}(\varphi, z) = C_{mnj}\, sin\frac{m\pi z}{L} cos(n\varphi) \tag{4.108}$$

and

$$U_{z,2mnj}(\varphi, z) = A_{mnj}\, cos\frac{m\pi z}{L} sin(n\varphi) \tag{4.109}$$

$$U_{\varphi,2mnj}(\varphi, z) = -B_{mnj}\, sin\frac{m\pi z}{L} cos(n\varphi) \tag{4.110}$$

$$U_{3,2mnj}(\varphi, z) = C_{mnj}\, sin\frac{m\pi z}{L} sin(n\varphi) \tag{4.111}$$

The displacements u_z, u_φ and u_3 can be found by employing modal expansion method for the two sets:

$$\begin{aligned} u_z(\varphi, z, t) &= \sum_{k=1}^{2}\sum_{m=1}^{\infty}\sum_{n=0}^{\infty}\sum_{j=1}^{3} \eta_{k,mnj}(t) U_{z,kmnj}(\varphi, z) \\ &\approx \sum_{k=1}^{2}\sum_{m=1}^{\infty}\sum_{n=0}^{\infty} \eta_{k,mn1}(t) U_{z,kmn1}(\varphi, z) \end{aligned} \tag{4.112}$$

$$\begin{aligned} u_\varphi(\varphi, z, t) &= \sum_{k=1}^{2}\sum_{m=1}^{\infty}\sum_{n=0}^{\infty}\sum_{j=1}^{3} \eta_{k,mnj}(t) U_{\varphi,kmnj}(\varphi, z) \\ &\approx \sum_{k=1}^{2}\sum_{m=1}^{\infty}\sum_{n=0}^{\infty} \eta_{k,mn1}(t) U_{\varphi,kmn1}(\varphi, z) \end{aligned} \tag{4.113}$$

$$u_3(\varphi, z, t) = \sum_{k=1}^{2}\sum_{m=1}^{\infty}\sum_{n=0}^{\infty}\sum_{j=1}^{3}\eta_{k,mnj}(t)U_{3,kmnj}(\varphi, z) \approx \sum_{k=1}^{2}\sum_{m=1}^{\infty}\sum_{n=0}^{\infty}\eta_{k,mn1}(t)U_{3,kmn1}(\varphi, z) \tag{4.114}$$

where $\eta_{k,mn}$ is the participation factor (or the time dependent part) for the combination m and n modes and j refers to the j^{th} natural frequency for the combination m and n modes. Since the ω_{1mn} (i.e., the lowest of ω_{jmn}) is associated with the mode where the transverse component dominates, one can use a simplification as shown in (4.112) to (4.114). Then the subscript j can be left out. By furnishing eqs. (4.6) through (4.8) for zero rotation with the viscous damping terms and substituting these into eqs. (4.112) to (4.114) for each set ($k = 1$ and $k = 2$) separately and exploiting eqs. (4.31) to (4.33), then summing these three equations and integrating over the shell surface and finally utilizing the orthogonality property of the modes, one can write following second order differential equation:

$$m_{k,mn}\ddot{\eta}_{k,mn} + c_{k,mn}\dot{\eta}_{k,mn} + k_{k,mn}\eta_{k,mn} = F_{k,mn,C} + F_{k,mn,G} \tag{4.115}$$

Here, $m_{k,mn}$, $c_{k,mn}$ and $k_{k,mn}$ are the modal mass, modal damping and modal stiffness corresponding to modes m, n, respectively. $F_{k,mn,C}$ is the modal force caused by the contact (grinding) forces and $F_{k,mn,G}$ is the modal force caused by the gravity (self-weight) load of the roll (see Figure 4.6). The modal mass, damping and stiffness members are defined as follows:

$$m_{k,mn} = \rho h N_{k,mn} \tag{4.116}$$

$$c_{k,mn} = 2\zeta\rho h\omega_{mn}N_{k,mn} \tag{4.117}$$

$$k_{k,mn} = \rho h\omega_{mn}^2 N_{k,mn} \tag{4.118}$$

where ζ is the viscous damping ratio and

$$N_{k,mn} = \int_0^{2\pi}\int_0^{L}\left[U_{z,kmn}(\varphi, z)^2 + U_{\varphi,kmn}(\varphi, z)^2 + U_{3,kmn}(\varphi, z)^2\right] a\, dz d\varphi \tag{4.119}$$

where L is the length of the roll. Eq. (4.119) can be further evaluated as

$$N_{1,mn} = \begin{cases} La\pi(A_{mn}^2 + C_{mn}^2), & n = 0, m \neq 0 \\ \dfrac{La\pi(A_{mn}^2 + B_{mn}^2 + C_{mn}^2)}{2}, & n \neq 0, m \neq 0 \end{cases} \quad (4.120)$$

$$N_{2,mn} = \begin{cases} La\pi(B_{mn}^2), & n = 0, m \neq 0 \\ \dfrac{La\pi(A_{mn}^2 + B_{mn}^2 + C_{mn}^2)}{2}, & n \neq 0, m \neq 0 \end{cases} \quad (4.121)$$

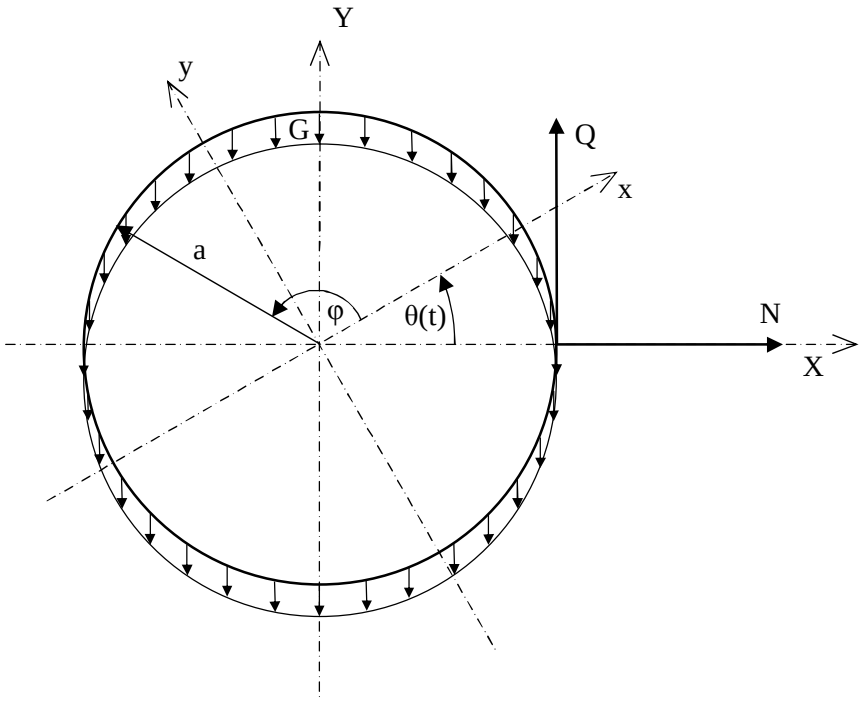

Figure 4.6: Load acting on the roll and rotating coordinates

$F_{mn,C}$ is defined as:

$$F_{k,mn,C} = \int_0^{2\pi} \int_0^{L} \left[q_z U_{z,kmn}(\varphi, z) + q_\varphi U_{\varphi,kmn}(\varphi, z) + q_3 U_{3,kmn}(\varphi, z)\right] a \, dz d\varphi \quad (4.122)$$

where

$$q_z = 0 \quad (4.123)$$

$$q_\varphi = Q\frac{1}{a}\delta(z - z^*)\delta(\varphi - \varphi^*) \tag{4.124}$$

$$q_3 = N\frac{1}{a}\delta(z - z^*)\delta(\varphi - \varphi^*) \tag{4.125}$$

By solving the integral in (4.122) one obtains

$$F_{k,mn,C} = \left[QU_{\varphi,kmn}(\varphi^*, z^*) + NU_{3,kmn}(\varphi^*, z^*)\right] \tag{4.126}$$

where superscript * indicates the position of the acting point force. $F_{mn,G}$ is defined as:

$$F_{k,mn,G} = \int_0^{2\pi}\int_0^{L}\left[g_\varphi U_{\varphi,kmn}(\varphi, z) + g_3 U_{3,kmn}(\varphi, z)\right]a\, dzd\varphi \tag{4.127}$$

where

$$g_\varphi = -G\, cos(\varphi - \varphi^*) \tag{4.128}$$

$$g_3 = -G\, sin(\varphi - \varphi^*) \tag{4.129}$$

and G is the distributed self-weight, where g is the gravity acceleration on Earth:

$$G = \rho hg \tag{4.130}$$

where φ^* defines also the direction of the gravitational acceleration. For $\varphi^* = 0$, the direction of the gravitational acceleration coincides with $-Y$ direction (see Figure 4.6). By solving the integral in (4.127) one obtains

$$F_{1,mn,G} = \begin{cases} 0, & n \neq 1 \vee m = 2,4,6,.. \\ -\dfrac{2LaG\, sin\,\varphi^*\,(B_{mn} - C_{mn})}{m}, & otherwise \end{cases} \tag{4.131}$$

and

$$F_{2,mn,G} = \begin{cases} 0, & n \neq 1 \vee m = 2,4,6,.. \\ \dfrac{2LaG\, cos(\varphi^*)\,(B_{mn} - C_{mn})}{m}, & otherwise \end{cases} \tag{4.132}$$

The initial conditions for the modal participation factor are defined as:

$$\eta_{k,mn}(0) = \int_0^{2\pi} \int_0^{L} \left[u_\varphi(z,\varphi,0) U_{\varphi,kmn}(\varphi,z) + u_3(z,\varphi,0) U_{3,kmn}(\varphi,z)\right] a \, dz d\varphi \qquad (4.133)$$

and for its time derivative:

$$\dot{\eta}_{k,mn}(0) = \int_0^{2\pi} \int_0^{L} \left[\dot{u}_\varphi(z,\varphi,0) U_{\varphi,kmn}(\varphi,z) + \dot{u}_3(z,\varphi,0) U_{3,kmn}(\varphi,z)\right] a \, dz d\varphi \qquad (4.134)$$

where $u_3(z,\varphi,0)$ and $u_\varphi(z,\varphi,0)$ are the initial displacements and $\dot{u}_3(z,\varphi,0)$ and $\dot{u}_\varphi(z,\varphi,0)$ are the initial velocities of any point of the shell centre surface in radial and tangential direction, respectively. In this case, the initial displacement is caused by the gravity or the roll self-weight and the initial velocity is zero.

Thus, the initial displacement corresponds to the static deflection caused by the self-weight. This can be obtained by reducing eq. (4.115) to the static situation and taking into account only the loading caused by gravity and substituting this equation into (4.113) and (4.114):

$$u_{\varphi,stat}(\varphi,z) = \sum_{k=1}^{2} \sum_{m=1}^{\infty} \sum_{n=0}^{\infty} \frac{F_{k,mn,G}}{k_{mn}} U_{\varphi,kmn}(\varphi,z) = u_\varphi(z,\varphi,0) \qquad (4.135)$$

$$u_{3,stat}(\varphi,z) = \sum_{k=1}^{2} \sum_{m=1}^{\infty} \sum_{n=0}^{\infty} \frac{F_{k,mn,G}}{k_{mn}} U_{3,kmn}(\varphi,z) = u_3(z,\varphi,0) \qquad (4.136)$$

With this approach one can find displacements u_φ and u_3 for any point on the centre surface of the shell whose position is defined by angle φ and position z at any time t as a response of excitation forces N and Q and the gravity load whose position and / or orientation is defined by angle φ^* and position z^* at any time t.

In general, in rotor dynamics [Genta 2005] a use of rotating coordinate frame that is attached to the rotor and rotates with the rotating speed of the roll finds great advantages. This approach is therefore used also in this study although it is not strictly necessary. Nevertheless, in case of including, e.g. imbalance of the roll, the use of the rotating frame would be advantageous.

So, the position of any point on the centre surface of the shell in an arbitrary cross-sectional plane at a distance $Z = z$ can be defined in the global fixed coordinate frame *XY* and also in the rotating coordinate frame *xy*, where the rotating coordinate frame *xy* rotates with a constant angular velocity $\dot{\theta}$ with respect to the fixed coordinate frame *XY* (see Figure 4.6).

Thus, by applying the rotation of the roll, one can obtain the response in both the stationary and the rotating coordinate system. Now, let us define the position φ^*, thus

$$\varphi^*(t) = -\theta(t) \tag{4.137}$$

Finally, the displacement u_φ and u_3 in the stationary coordinates, let us call them $u_{\varphi,stationar}$ and $u_{3,stationar}$, can be found as

$$u_{\varphi,stationar}(\varphi, z, t) = u_\varphi(\varphi - \theta, z, t) \tag{4.138}$$

$$u_{3,stationar}(\varphi, z, t) = u_3(\varphi - \theta, z, t) \tag{4.139}$$

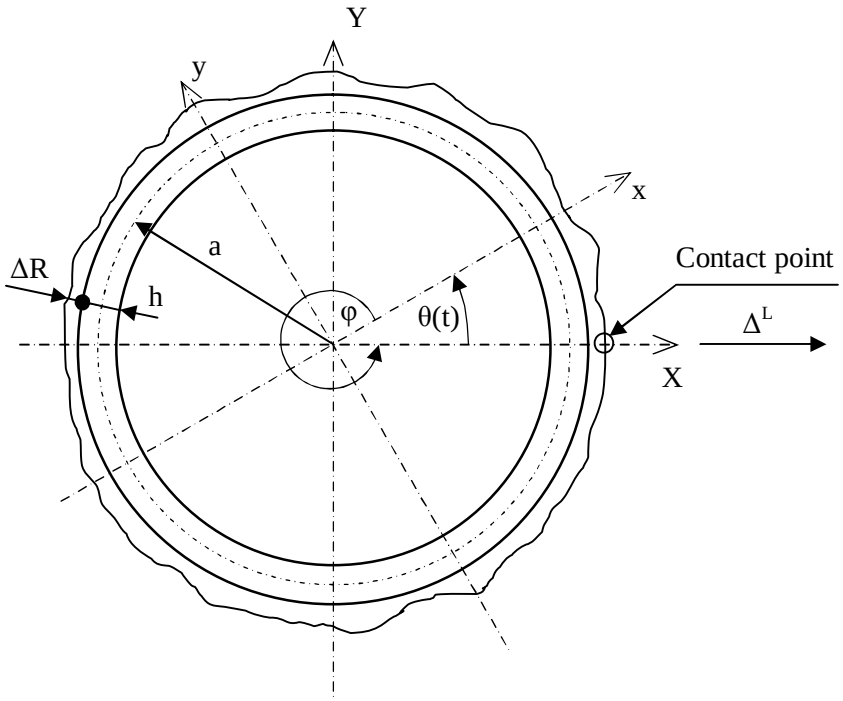

Figure 4.7: Shell dimensions and the contact point

Now, let us define the contact conditions. Let us take an assumption that the contact between the roll and the grindstone is always only on the level of the horizontal plane going through the *X* axes of the roll (see Figure 4.7) and that it is a point contact.

For this point of the roll, the radial $u_{3,stationar}(0,z,t)$ and tangential $u_{\varphi,stationar}(0,z,t)$ displacements in the stable coordinates and correspondingly the radial $u_3(-\theta(t),z,t)$ and tangential $u_\varphi(-\theta(t),z,t)$ displacements in the rotating coordinates can be found.

Now, the position of the contact point is defined as a summation of the displacement $u_3(\varphi,z,t) = u_3(-\theta(t),z,t)$ and the surface error $\Delta R(\varphi,z) = \Delta R(-\theta(t),z)$.

Thus,

$$\Delta^L = u_3(-\theta(t), z, t) + \Delta R(-\theta, z) \tag{4.140}$$

And by executing its time derivative the velocity in the radial direction is:

$$\dot{\Delta}^L = \dot{u}_3(-\theta(t), z, t) \tag{4.141}$$

Similarly, the tangential velocity of the contact point of the roll is defined:

$$\dot{\tau}_r^L = \dot{u}_\varphi(-\theta(t), z, t) + \dot{\theta}(t)\left(a + \frac{h}{2}\right) \tag{4.142}$$

Now let us derive the equation of motion for the torsional vibration of the roll. For sake of simplicity the free-body method is used here. The directions of the driving torques and loading forces and torques are apparent from Figure 4.8. If θ shows the positive direction of the angular position, *X* and *Y* the positive directions of the rectilinear positions, then T_r denotes the driving torque of the roll, M_μ the bearing friction torque, *G* the gravitational load (or self-weight) and *N* and *Q* the normal and tangential grinding force respectively.

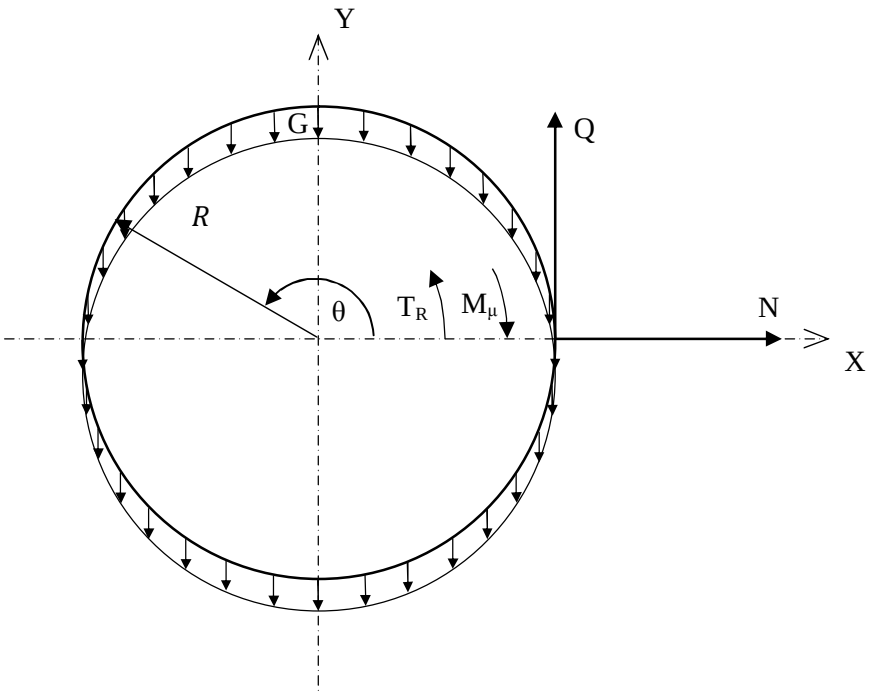

Figure 4.8: Loading acting on the roll including drive torque and bearing friction

The friction resistance of bearings M_μ can be written as

$$M_\mu = \frac{1}{2}\rho A g \mu_{fr} d \, sgn(\dot{\theta}) \tag{4.143}$$

where d is the diameter of the roll ending shaft and μ_{fr} is the friction coefficient. Then the equation of motion takes following form:

$$\rho I_z L \ddot{\theta} = T_R - M_\mu + QR \tag{4.144}$$

4.3 Euler-Bernoulli beam model

4.3.1 Equations of motion of an Euler-Bernoulli beam

The equations of motion of the Euler-Bernoulli beam can be derived directly from basic principles. Nevertheless, they can be derived also indirectly from the Love's equations for the circular cylindrical shell. In case of a beam it is set

$$N_{\varphi\varphi} = 0\ ,\ M_{\varphi\varphi} = 0,\ N_{\varphi z} = N_{z\varphi} = 0\ ,\ M_{\varphi z} = M_{z\varphi} = 0 \tag{4.145}$$

Thus, eqs. (4.6) and (4.8) become for non-rotating situation:

$$\frac{\partial N_{zz}}{\partial z} + q_z = \rho h \frac{\partial^2 u_z}{\partial t^2} \tag{4.146}$$

$$\frac{\partial^2 M_{zz}}{\partial z^2} + q_3 = \rho h \frac{\partial^2 u_3}{\partial t^2} \tag{4.147}$$

and eq. (4.7) vanishes. Also eqs. (4.12), (4.15), (4.26) and (4.27) reduce to

$$N_{zz} = K\varepsilon^{\circ}_{zz} \tag{4.148}$$

$$M_{zz} = Dk_{zz} \tag{4.149}$$

$$K = Eh \tag{4.150}$$

$$D = \frac{Eh^3}{12} \tag{4.151}$$

Substituting this into eqs. (4.146) and (4.147) and taking into account the cross-section geometry gives

$$EA\frac{\partial^2 u_z}{\partial z^2} + q_z^{'} = \rho A_R \frac{\partial^2 u_z}{\partial t^2} \tag{4.152}$$

$$-EI\frac{\partial^4 u_3}{\partial z^4} + q_3^{'} = \rho A_R \frac{\partial^2 u_3}{\partial t^2} \tag{4.153}$$

Here, I is the second moment of area and A_R the cross-sectional area of the beam. $q_z^{'}$ and $q_3^{'}$ are forces per unit length. The transverse vibration is described by the eq. (4.153). Eq. (4.152) describes the longitudinal vibrations and is not of interest in this work.

4.3.2 Natural frequencies and modes of a non-rotating beam

For the eigenvalue problem $q_3^{'} = 0$ in eq. (4.153). Similarly as in the case of the shell one can utilize eq. (4.30) and eq. (4.153) becomes

$$EI\frac{\partial^4 U_3}{\partial z^4} - \omega^2 \rho A_R U_3 = 0 \tag{4.154}$$

The boundary conditions of the circular cylindrical shell reduce only to eqs. (4.34), (4.36), (4.38), and (4.40) and the solution eq. (4.44) can be used by leaving out the circumferential term and it can be written as

$$U_3(z,\varphi) = C\, sin\frac{m\pi z}{L} \tag{4.155}$$

Now, if eq. (4.155) is substituted into eq. (4.154) and solved for ω, one obtains

$$\omega_m = \frac{\pi^2 m^2}{L^2}\sqrt{\frac{EI}{\rho A_R}} \tag{4.156}$$

ω_m is the natural frequency of the beam for m^{th} mode.

Eq. (4.155) is the mode shape of the transversely vibrating beam where C is an arbitrary constant.

4.3.3 Forced response

The Euler-Bernoulli beam theory assumes that in an arbitrary plane perpendicular to the centre line the distance between a centre line and an arbitrary point of the cross-section is constant at all times. Due to this fact the lateral vibration of a beam can be expressed as a displacement of any point of its centre line in its cross-sectional plane as a combination of two components, representing displacements in the directions of the main axes of its coordinate system (see Figure 4.6).

Therefore, the total displacement of the centreline can be obtained by a superposition of the lateral displacements U and V, in the fixed coordinates X and Y, and u and v, in the rotating coordinates x and y. And eq. (4.153) can be written for the two directions:

$$EI_y\frac{\partial^4 u(z,t)}{\partial z^4} + \rho A_R\frac{\partial^2 u(z,t)}{\partial t^2} = q_x' \tag{4.157}$$

$$EI_x\frac{\partial^4 v(z,t)}{\partial z^4} + \rho A_R\frac{\partial^2 v(z,t)}{\partial t^2} = q_y' \tag{4.158}$$

where for circular cross-section $I_y = I_x = I$. The relation between the displacements in rotating and stationary coordinate frame is

$$\begin{bmatrix} U(z,t) \\ V(z,t) \end{bmatrix} = \begin{bmatrix} cos\,\theta(t) & -sin\,\theta(t) \\ sin\,\theta(t) & cos\,\theta(t) \end{bmatrix} \begin{bmatrix} u(z,t) \\ v(z,t) \end{bmatrix} \tag{4.159}$$

Similarly as in the shell case, one can find the displacements in terms of modal expansion

$$u(z,t) = \sum_{m=1}^{\infty} \eta_m^u(t) U_{3,m}(z) \tag{4.160}$$

$$v(z,t) = \sum_{m=1}^{\infty} \eta_m^v(t) U_{3,m}(z) \tag{4.161}$$

And eq. (4.115) takes form

$$m_m \ddot{\eta}_m^u + c_m \dot{\eta}_m^u + k_m \eta_m^u = -F_{m,G}\, sin\,\theta + F_{m,N}\, cos\,\theta + F_{m,Q}\, sin\,\theta \tag{4.162}$$

$$m_m \ddot{\eta}_m^v + c_m \dot{\eta}_m^v + k_m \eta_m^v = -F_{m,G}\, cos\,\theta - F_{m,N}\, sin\,\theta + F_{m,Q}\, cos\,\theta \tag{4.163}$$

and where

$$m_m = \rho A_R N_m \tag{4.164}$$

$$c_m = 2\zeta \rho A_R \omega_{mn} N_m \tag{4.165}$$

$$k_m = \rho A_R \omega_{mn}^2 N_m \tag{4.166}$$

N_m is defined as

$$N_m = \int_0^L \left[U_{3,m}(z)^2\right] dz \tag{4.167}$$

$F_{m,G}$, $F_{m,N}$ and $F_{m,Q}$ are modal forces for the m^{th} mode and related to the gravitational (distributed) load G, the normal grinding force N and the tangential grinding force Q, respectively. The definitions of the modal forces are as follows:

$$F_{m,G} = \int_0^L G U_{3,m}(z) dz \tag{4.168}$$

$$F_{m,N} = \int_0^L [N(t)\delta(z - z^*)] U_{3,m}(z) dz = N(t) U_{3,m}(z^*) \tag{4.169}$$

$$F_{m,Q} = \int_0^L [Q(t)\delta(z - z^*)]U_{3,m}(z)dz = Q(t)U_{3,m}(z^*) \tag{4.170}$$

where *G* must be this time a distributed line load

$$G = \rho A_R g \tag{4.171}$$

The initial conditions for eqs. (4.162) and (4.163) are defined as:

$$\eta_m^u(0) = \int_0^L \left[u(z,0)U_{3,m}(z)\right] dz \tag{4.172}$$

$$\eta_m^v(0) = \int_0^L \left[v(z,0)U_{3,m}(z)\right] dz \tag{4.173}$$

and

$$\dot{\eta}_m^u(0) = \int_0^L \left[\dot{u}(z,0)U_{3,m}(z)\right] dz \tag{4.174}$$

$$\dot{\eta}_m^v(0) = \int_0^L \left[\dot{v}(z,0)U_{3,m}(z)\right] dz \tag{4.175}$$

Again, for this case the initial displacements *u(z,0)* and *v(z,0)* correspond to the static deflection caused by the gravity and the initial velocities $\dot{u}(z,0)$ and $\dot{v}(z,0)$ equal zero. Thus, *u(z,0)* and *v(z,0)* can be found by reducing eqs. (4.162) and (4.163) to the static situation and taking into account only the loading caused by gravity and substituting eq. (4.162) into (4.160) and (4.163) into (4.161) one obtains:

$$u_{stat}(z) = \sum_{i=1}^{\infty} \frac{-F_{m,G}\, sin\,\theta}{k_m} U_{3,m}(z) = u(z,0) \tag{4.176}$$

$$v_{stat}(z) = \sum_{i=1}^{\infty} \frac{-F_{m,G}\, cos\,\theta}{k_m} U_{3,m}(z) = v(z,0) \tag{4.177}$$

And again the contact conditions follow the same principles as in the case of the shell. Thus

$$\Delta^E(z,t) = u(z,t)\cos\theta - v(z,t)\sin\theta + \Delta R(z,-\theta) \tag{4.178}$$

and its time derivative

$$\dot{\Delta}^E(z,t) = \dot{u}(z,t)\cos\theta - \dot{v}(z,t)\sin\theta \tag{4.179}$$

In a similar manner one can define also the tangential velocity of the contact point on the roll:

$$\dot{\tau}_r^E(z,t) = \dot{u}(z,t)\sin\theta + \dot{v}(z,t)\cos\theta + \dot{\theta}\left(a + \frac{h}{2}\right) \tag{4.180}$$

Equation for the torsional vibration eq. (4.144) remains unchanged.

4.4 Grinding stone subsystem

The grinding wheel subsystem is defined by the angular position of the drive σ and the deviation in the angular position $\Delta\sigma$, which is caused by the flexibility of the transmission belt (see Figure 4.9).

In order to find the equations of motion, one can apply the power equilibrium method. First, the kinetic energy of the stone subsystem is defined:

$$K_S = \frac{1}{2}J_d\dot{\sigma}^2 + \frac{1}{2}J_s\left(\kappa\dot{\sigma} + \dot{\Delta\sigma}\right)^2 \tag{4.181}$$

where J_d and J_s are the mass moment of inertia of the stone drive and the stone, respectively and κ is the transmission ratio. The strain energy can be written as:

$$E_S = 2\frac{1}{2}k_b(r_s\Delta\sigma)^2 \tag{4.182}$$

where k_b is the stiffness of the transmission belt and r_s is the radius of the grindstone sheave. The power relation can be found:

$$P_S = T_S\dot{\sigma} + Qr\left(\kappa\dot{\sigma} + \dot{\Delta\sigma}\right) \tag{4.183}$$

where T_S is torque of the stone drive and r is radius of the grindstone.

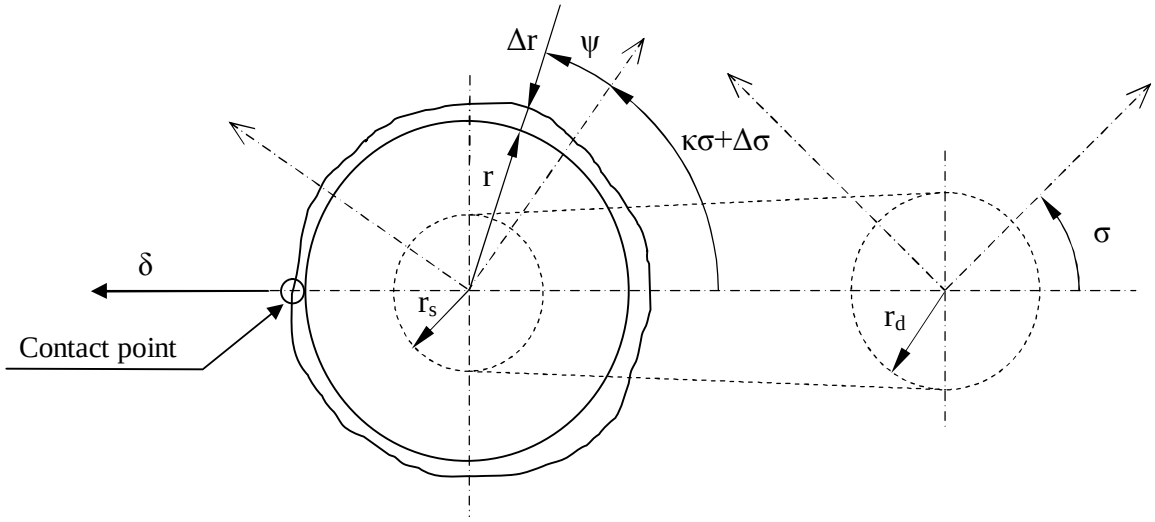

Figure 4.9: Grinding wheel subsystems

Now, the substitution into the relation for power equilibrium is carried out:

$$\frac{d}{dt}(K_S + E_S) = P_S \tag{4.184}$$

Finally, the equations of motion for the torsional vibration of the grinding wheel subsystem are obtained:

$$(J_d + \kappa^2 J_s)\ddot{\sigma} + \kappa J_s \Delta\ddot{\sigma} = T_S + Qr\kappa \tag{4.185}$$

$$\kappa J_s \ddot{\sigma} + J_s \Delta\ddot{\sigma} + 2k_b r_s^2 \Delta\sigma = Qr \tag{4.186}$$

Now, let us derive the horizontal displacement of the contact point of the grinding stone:

$$\delta = \Delta r\big(\pi - (\kappa\sigma + \Delta\sigma)\big) + x_s \tag{4.187}$$

where $\Delta r(\psi)$ is surface error of the grindstone as a function of its angular position. Thus, for the contact $\Delta r = \Delta r(\pi-(\kappa\sigma+\Delta\sigma))$. x_s is the nominal infeed of the stone. The tangential velocity of the stone is then:

$$\dot{\tau}_s = r\big(\kappa\dot{\sigma} + \dot{\Delta\sigma}\big) \tag{4.188}$$

4.5 Grinding forces

The contact between the grindstone and the roll appears to be a surface, in an ideal case a line contact. Nevertheless, in modelling of cutting forces the line contact is often simplified to a point contact [Altintas 2000, Keskinen 1999]. This is also the case of this analysis.

The grinding forces are considered as contact forces N and Q between the roll and the grinding stone, where N denotes the normal and Q the tangential force (see Figure 4.10[1]). The forces are derived based on the classic wear theory [Altintas 2000, Keskinen 1999], i.e. the cutting forces are dependent on the chip thickness x_s, feed speed $\dot{z}_s$, the relative cutting speed $\dot{\tau}$ and the depth of penetration ε. The direction of acting the cutting forces on both the roll and the grindstone is depicted in Figure 4.10.

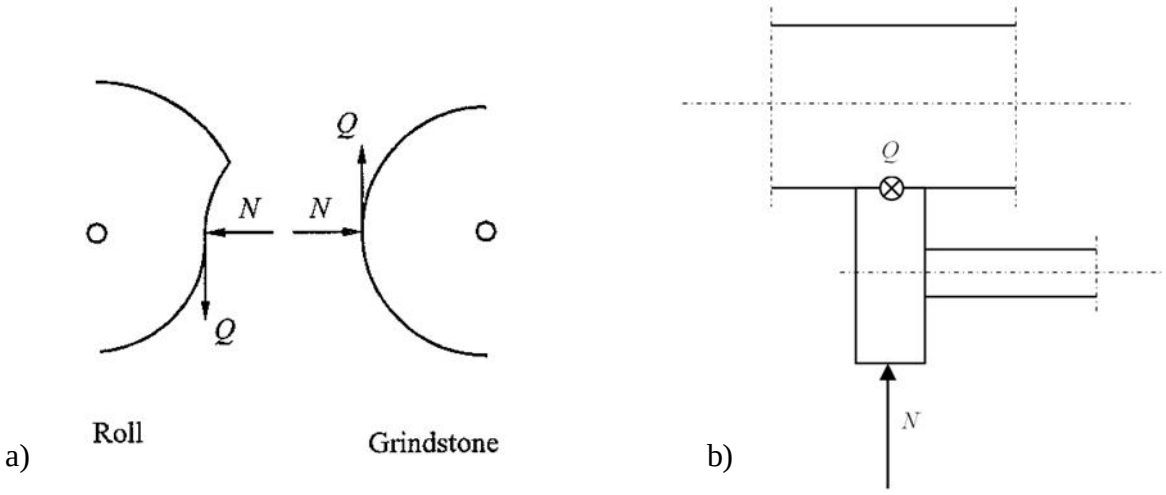

Figure 4.10: Acting of grinding forces

The total penetration of the stone into the roll surface is defined slightly differently for the two different theories (Euler-Bernoulli and shell theory). Thus, the total penetration related to Love's equations ε^L is defined as:

$$\varepsilon^L = \Delta^L + \delta \tag{4.189}$$

[1] Figure 4.10 shows the actual direction of the forces without using any coordinate system, while earlier in the text the direction of the forces was chosen in the positive direction of axes X and Y for derivation of the equations of motion. That is why the resulting forces will have negative values.

which means

$$\varepsilon^L = u_3(-\theta(t), z, t) + \Delta R(-\theta(t), z) + \Delta r\big(\pi - (\kappa\sigma + \Delta\sigma)\big) + x_s \tag{4.190}$$

and the total penetration related to Euler-Bernoulli beam theory ε^E reads:

$$\varepsilon^E = \Delta^E + \delta \tag{4.191}$$

which can be written

$$\varepsilon^E = u(t,z)cos\,\theta - v(t,z)sin\,\theta + \Delta R(-\theta(t), z) + \Delta r\big(\pi - (\kappa\sigma + \Delta\sigma)\big) + x_s \tag{4.192}$$

In the following, only symbol ε is used for the total penetration and it means ε^L in case of using the shell model and ε^E in case of using the Euler-Bernoulli model. The expressions for the cutting forces are formulated as:

$$N = \frac{w\dot{\tau}_r}{k_w(\dot{\tau}_r + \dot{\tau}_s)}[\varepsilon(t) - \alpha\beta\varepsilon(t-\tau)] \tag{4.193}$$

$$Q = c_e k_w N \tag{4.194}$$

where

$$\tau = \frac{2\pi}{\dot{\theta}} \tag{4.195}$$

In equation (4.193), the penetration ε is a function of time, where the term τ is the delay constant and it equals time of one revolution of the roll, α and β are delay control parameters, c_e is the specific energy consumption factor, k_w is wear factor and w is the width of the stone.

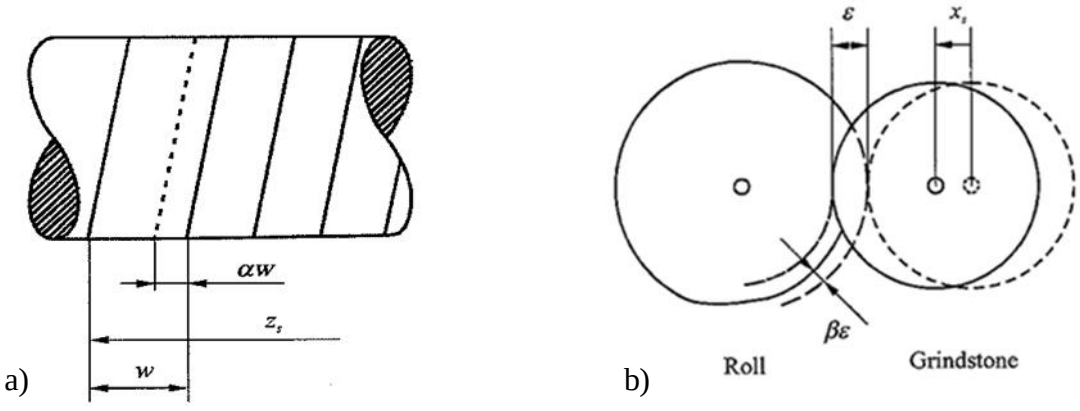

Figure 4.11: Over-lapping and recovering contact elasticity [Keskinen 1999]

In the grinding process and its stability the time delay phenomenon plays a crucial role. The delay control parameter α expresses the overlapping in grinding, i.e. a situation when the grinding stone enters a zone on the roll surfaces that has already been ground (see Figure 4.11 a)). The parameter α can reach values *(0, 1)* where *0* means no overlapping. Intuitively, the parameter α is dependent on the stone axial feed velocity $\dot{z}_s$, the rotational speed of the roll $\dot{\theta}$ and the stone width *w*. Thus one can write:

$$\alpha = 1 - \frac{2\pi \dot{z}_s}{\dot{\theta} w} \tag{4.196}$$

The grinding parameters are typically set in such a way that α usually reaches values close to *0.1*.

The other delay control parameter β describes the contact elasticity between the roll and the stone (see Figure 4.11 b)). As a result the actual depth of cut never reaches the nominal total penetration. The parameter β is also called a reduction parameter [Yuan 2002] and it reduces the penetration by a factor *(0, 1)*, where for steels β corresponds to value *0.9*.

Another significant factor in roll grinding is the shape error (or the out-of-roundness) of both the roll and the grindstone. It has been observed by measurements [Järvinen 1998, Yuan 2002] that the frequency of the periodic shape error is related to the first natural frequency of the system ω_n. Based on this knowledge the roll shape error can be modelled as:

$$\Delta R(z, \varphi) = E_1 sin\,(\iota \dot{\theta} t) \tag{4.197}$$

where E_1 is the amplitude of the out-of-roundness and ι is the number of waves on the surface of the roll. And in that case ι satisfies the relationship:

$$\iota = \frac{\omega_n}{\dot{\theta}} \tag{4.198}$$

The shape error of the stone can take various forms. It can be random, eccentric, oval, triangular, rectangular etc. For simulations, the symmetric and antisymetric shapes are easy to model:

$$\Delta r(z, \psi) = E_2\, cos(\kappa\sigma) + E_3\, cos(2\kappa\sigma) + E_4\, cos(3\kappa\sigma) + \cdots \tag{4.199}$$

where the terms $\Delta\sigma$ are neglected, E_2, E_3, E_4, ... are the amplitudes of the shape errors of the stone and the first term corresponds to the eccentric shape, the second term corresponds to the oval shape etc. One can also form their combinations as in eq. (4.199).

4.6 Drive models

Older machine tools as, e.g., a roll grinder being analyzed here are usually driven by DC motors. DC drives can be modelled by simple linear models [Keskinen 1999]. In grinding, it is advisable to run the process under constant speed conditions, i.e. by reaching a desirable rotational speed and keep it there in some acceptable range. So, in DC motors the driving torque will be controlled in such a way that the speed will be near the desired one although the amplitudes of the loading forces (torques) are changing.

If PD control is applied the torque of the roll drive gets expression [Dutton 1997]

$$T_R = K_P^r\left(\dot{\theta}_d t - \theta\right) + K_D^r\left(\dot{\theta}_d - \dot{\theta}\right) \tag{4.200}$$

in which $\dot{\theta}_d$ is the desired value of the roll speed and K_P^r and K_D^r are the gains of position and speed errors. Similarly, the torque of the grinding stone drive is given by

$$T_S = K_P^s(\dot{\sigma}_d t - \sigma) + K_D^s(\dot{\sigma}_d - \dot{\sigma}) \tag{4.201}$$

where $\dot{\sigma}_d$ is the desired value of the grindstone (if the variation $\Delta\dot{\sigma}$ is neglected), corresponding to the desired tangential speed in grinding zone:

$$\dot{\tau}_d = R\dot{\theta}_d + r\kappa\dot{\sigma}_d \tag{4.202}$$

5. Numerical solution

This chapter deals with the numerical solution of the equations defining the grinding system introduced in chapter 4. Several numerical methods for solving ordinary and delay differential equations are qualitatively compared.

5.1 Governing equations

The grinding system was described mathematically in chapter 4. The model was developed in two ways. In the first case, the roll was modelled as a thin shell, in the second case as an elastic beam. The system is governed by following sets of differential equations for the two cases (in rotating coordinates):

Shell:

$$m_{k,mn}\ddot{\eta}_{k,mn} + c_{k,mn}\dot{\eta}_{k,mn} + k_{k,mn}\eta_{k,mn} = F_{k,mn,C} + F_{k,mn,G} \tag{5.1a}$$

$$\rho I_z L\ddot{\theta} = T_R - M_\mu + QR \tag{5.1b}$$

$$(J_d + \kappa^2 J_s)\ddot{\sigma} + \kappa J_s \Delta\ddot{\sigma} = T_S + Qr\kappa \tag{5.1c}$$

$$\kappa J_s \ddot{\sigma} + J_s \Delta\ddot{\sigma} + 2kr_s^2 \Delta\sigma = Qr \tag{5.1d}$$

with

$$u_\varphi(\varphi, z, t) = \sum_{k=1}^{2}\sum_{m=1}^{\infty}\sum_{n=0}^{\infty} \eta_{k,mn}(t) U_{\varphi,kmn}(\varphi, z) \tag{5.1e}$$

$$u_3(\varphi, z, t) = \sum_{k=1}^{2}\sum_{m=1}^{\infty}\sum_{n=0}^{\infty} \eta_{k,mn}(t) U_{3,kmn}(\varphi, z) \tag{5.1f}$$

Beam:

$$m_m\ddot{\eta}_m^u + c_m\dot{\eta}_m^u + k_m\eta_m^u = -F_{m,G}\sin\theta + F_{m,N}\cos\theta + F_{m,Q}\sin\theta \tag{5.2a}$$

$$m_m\ddot{\eta}_m^u + c_m\dot{\eta}_m^u + k_m\eta_m^u = -F_{m,G}\cos\theta - F_{m,N}\sin\theta + F_{m,Q}\cos\theta \tag{5.2b}$$

$$\rho I_z L\ddot{\theta} = T_R - M_\mu + QR \tag{5.2c}$$

$$(J_d + \kappa^2 J_s)\ddot{\sigma} + \kappa J_s \Delta\ddot{\sigma} = T_S + Qr\kappa \tag{5.2d}$$

$$\kappa J_s \ddot{\sigma} + J_s \Delta\ddot{\sigma} + 2kr_s^2 \Delta\sigma = Qr \tag{5.2e}$$

with

$$u(z,t) = \sum_{m=1}^{\infty} \eta_m^u(t) U_{3,m}(z) \tag{5.2f}$$

$$v(z,t) = \sum_{m=1}^{\infty} \eta_m^v(t) U_{3,m}(z) \tag{5.2g}$$

In both cases, excitation terms $F_{k,mn,C}$, $F_{m,N}$ and $F_{m,Q}$ contain the time delay term that raises these two sets of differential equations to sets of delay differential equations.

The concept of use of the rotating frame that rotates with the rotor can be also seen as an inverse problem to a rotating rotor subjected to stationary forces, i.e. as a stationary rotor subjected to rotating forces. In case of this model, the use of a non-rotating frame turns out to be more suitable.

In this analysis, grinding in the middle area of the roll is assumed. Therefore, only first bending (beam) mode is used ($m = 1$). Emphasis is put on the accuracy of the circumferential displacements. Therefore, the first *6* ring modes are used ($n = 0, 1, 2, 3, 4, 5$). Thus, for the case of a roll as a shell one obtains a system of *15* degrees of freedom (DOF), for the case of a roll as a beam one obtains a system of *5* DOF.

5.2 Numerical methods

In general, an ordinary differential equation can be written as:

$$\boldsymbol{y}'(t) = \boldsymbol{f}(t, \boldsymbol{y}(t)) \tag{5.3}$$

that is solved on $a \leq t \leq b$ with initial values defined as

$$\boldsymbol{y}(a) = \boldsymbol{y_a} \tag{5.4}$$

Whereas the delay differential equation with one constant delay can be written as:

$$\boldsymbol{y}'(t) = \boldsymbol{f}(t, \boldsymbol{y}(t), \boldsymbol{y}(t-\tau)) \tag{5.5}$$

that is solved on $a \leq t \leq b$ with a given history

$$\boldsymbol{y}(t) = \boldsymbol{S}(t) \qquad for\ t \leq a \tag{5.6}$$

One can see that the difference between ODE and DDE is that the initial state of ODE is defined by a constant while in case of DDE the value of the solution at the initial point is not enough and the whole history, the solution ***S(t)*** at times prior to the initial point, is needed. Usually the problem is to determine the history ***S(t)***.

However, in the studied case, the delay effect starts to act exactly after one revolution of the roll when the grindstone enters the zone that has already been ground, which equals the time of the delay. That is, if the process starts at $t = t_0$, during the first revolution of the roll, the normal grinding force is

$$N = \frac{w\dot{t}_r}{k_w(\dot{t}_r+\dot{t}_s)}\varepsilon(t) \qquad for\ t_0 \leq t < \tau \tag{5.7}$$

which means that the differential equation can be viewed as ODE on $t_0 \leq t < \tau$ with initial conditions of the roll being in rest. Its solution in terms of eqs. (5.3) and (5.4), ***y(t)***, can be used as the history of DDE in terms of eqs. (5.5) and (5.6), ***S(t)***. And also after the first revolution of the roll the normal grinding force is

$$N = \frac{w\dot{t}_r}{k_w(\dot{t}_r+\dot{t}_s)}[\varepsilon(t) - \alpha\beta\varepsilon(t-\tau)] \qquad for\ \tau \leq t \leq b \tag{5.8}$$

which corresponds to DDE.

In this case, both the ODE and DDE can be solved by employing integration over the whole time of the simulation. Available methods for solving initial value problems of differential equations can be divided into two groups: so called one-step methods and methods with memory [Shampine 2003]. To the first group of methods belong the following methods that have been tested: Euler's method, Euler's first improved method, Heun's method (or also called Euler's second improved method or Euler-Cauchy method) and classical Runge-Kutta method. All the mentioned methods are explicit. To the second group of methods belongs the Euler's second improved method with an iterative process (or also Trapezoidal method using predictor-corrector procedure), which is an implicit method.

The basic formulas for these methods can be found in every textbook on numerical methods [Eldén 2004, Shampine 2003, Kopchenova 1981]. Nevertheless, for clear comparison, the formulas of these methods are listed below.

Euler's method:

$$y_{i+1} = y_i + hf(x_i, y_i) \tag{5.9}$$

Euler's first improved method:

$$y_{i+1} = y_i + hf\left(x_{i+1/2}, y_{i+1/2}\right) \tag{5.10a}$$

$$x_{i+1/2} = x_i + \frac{h}{2} \tag{5.10b}$$

$$y_{i+1/2} = y_i + \frac{h}{2} f(x_i, y_i) \tag{5.10c}$$

Heun's method:

$$y_{i+1} = y_i + \frac{h}{2}(\kappa_1 + \kappa_2) \tag{5.11a}$$

$$\kappa_1 = f(x_i, y_i) \tag{5.11b}$$

$$\kappa_2 = f(x_i + h, y_i + h\kappa_1) \tag{5.11c}$$

Trapezoidal method:

$$y_{i+1} = y_i + \frac{h}{2}\left(f(x_i, y_i) + f(x_{i+1}, y_{i+1})\right) \tag{5.12a}$$

predictor-corrector procedure:

$$y_{i+1}^{[0]} = y_i + hf(x_i, y_i) \tag{5.12b}$$

$$y_{i+1}^{[k+1]} = y_i + \frac{h}{2}\left(f(x_i, y_i) + f\left(x_{i+1}, y_{i+1}^{[k]}\right)\right) \tag{5.12c}$$

Classical Runge-Kutta method:

$$y_{i+1} = y_i + \frac{h}{6}(\kappa_1 + 2\kappa_2 + 2\kappa_3 + \kappa_4) \tag{5.13a}$$

$$\kappa_1 = f(x_i, y_i) \tag{5.13b}$$

$$\kappa_2 = f\left(x_i + \frac{h}{2}, y_i + \frac{h}{2}\kappa_1\right) \tag{5.13c}$$

$$\kappa_3 = f\left(x_i + \frac{h}{2}, y_i + \frac{h}{2}\kappa_2\right) \tag{5.13d}$$

$$\kappa_4 = f(x_i + h, y_i + h\kappa_3) \tag{5.13e}$$

All of these methods could be used for this problem. However, the methods differ in their accuracy and speed of convergence. A numerical test has been carried out in order to compare the performance of the above mentioned methods. Tables 5.1 and 5.2 show results for two simple ODEs: $y' = x + 2y$, *y(0)* = 0 and $y' = y - 2x/y$, *y(0) = 1*, respectively. The values of the exact solutions are compared with the results gained by the particular methods with their time costs (by taking average value of Matlab functions tic-toc). The integration step has been chosen *h = 0.2* and the integration has been carried out on the interval $\langle 0,1 \rangle$.

Table 5.1: Solution of $y' = x + 2y$, *y(0) = 0 on* $x \in \langle 0,1 \rangle$, *h = 0.2*

x	***0.2***	***0.4***	***0.6***	***0.8***	***1***	**time [ms]**
Exact solution	*0.0230*	*0.1064*	*0.2800*	*0.5883*	*1.0973*	
Euler's method	*0.0000*	*0.0400*	*0.1360*	*0.3104*	*0.5946*	*2.0*
Euler's first improved method	*0.0200*	*0.0976*	*0.2605*	*0.5495*	*1.0252*	*2.2*
Heun's method	*0.0200*	*0.0976*	*0.2605*	*0.5495*	*1.0252*	*2.2*
Trapezoidal method (6 iterations)	*0.0250*	*0.1125*	*0.2937*	*0.6155*	*1.1483*	*3.5*
Trapezoidal method (1 iteration)	*0.0200*	*0.0976*	*0.2604*	*0.5495*	*1.0252*	*3.0*
Classical Runge-Kutta	*0.0229*	*0.1063*	*0.2799*	*0.5880*	*1.0967*	*2.8*

Table 5.2: Solution of $y' = y - 2x/y$, $y(0) = 1$ on $x \in \langle 0,1 \rangle$, $h = 0.2$

x	***0.2***	***0.4***	***0.6***	***0.8***	***1***	**time [ms]**
Exact solution	*1.1832*	*1.3416*	*1.4832*	*1.6124*	*1.7320*	
Euler's method	*1.2000*	*1.3733*	*1.5315*	*1.6811*	*1.8269*	*2.0*
Euler's first improved method	*1.1836*	*1.3427*	*1.4850*	*1.6152*	*1.7362*	*2.2*
Heun's method	*1.1867*	*1.3483*	*1.4937*	*1.6279*	*1.7542*	*2.2*
Trapezoidal method (6 iterations)	*1.1847*	*1.3443*	*1.4873*	*1.6183*	*1.7404*	*3.5*
Trapezoidal method (1 iteration)	*1.1867*	*1.3483*	*1.4937*	*1.6279*	*1.7542*	*3.0*
Classical Runge-Kutta	*1.1832*	*1.3417*	*1.4833*	*1.6125*	*1.7321*	*2.8*

Based on this analysis, one could say that Euler's method is fast but the accuracy is low. For increasing the accuracy the integration step *h* would have to be shortened, which would slow down the process. Euler's first improved method gives good accuracy and is rather fast. The Heun's method is still simple and so rather fast but the accuracy is lower than in the former case. The trapezoidal method with the predictor-corrector procedure has the advantage that the accuracy can be set by controlling the iteration procedure. On the other hand, for higher accuracy, more iterative steps are needed and the time costs increase. And finally the classical Runge-Kutta method provides excellent accuracy, but it is slower because of multiple evaluation of the function *f*. Of course, one could argue that with this method one could use longer integration steps and so shorten the computational time.

It should be noted that this analysis does not necessarily select the most efficient integration method for the main model, for the effectiveness of these methods is specific to the nature of the differential equation. Nevertheless, this simple analysis is giving an overview of some available methods and their performance for two specific differential equations.

Nonetheless, the Euler's first improved method was selected. The method uses constant steps for easier determination of the delay terms in the DDE.

As an alternative to these methods, predefined solvers in MATLAB® are available. Basically any of the ode solvers (ode23, ode45, ode113, ode15s, ode23s, ode23t, ode23tb) can be used by a special treatment of the delay terms. MATLAB® provides also dde23 solver for DDE with constant delay. These methods were also tested and gave the same result as the non-commercial solvers mentioned above.

6. System response

In this chapter numerical results of equations introduced in chapters 4 and 5 describing the dynamic grinding system are presented and discussed. The system parameters listed in Table 6.1 are used in the simulation, if not said otherwise. First, the effect of the self-weight and its negligibility in this study is discussed. Then, the origin of the roll waviness and its relation to the natural frequency of the system is studied. Finally, the time domain response of the system is obtained for three cases corresponding to different wall thicknesses.

Table 6.1: System parameters

System parameters	
Roll	
Length	$L = 7.15\ m$
Radius	$R = 0.2235\ m$
Wall thickness	$h = 10\ mm;\ 5\ mm;\ 2.5\ mm$
Young's modulus	$E = 200\ GPa$
Density	$\rho = 7874\ kg/m^3$
Damping ratio	$\zeta = 0.025$
Angular velocity	$\dot{\theta} = -1.05\ rad/s$
Grinding stone	
Width	$w = 0.08\ m$
Radius	$r = 0.25\ m$
Mass moment of inertia	$J_s = 1.2\ kgm^2$
Grinding stone drive	
Mass moment of inertia	$J_d = 1\ kgm^2$
Angular velocity	$\dot{\sigma} = 62.8\ rad/s$
Belt stiffness	$k = 155\ kN/m$
Transmission ratio	$\kappa = 1$
Process	
Specific wear factor	$k_w = 1.168x10^{-10}\ m^2/N$
Specific energy consumption	$c_e = 8.5616x10^9\ N/m^2$
Reduction parameter	$\beta = 0.9$
Radial feed	$x_s = 50\ \mu m$
Axial feeding velocity	$\dot{z}_s = 0.0105\ m/s$

6.1 Gravity effect

The effect of self-weight is very often left out in dynamic analyses. The reason for that is that the self-weight loading represents only a static load that does not contribute to the dynamic response. Of course, it can always be included in the dynamic analysis as presented in chapter 4. Then, one can use zero initial conditions, which would cause a drop of the roll and damped free vibrations at the beginning of the simulation. To avoid this, one can apply the initial conditions that equal the static deflection for the initial displacement and null for the initial velocity. In both cases, one obtains the absolute displacement of the roll with respect to the global coordinate frame fixed in the boundary of the roll. This could seem to be a "good" interpretation of the response, however, due to the fact that the static displacement is typically by one or more orders greater than the dynamic displacement, it is convenient in dynamic analysis to either leave out the gravity load or study the vibration about the static equilibrium position. The former has been chosen in this work.

Nevertheless, in case of thin-walled rolls and use of the shell theory, it is desirable to study also the effect of the gravity load on the static response. The shape of the cross-section in particular is of interest. This section is devoted to this problem.

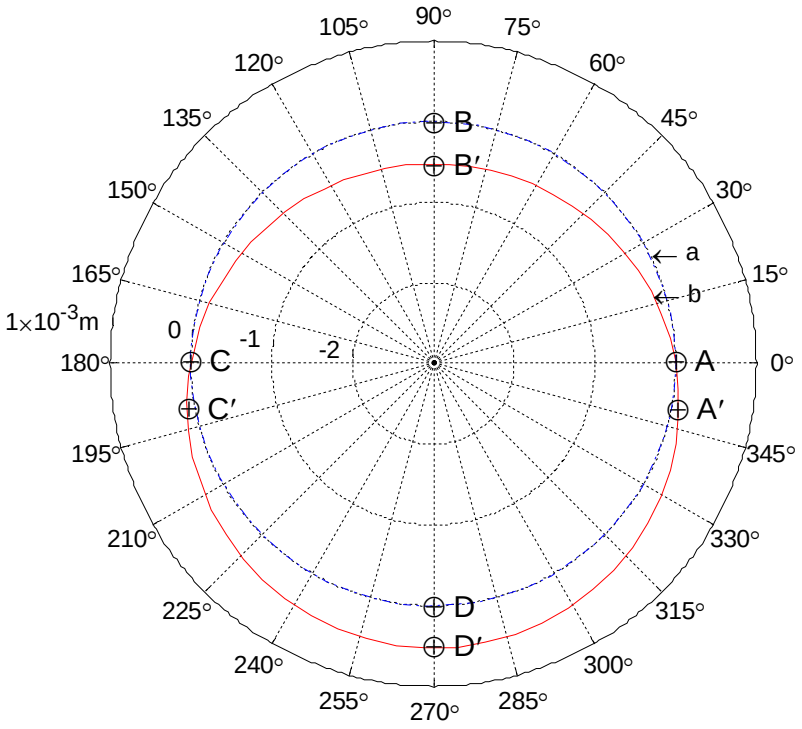

Figure 6.1: Static deflection caused by the gravity load;
a: zero loading, b: gravity loading

The static radial $u_{3,stat}(\varphi, z)$ and tangential $u_{\varphi,stat}(\varphi, z)$ displacement can be obtained by utilizing equations (4.135) and (4.136). If these equations are applied exploiting roll parameters given in Table 6.1, selecting the wall thickness *h = 2.5 mm* and applying the gravity load, one obtains the shape of the roll cross-section in axial position *z = 3 m*, which is presented in Figure 6.1. In this case one beam mode *m = 1* and *6* circumferential modes n_{max} *= 5* have been used. If one concentrates on selected points *A, B, C* and *D* on the unloaded cross-section and their deflected positions on the deformed cross-section named *A', B', C'* and *D'*, one can notice that the shape is neither circular nor elliptic. The exact values of these points are tabulated in Table 6.2 for three different wall thicknesses: *h = 10 mm*, *5 mm* and *2.5 mm*. From the computed values it is apparent that the points *A* and *C* experience larger displacement than points *B* and *D*. The reason for that can be viewed in the load distribution. If it is assumed that the mass of each point of the circular cylindrical shell acts in the direction of the gravity acceleration, it can be agreed that the mass density is higher in the neighbourhood of the side horizontal lines of the roll (going through points *A* and *C*). As a consequence, the load is higher in these areas and therefore the displacement is larger too.

Table 6.2: Displacement caused by the gravity load, Love's equations

h [mm]	**10**	**5**	**2.5**
A'($u_{3,stat}$, $u_{\varphi,stat}$) [mm]	(0, -0.5430)	(0, -0.5341)	(0, -0.5289)
B'($u_{3,stat}$, $u_{\varphi,stat}$) [mm]	(-0.5415, 0)	(-0.5326, 0)	(-0.5275, 0)
C'($u_{3,stat}$, $u_{\varphi,stat}$) [mm]	(0, 0.5430)	(0, 0.5341)	(0, 0.5289)
D'($u_{3,stat}$, $u_{\varphi,stat}$) [mm]	(0.5415, 0)	(0.5326, 0)	(0.5275, 0)

Table 6.3: Displacement caused by the gravity load, beam theory

h [mm]	**10**	**5**	**2.5**
S'(V_{stat}) [mm]	(-0.5347)	(-0.5229)	(-0.5171)

A comparison with Euler-Bernoulli beam theory can be obtained by utilizing equation (4.177) that defines static displacement of the roll centre line in rotating coordinates v_{stat}. After transforming v_{stat} into non-rotating coordinate frame, one gets static displacement V_{stat} of point *S* on the centre line, which is displaced by the gravity to the point *S'*. Similarly as in the previous case the value

corresponds to the axial position $z = 3\ m$ on the roll and one beam mode has been used $m = 1$. The values of the calculated static displacements for the beam theory are tabulated in Table 6.3. One can notice that the values are slightly higher for the shell model. In particular, the difference is for thickness $h = 2.5\ mm$ ca. *2.1 %*, for $h = 5\ mm$ ca. *2.0 %* and for $h = 10\ mm$ ca. *1.4 %*. It also indicates that for larger thicknesses both models yield similar values. The difference is caused by the membrane stiffness that allows for higher flexibility of the roll in case of the shell model.

6.2 Roll surface waviness

The surface waviness represents as a matter of fact the excitation mechanism causing the self-excited or chatter vibration. It has been discussed in the previous chapters that this type of waviness is caused by the relative movement between the work-piece and the tool. This is a very commonly used statement in many research works and it is considered to be a fact. But what does actually form the waves? If an ideally round roll and an ideally round grinding stone is assumed and the cutting conditions at the beginning of the roll are applied, the response in the time domain will look very steady – no vibrations! The plots of the tangential grinding force, chip thickness, the radial and tangential displacement of the contact point using the shell theory, for the wall thickness $h = 5\ mm$, are depicted in Figure 6.2 and Figure 6.3.

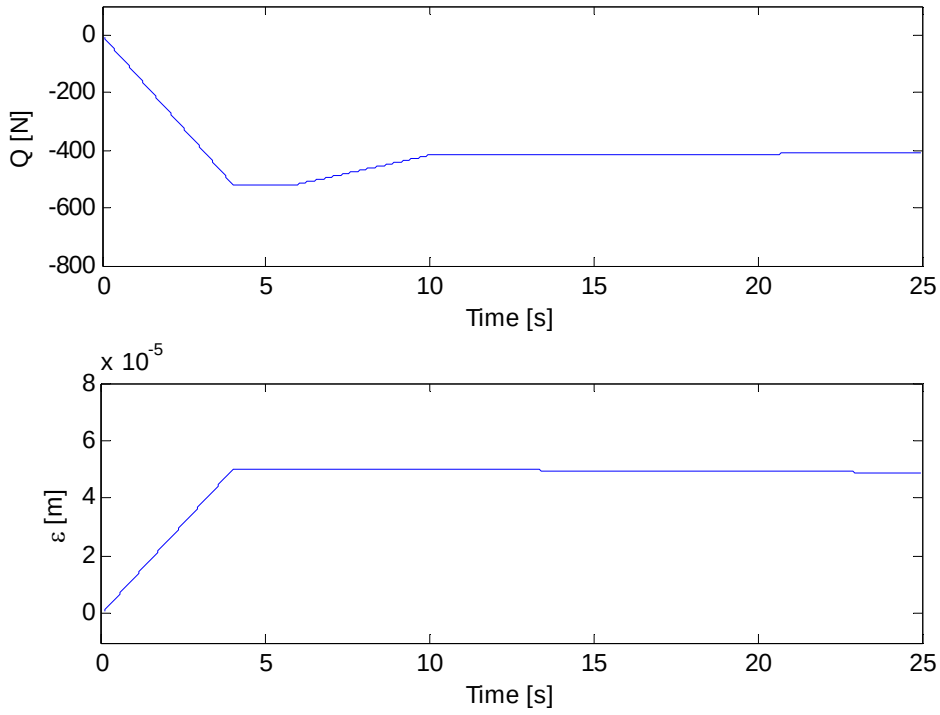

Figure 6.2: Ideally round roll: tangential grinding force and chip thickness

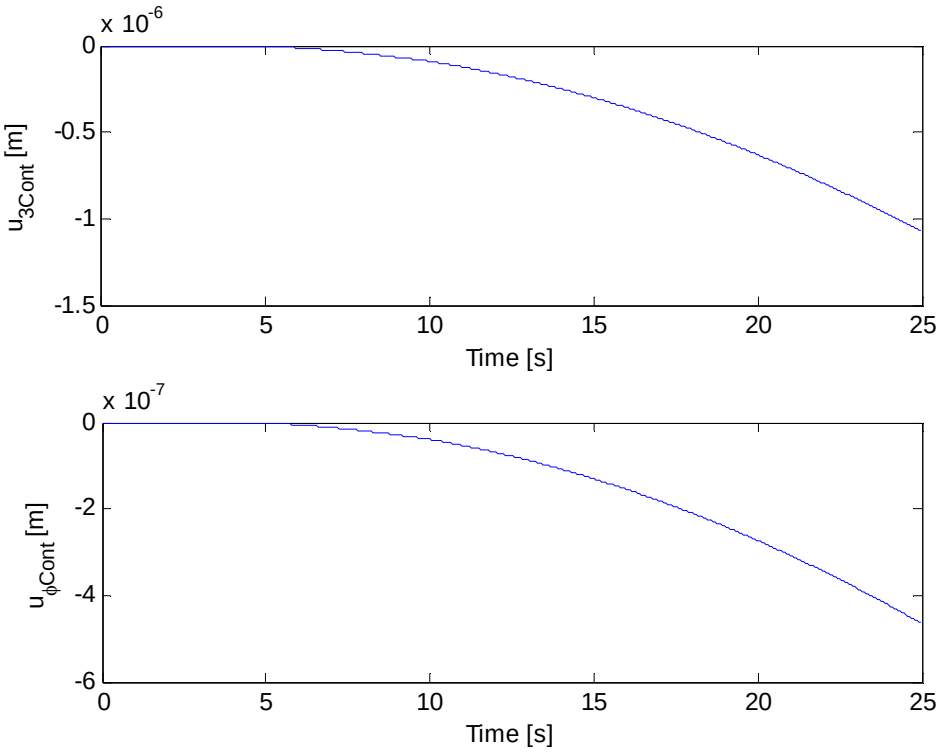

Figure 6.3: Ideally round roll: radial and tangential displacement of the contact point

One of the very few sources that mention the origin of the waviness is [Tlustý 1980], which only says that „the waviness is produced by externally excited vibrations". In practice, it could mean irregularities in the surface profile caused by the weld joint, surface quality errors, the first contact of the grindstone with the roll, which creates a small impact etc. Now, let us assume that the roll is not ideally round. One can simulate this e.g., as random sudden changes in the roll surface. As a matter of fact, these "surface errors" create free vibrations that make the roll vibrate with the natural frequency of the system and so it forms the waves on the surface of the roll related to this frequency. The plots of the tangential grinding force, chip thickness, the radial and tangential displacement of the contact point using the shell theory are depicted in Figure 6.4 and Figure 6.5. This time there are three sudden changes in the roll surface, in the plot visible at time $t = 5\ s$, *13 s* and *16 s*. The secondary effect of the time delay is also visible. In this case the delay $\tau = 6\ s$. If one takes Fast Fourier Transform (FFT) of the power history for this case, Figure 6.6 can be obtained. This figure clearly shows the natural frequency of the system.

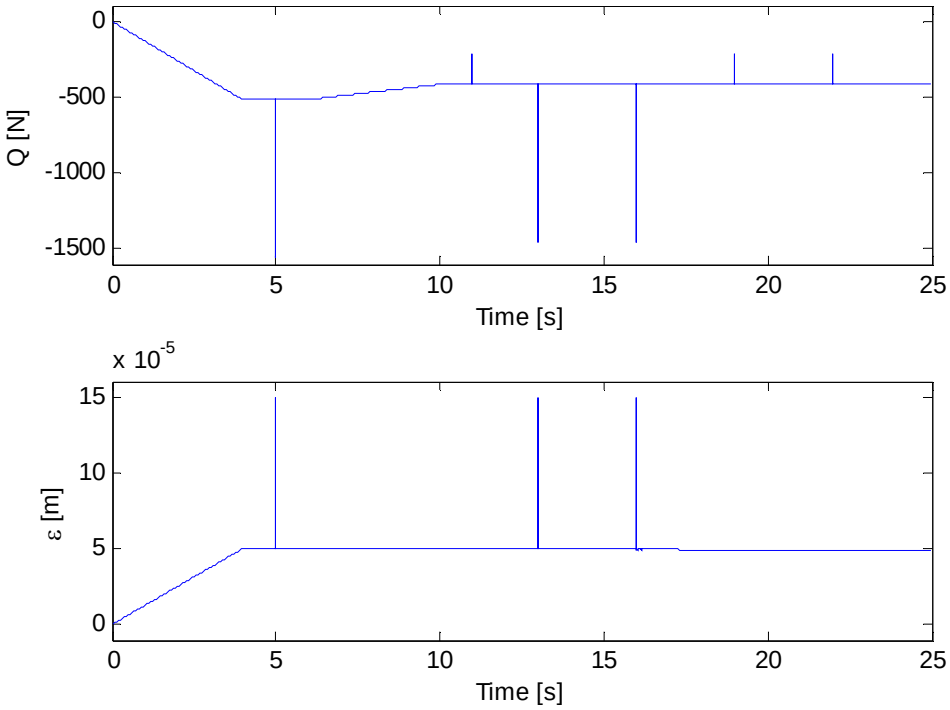

Figure 6.4: Random irregularities on the roll surface: tangential grinding force and chip thickness

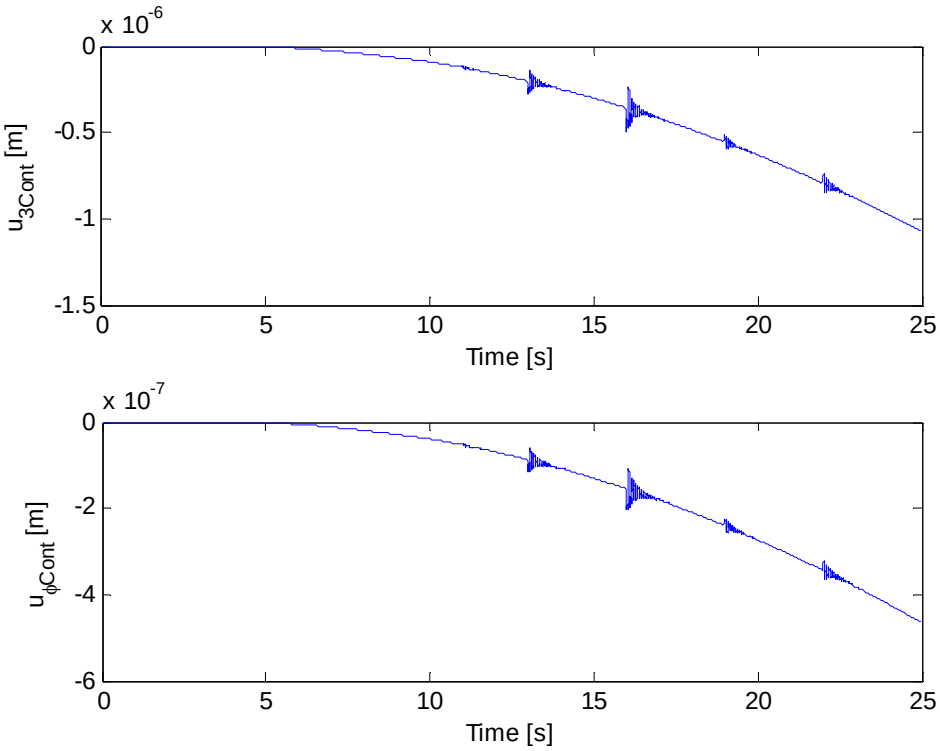

Figure 6.5: Random irregularities on the roll surface: radial and tangential displacement of the contact point

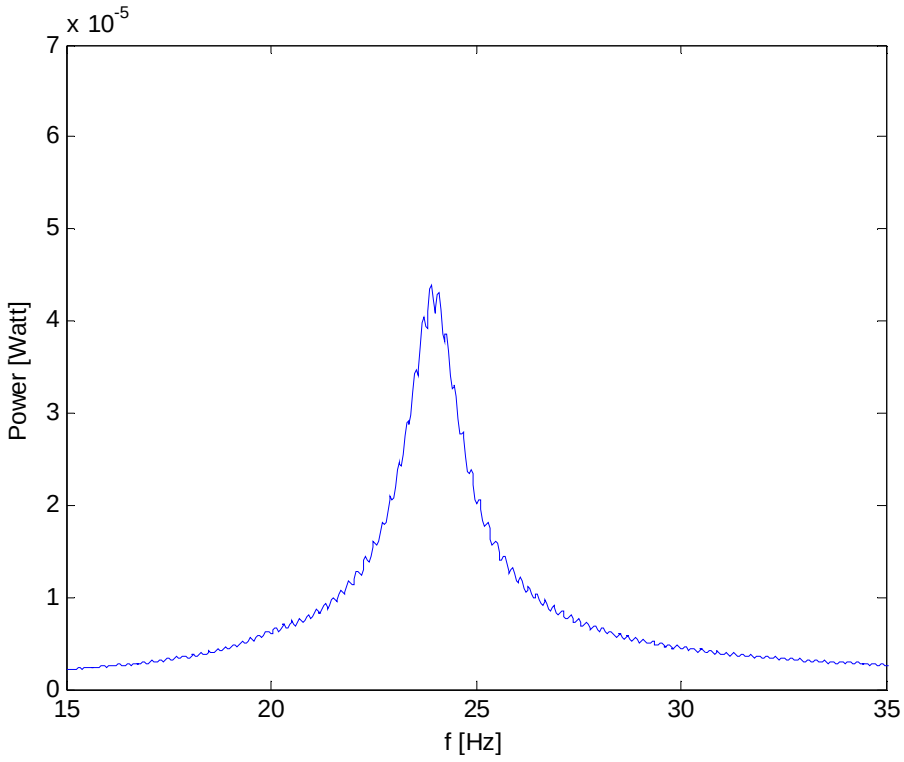

Figure 6.6: FFT of the power history

In the main model, this kind of waviness, ΔR, is assumed to be present from the beginning of the simulation in order to avoid too long simulations.

Now, another questions pops up: what is actually the lowest natural frequency of the system? In the literature, there is often written that the lowest natural frequency of the grinding system is very close to the lowest bending frequency of the roll. Certainly, this holds true for the standard thick-walled and solid rolls. Nevertheless, by taking FFT of various responses in the time domain of a thin-walled roll under grinding conditions, one observes that the frequency of the vibration might be far away from the lowest bending frequency and even more, it can vary.

The cause can be found in the eigenvalue analysis of a simplified single degree of freedom (SDOF) model for the beam (see Figure 6.7). The grinding system reduces to a SDOF mass-spring-damper model by evaluating the response to only a normal grinding force, in the contact plane and using only the first mode.

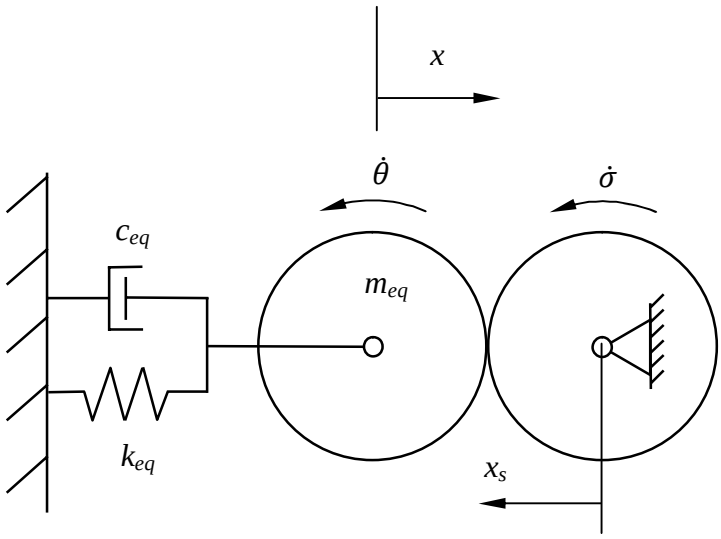

Figure 6.7: Simplified single degree of freedom (SDOF) model

Then, from eq. (4.162) by using the non-rotating coordinates one can derive:

$$m\ddot{\eta} + c\dot{\eta} + k\eta = NU_3(z_s) \tag{6.1}$$

where

$$N = k_N[\varepsilon(t) - \alpha\beta\varepsilon(t-\tau)] \tag{6.2}$$

k_N is the contact stiffness and it is defined as

$$k_N = \frac{w\dot{\tau}_r}{k_w(\dot{\tau}_r + \dot{\tau}_s)} \tag{6.3}$$

and

$$\varepsilon(t) = x(t) + x_s \tag{6.4}$$

Now, the response in terms of modal expansion is

$$x = \eta U_3(z_s) \tag{6.5}$$

Substituting eqs. (6.5), (6.4) and (6.2) into eqs. (6.1) yields

$$\frac{m}{U_3(z_s)}\ddot{x} + \frac{c}{U_3(z_s)}\dot{x} + \frac{k}{U_3(z_s)}x = k_N[x + x_s(1-\alpha\beta) - \alpha\beta x(t-\tau)]U_3(z_s) \tag{6.6}$$

and the term $\frac{m}{U_3(z_s)}$ can be called the equivalent mass m_{eq}, term $\frac{c}{U_3(z_s)}$ the equivalent damping c_{eq} and term $\frac{k}{U_3(z_s)}$ the equivalent stiffness k_{eq} (see Figure 6.7).

Finally, it can be written:

$$\frac{m}{U_3(z_s)}\ddot{x} + \frac{c}{U_3(z_s)}\dot{x} + \frac{k - k_N U_3(z_s)^2}{U_3(z_s)}x = [x_s(1 - \alpha\beta) - \alpha\beta x(t - \tau)]U_3(z_s) \qquad (6.7)$$

From this can be easily seen that the natural frequency of this system is:

$$\omega_{SDOF} = \sqrt{\frac{k - k_N U_3(z_s)^2}{m}} \qquad (6.8)$$

This result matches well with the frequencies obtained by means of FFT of the time response of both the beam and the shell based on multi degree of freedom (MDOF) models.

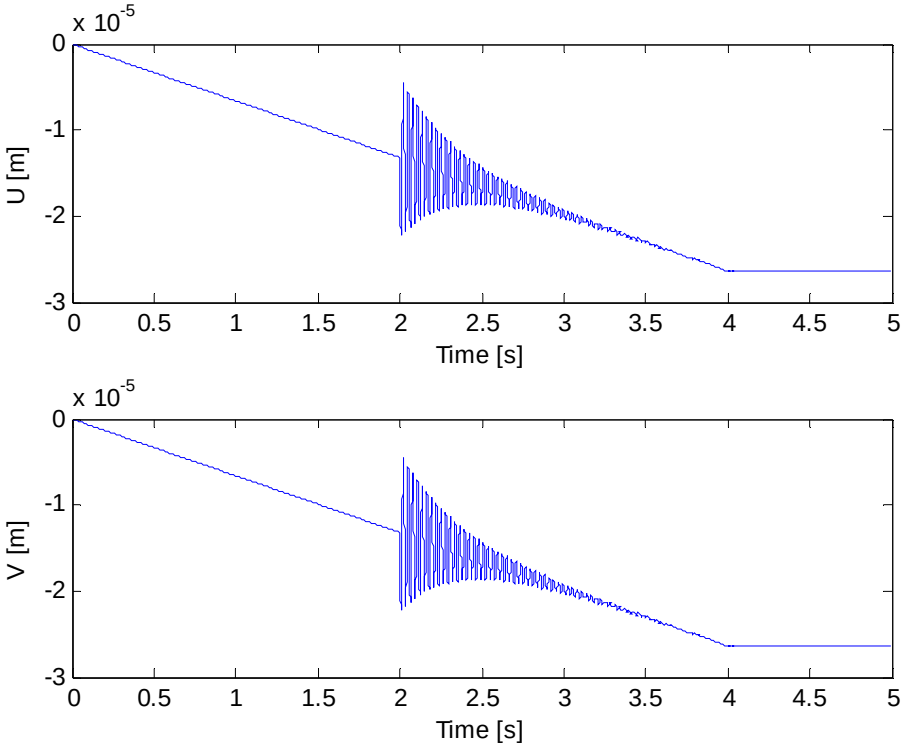

Figure 6.8: Irregularity on the roll surface at *t = 2 s*: displacements of the contact point in *X* and *Y* directions

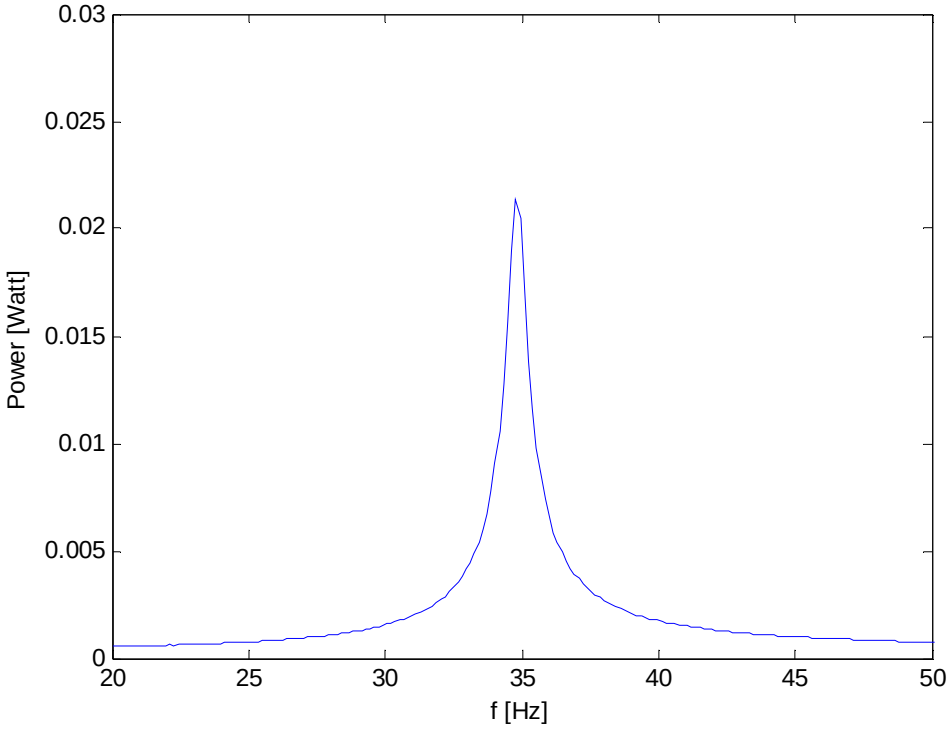

Figure 6.9: FFT of the power history

To support this statement quantitatively, let us consider a special case of grinding a roll, whose parameters are given in Tab. 6.1 and its wall thickness is $h = 10\ mm$. Let us assume that the roll is ideally round and the grinding process starts at axial position $z = 3\ m$. After $2\ s$ there is a sudden change in the roll surface, similarly as in the previous case. A beam model is used here. Figure 6.8 shows the time domain response of the roll in the grinding plain in the X and Y directions. Figure 6.9 shows then an FFT analysis of the power history, from which can be seen that the system frequency is about $f = 34.79\ Hz$. If one applies introduced eq. (6.8) and utilizes eq. (6.3) for the contact stiffness, one obtains a value $\omega_{SDOF} = 219.28\ rad/s$ that corresponds to a value $34.90\ Hz$. It should be noticed that the first bending natural frequency for this case using beam theory is $f_n = 23.93\ Hz$.

From eq. (6.8) it is apparent that the natural frequency of the roll is affected by the contact stiffness k_N. Furthermore, if one has a closer look at the contact stiffness as it is defined for the beam and for the shell, respectively:

$$k_N = \frac{w}{k_w} \frac{\left|\dot{u}_\varphi(-\theta(t), z, t) + R\dot{\theta}\right|}{\left|\dot{u}_\varphi(-\theta(t), z, t) + R\dot{\theta}\right| + \left|r\left(\kappa\dot{\sigma} + \dot{\Delta\sigma}\right)\right|} \quad \text{for the shell} \quad (6.9)$$

$$k_N = \frac{w}{k_w} \frac{\left|\dot{V} + R\dot{\theta}\right|}{\left|\dot{V} + R\dot{\theta}\right| + \left|r\left(\kappa\dot{\sigma} + \dot{\Delta\sigma}\right)\right|} \quad \text{for the beam} \quad (6.10)$$

one can see that for solid or thick-walled rolls the bending stiffness k is much larger than the contact stiffness k_N and so the natural frequency of the system is very close to the natural frequency of the roll. Moreover, the contact stiffness is a function of the tangential velocity of the contact point, $\dot{u}_\varphi(-\theta(t), z, t)$ and $\dot{V}$, for the shell and the beam, respectively. This means that the contact stiffness changes its value and it can be called a dynamic stiffness. And finally, for all types of rolls, the contact stiffness varies with the axial position on the roll because in eq. (6.8) k_N is multiplied by $U_3(z_s)^2$ and due to the change in the tangential velocities in different axial positions of the roll. Nevertheless, the oscillation of the dynamic contact stiffness does not have great effect on the natural frequency of the system, because the change is very small and even its mean value could be used.

It should also be noted that the natural frequencies of the system of the shell and the beam model differ due to the fact that the tangential velocities of the contact point are different. In general, the natural frequency of the system using the beam theory is rather overestimated. The reason for this is that the vertical displacement and velocity of the modelled thin-walled beam is larger than it is in reality. This will be discussed later on in this text.

6.3 Grinding response under the grindstone

This section presents three cases of roll grinding and its response in time domain. Only one parameter is changed and it is the wall thickness that takes values *10 mm*, *5 mm* and *2.5 mm*. Each case shows results using both the shell theory and the beam theory for comparison and discussion.

The simulation begins with full speed of the roll and stone drive. The stone starts to penetrate the roll at the axial position $z = 3\ m$ and reaches the full nominal depth of cut in *4s*. After that it starts to move axially keeping the nominal depth of cut. The simulation lasts *25 s*.

CASE 1: h = 10 mm

Figures 6.10 through 6.17 depict the response in the studied Case 1. It can be observed that the process is rather stable. At the beginning of the simulation there is a visible small peak caused by the initial contact of the grindstone with the roll. The grinding forces as well as the vibration of the roll increase as the stone penetrates the roll. At time $t = 4\ s$ the amplitudes stabilize as the nominal depth of cut has been reached. After one revolution of the roll, the grindstone enters the zone that was already ground (at $t = 6\ s$). The interaction causes chatter vibration that repeats with a period of *6 s*; this is the time of one revolution of the roll and it is the delay time τ, too.

Figures 6.10 and 6.11 show the first set of plots of the tangential grinding force Q and the instantaneous chip thickness ε, related to the shell and beam model, respectively. The normal grinding force N is not presented here, for it is set to be of the same value as the tangential grinding force. It is apparent that the grinding force is proportional to the chip thickness as expected. Also the chip thickness and the grinding force are reaching their zero values that indicates the loss of the contact between the grindstone and the roll. If the two models are compared, one can see that the behaviour of both of them is very similar for this wall thickness. The only difference is in the maximum absolute value of the grinding force in the case of the beam model.

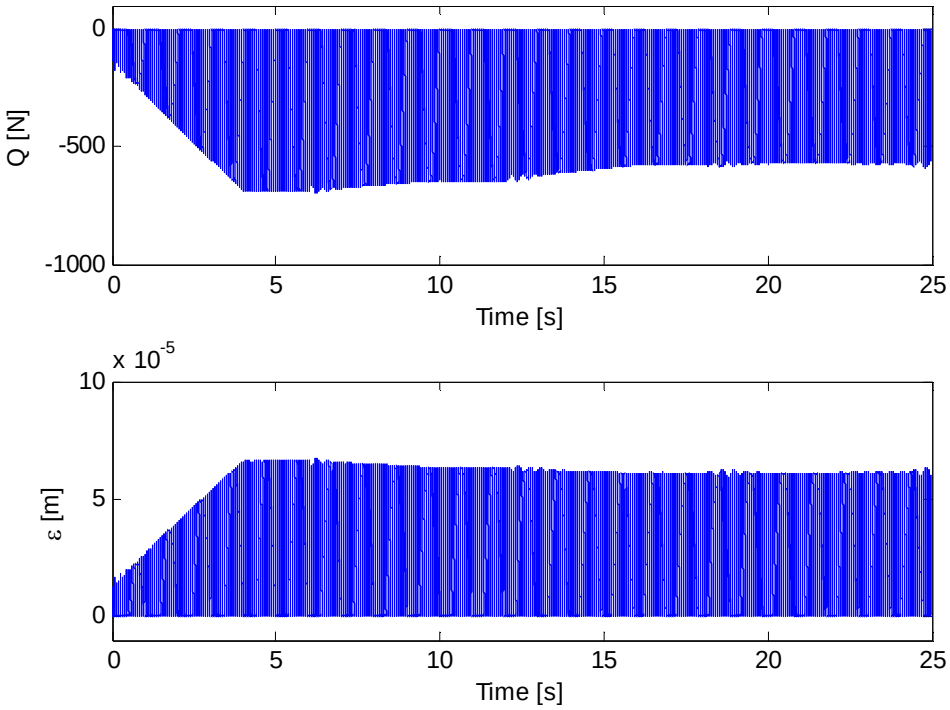

Figure 6.10: Tangential grinding force Q and chip thickness ε, Love's equations

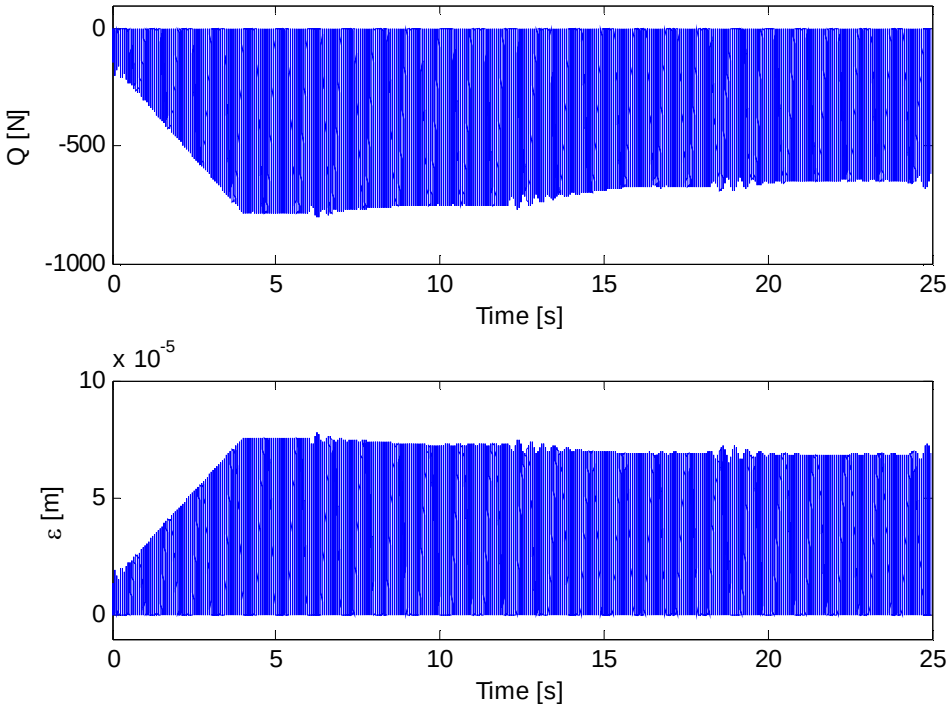

Figure 6.11: Tangential grinding force and chip thickness, beam theory

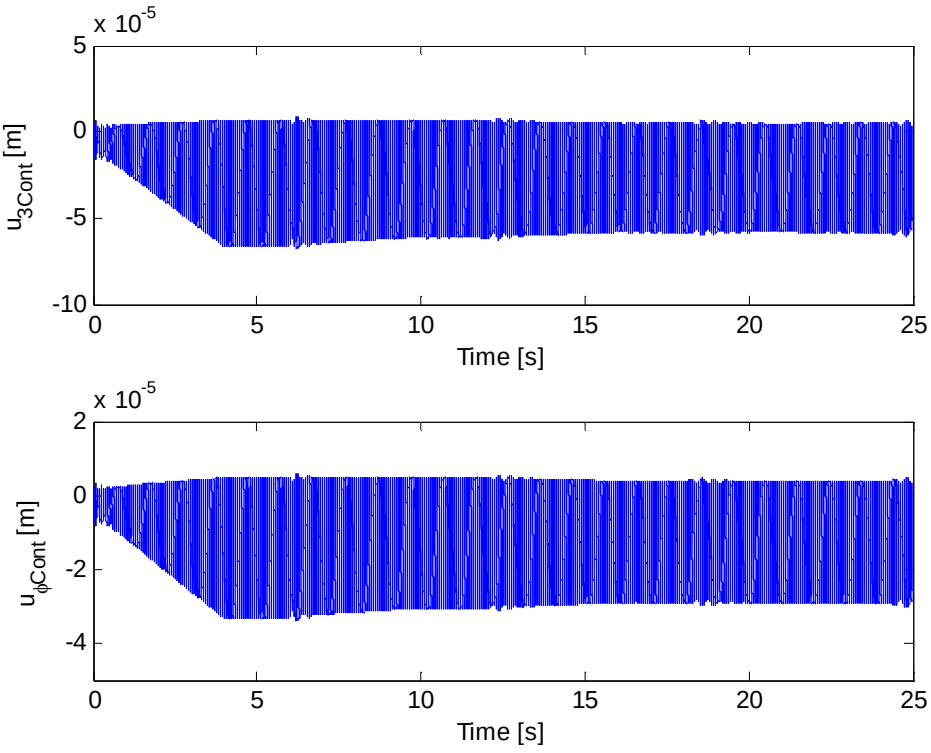

Figure 6.12: Radial and tangential displacement of the contact point, Love's equations

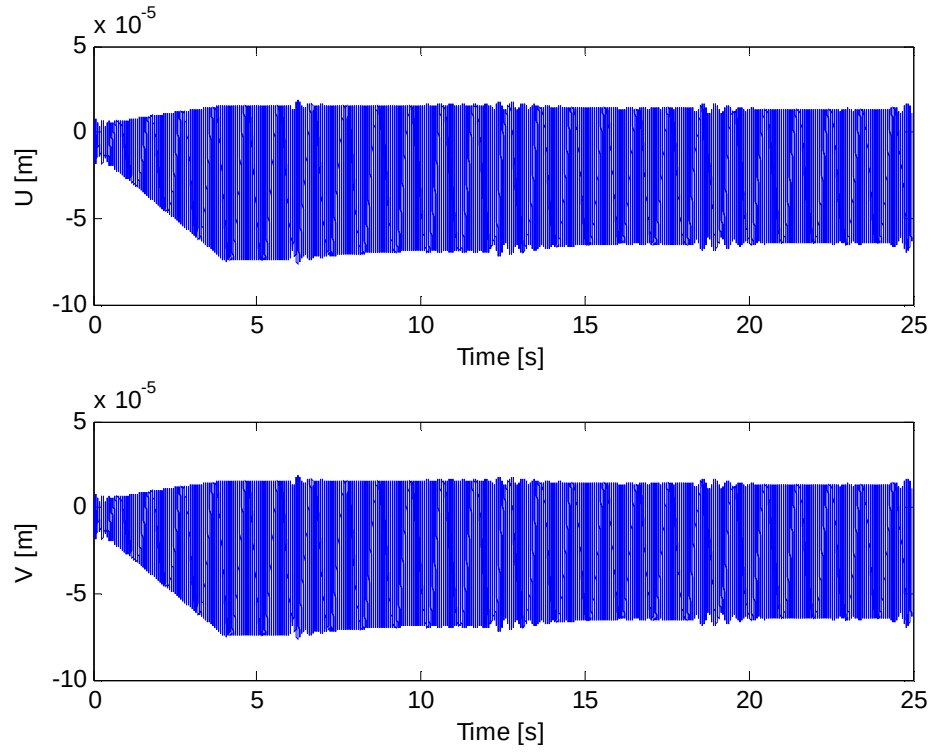

Figure 6.13: Horizontal and vertical displacement of the roll, beam theory

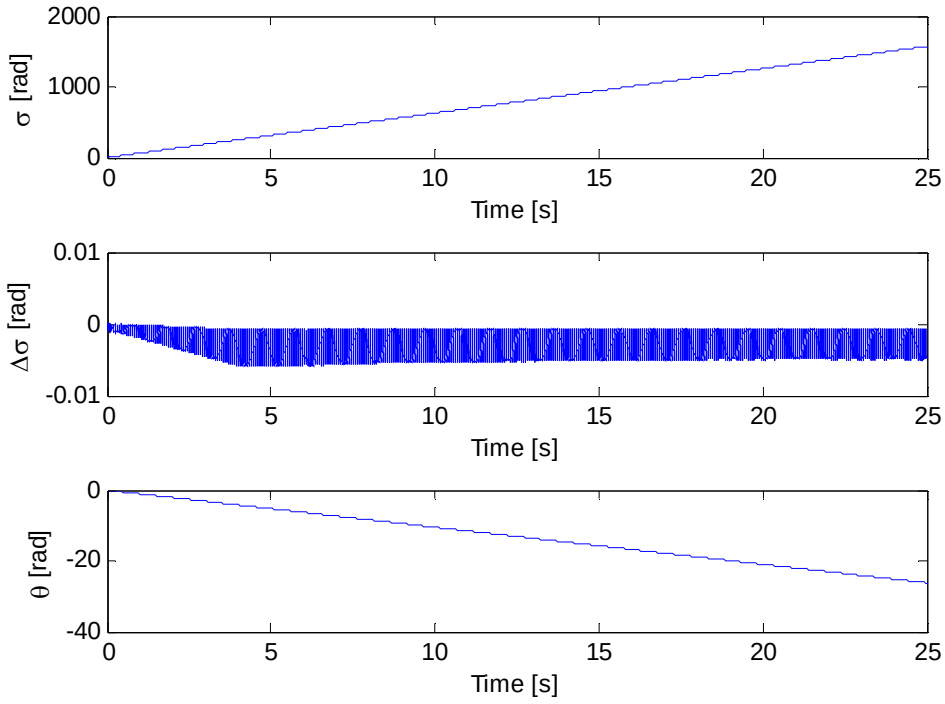

Figure 6.14: Angular position of the stone drive, deviation in the angular position of the stone and angular position of the roll drive, Love's equations

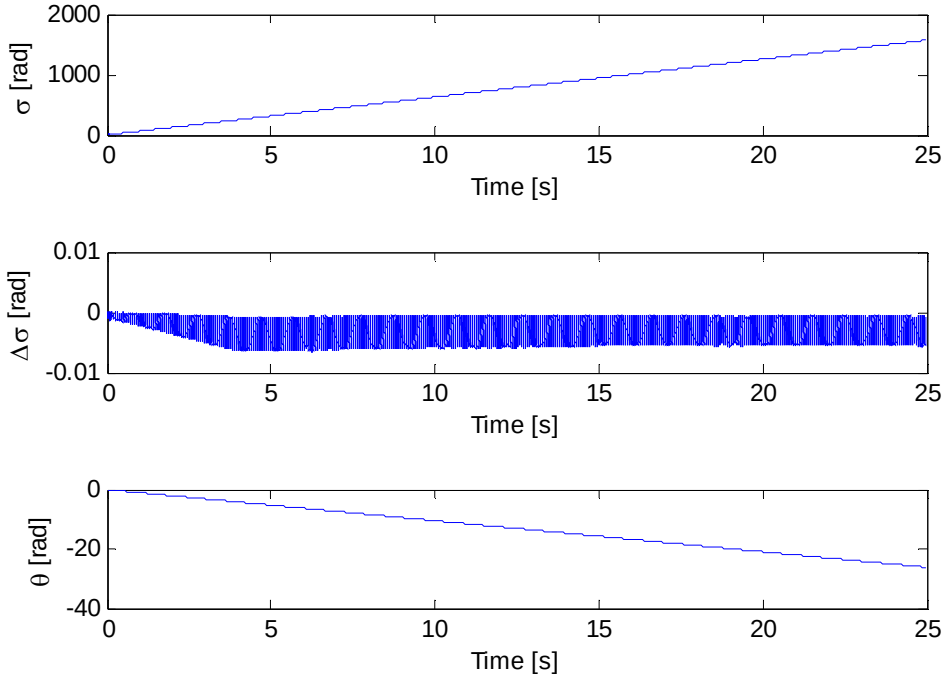

Figure 6.15: Angular position of the stone drive, deviation in the angular position of the stone and angular position of the roll drive, beam theory

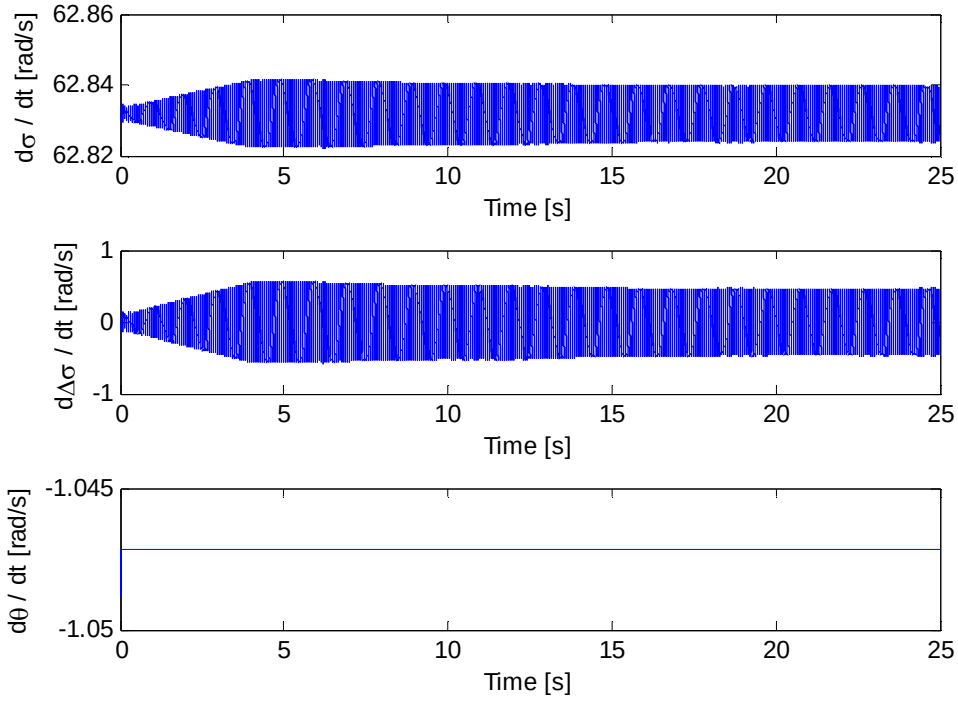

Figure 6.16: Angular velocity of the stone drive, change of the deviation in the angular position of the stone and angular velocity of the roll drive, Love's equations

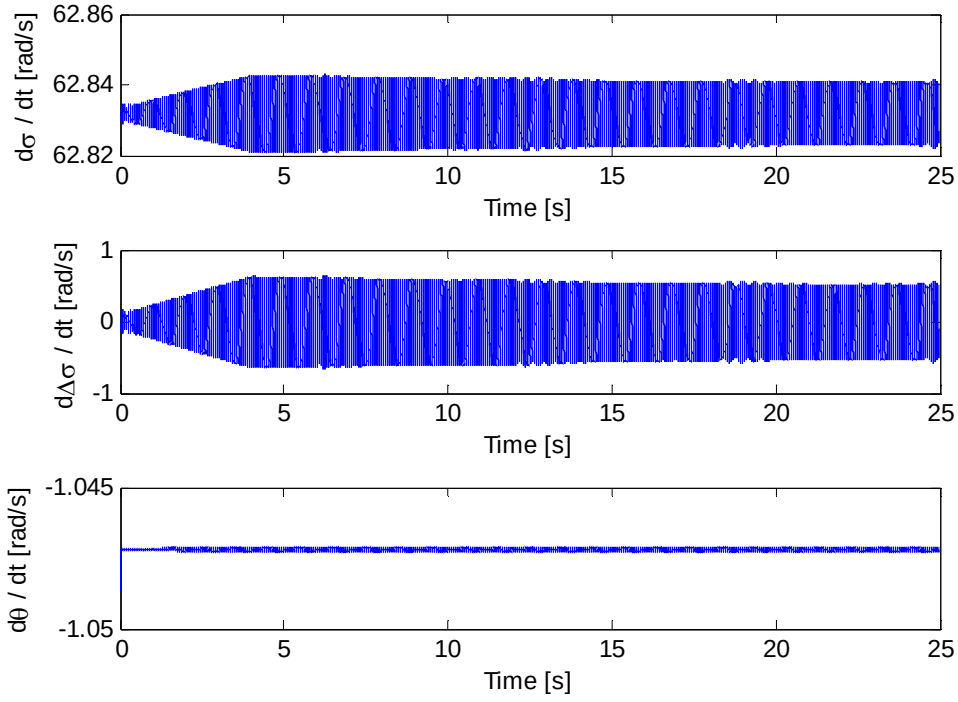

Figure 6.17: Angular velocity of the stone drive, change of the deviation in the angular position of the stone and angular velocity of the roll drive, beam theory

Now, in case of the beam theory, the tangential grinding force is handled as transverse force acting in the Y direction (see Figure 4.8). Therefore, the displacements U and V are identical and in this case the roll vibrates in the diagonal direction. In the case of Love's equations, the tangential force in handled as a proper tangential force. And since the stiffness in the tangential direction is higher than in the radial direction, the displacement in the tangential direction is smaller than that in the radial direction. Therefore, also the velocity of the roll in the Y direction, in case of the beam model, is greater than the velocity in the tangential direction of the contact point, in case of the shell model. Finally, by studying eqs. (6.7), (6.8) and (6.2) one can see that this is the reason why the grinding force is higher in the beam model. Of course, in turn, this higher force produces higher vibrations in both directions X and Y. It is also visible in comparison of Figures 6.12 and 6.13. The difference in the tangential velocities is also a reason for the fact that the modelled natural frequency of the system is higher in case of the beam model.

Figures 6.14 and 6.15 compare the angular position of the stone drive σ, the deviation in the angular position of the stone $\Delta\sigma$ and the angular position of the roll drive θ of the two models. The plots appear to be almost identical. The angular positions σ and θ behave linearly as expected. The deviation in the angular position of the stone $\Delta\sigma$ is caused by the flexibility of the transmission belt and it is caused by the tangential grinding force.

Angular velocity of the stone drive, change of the deviation in the angular position of the stone and angular velocity of the roll drive for the shell and the beam model are depicted in Figures 6.16 and 6.17, respectively. These plots show the performance of the speed controllers. They appear to work properly as the speeds vary in a small range, i.e., they keep the speeds nearly constant as desired. The variation of the speed of the roll in the beam model is slightly higher than in the shell model. It is again a consequence of the overestimated tangential velocities in the beam model that has already been discussed above. Otherwise, the speed performance of both models is again nearly the same for this case. It is rather difficult to compare the two models qualitatively at this stage, because the effect of the overestimated tangential velocities increases with the decreasing of the wall thickness. That will be apparent from the following cases. A quantitative comparison of these two models is carried out at the end of this chapter, where a specific coefficient that specifies a suitability of the models is introduced.

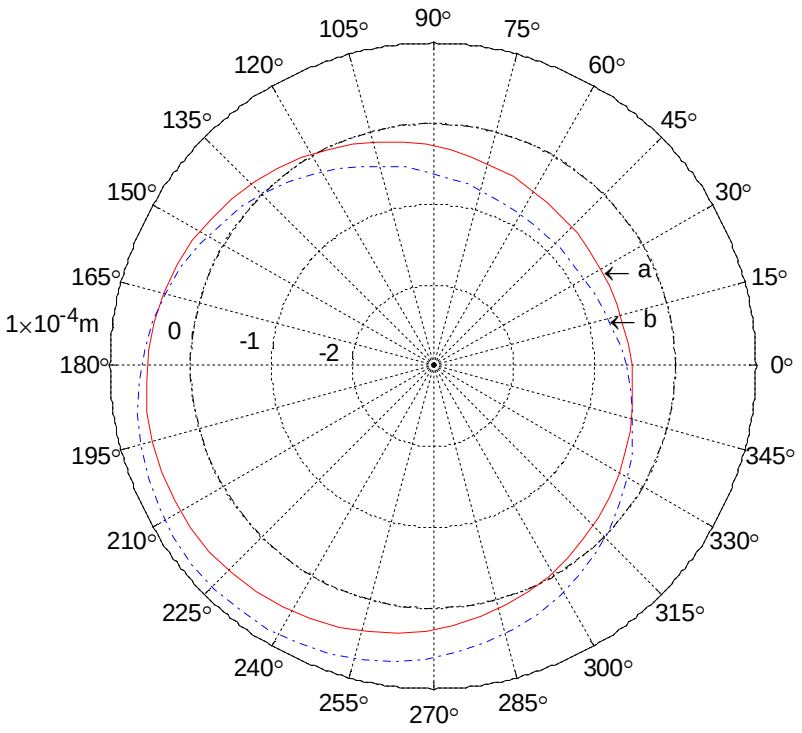

Figure 6.18: Shape and position of the cross-section of the roll at time *t = 15 s*;
a: Love's equations, b: beam theory

A direct comparison of cross-sections of the two models is presented in Figure 6.18. The figure shows the position and the shape of the whole cross-section of the roll in the contact plane utilizing both the shell and the beam theory, for one selected instance from the time domain response: *t = 15 s*. Both cross-sections are circular, which means that the wall thickness is so large that even in the case of the shell model the roll does not experience any circumferential deformation. The difference can be seen in the direction and the amplitude of the vibrations. In case of the beam model the direction is clearly diagonal due to the equal contributions of the horizontal and vertical displacements in contrast to the shell model as explained earlier. Also the amplitude of the vibration is larger in the beam model due to larger grinding forces.

As a conclusion to Case 1, one can summarize that because of the relatively large wall thickness of the roll both the shell and the beam theory are applicable in this case and both describe the dynamic system nearly identically. The difference in the response is caused by a necessary simplification in the case of the beam model. Therefore, it can be also concluded that the shell model yields a more realistic response.

CASE 2: h = 5 mm

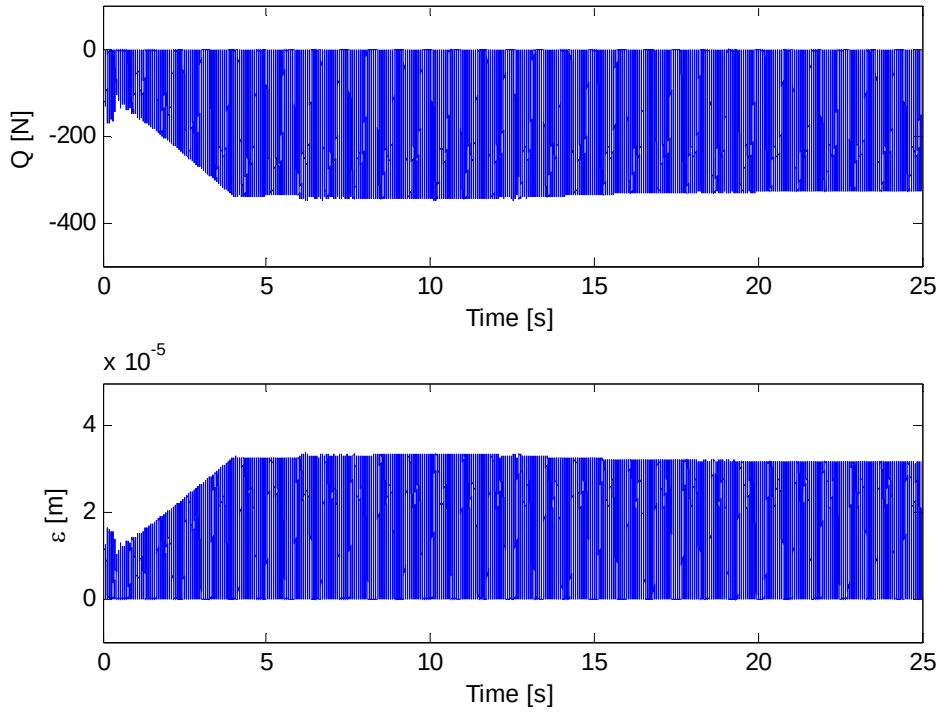

Figure 6.19: Tangential grinding force Q and chip thickness ε, Love's equations

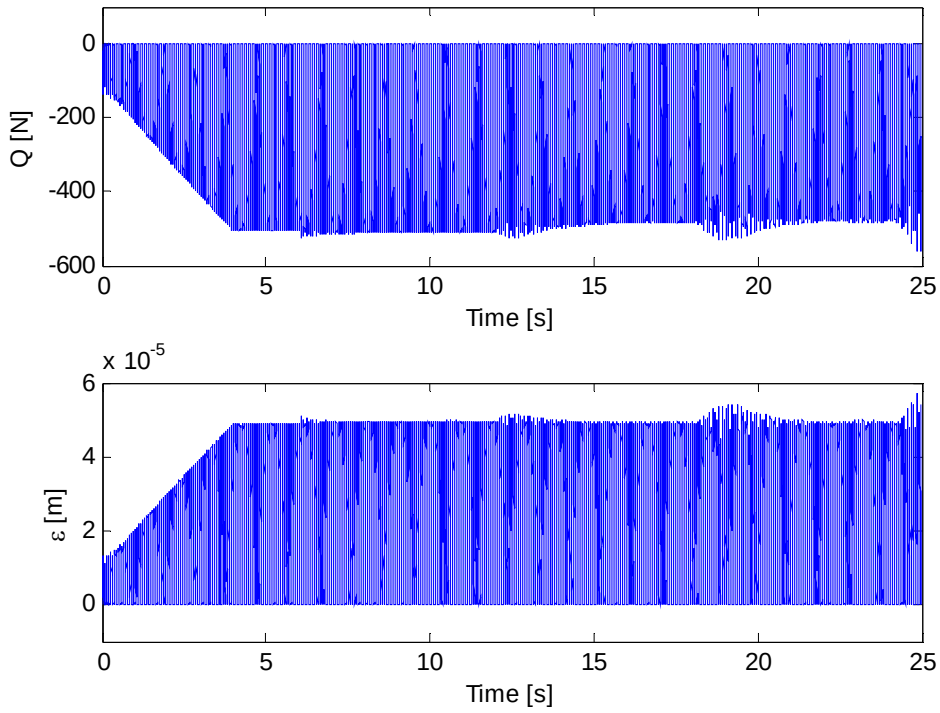

Figure 6.20: Tangential grinding force Q and chip thickness ε, beam theory

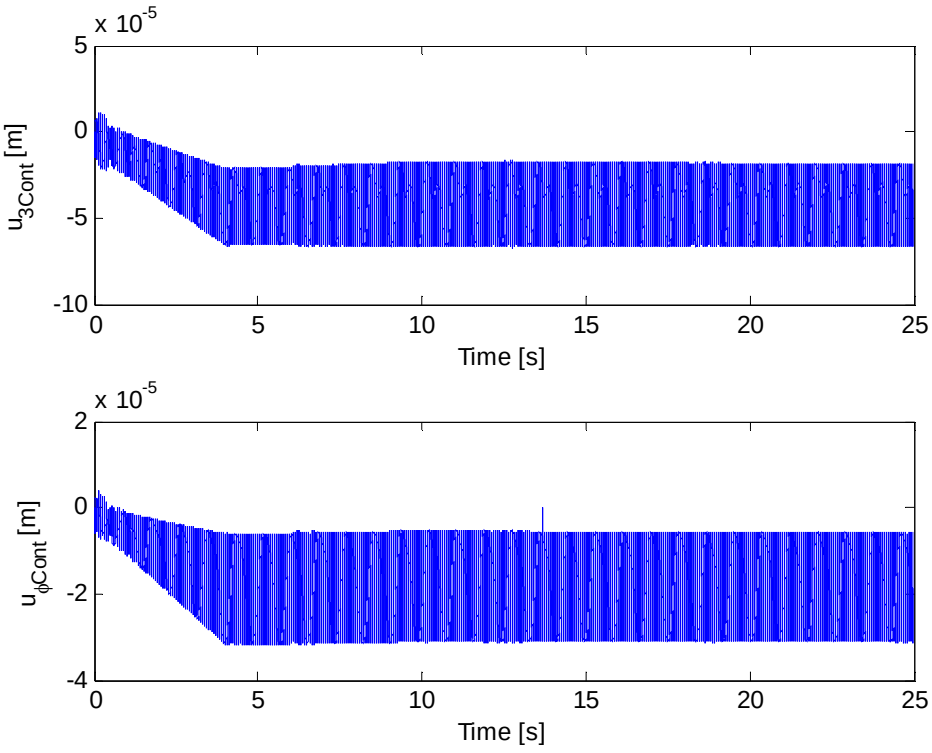

Figure 6.21: Radial and tangential displacement of the contact point, Love's equations

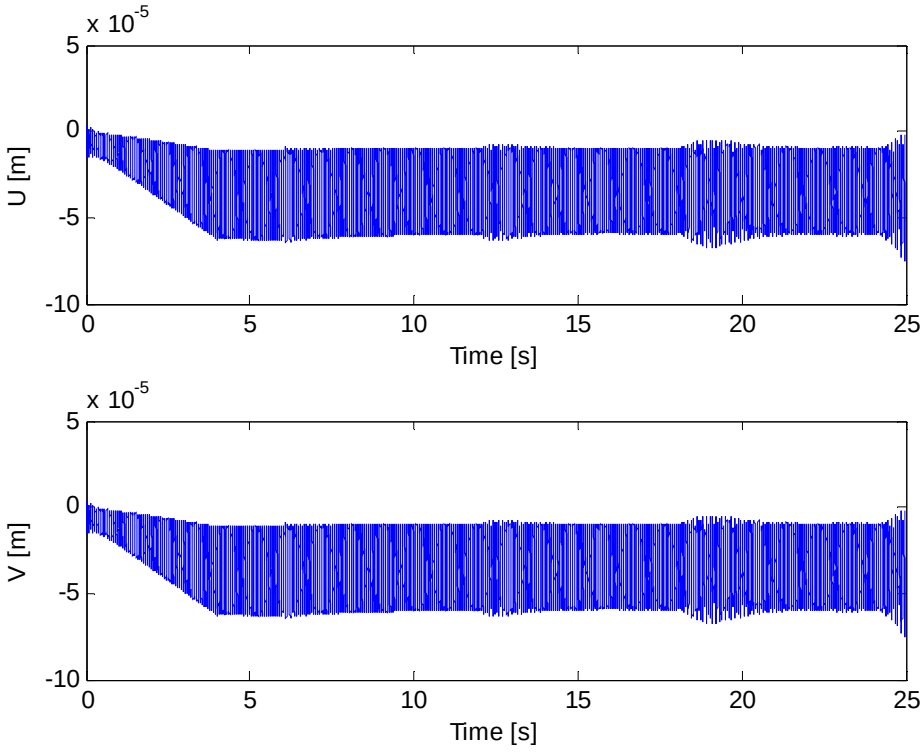

Figure 6.22: Horizontal and vertical displacement of the roll, beam theory

Figures 6.19 and 6.20 compare again the tangential grinding force Q and the chip thickness ε for the two models. In this case, the difference in the maximum absolute values of the grinding force is even larger than in the previous case. The reason in addition to the reasons mentioned in Case 1 is that with decreasing wall thickness the membrane stiffness of the shell gains the importance. It is also apparent from the chip thickness, which is larger in the beam model. In other words, due to the membrane stiffness, the shell-like roll is more flexible and cannot be penetrated by the grindstone as much as in the beam model. One can also see that in the case of the shell model the response is rather stable compared to the beam model. Nevertheless, the chatter vibrations are visible in both cases repeating with delay time.

The radial u_{3Cont} and tangential $u_{\varphi Cont}$ displacements of the contact point and the horizontal U and vertical V displacement of the roll is presented in Figures 6.21 and 6.22 for the shell and the beam model, respectively. Apart from the difference in the tangential displacement $u_{\varphi Cont}$ of the shell model and the vertical displacement V of the beam model, which was clarified above, one could incorrectly conclude that the dynamic behaviour of both models is very similar again. This affinity holds true only for the contact point. The proof that this is not true for other points of the cross-section of the shell is given in Figure 6.23.

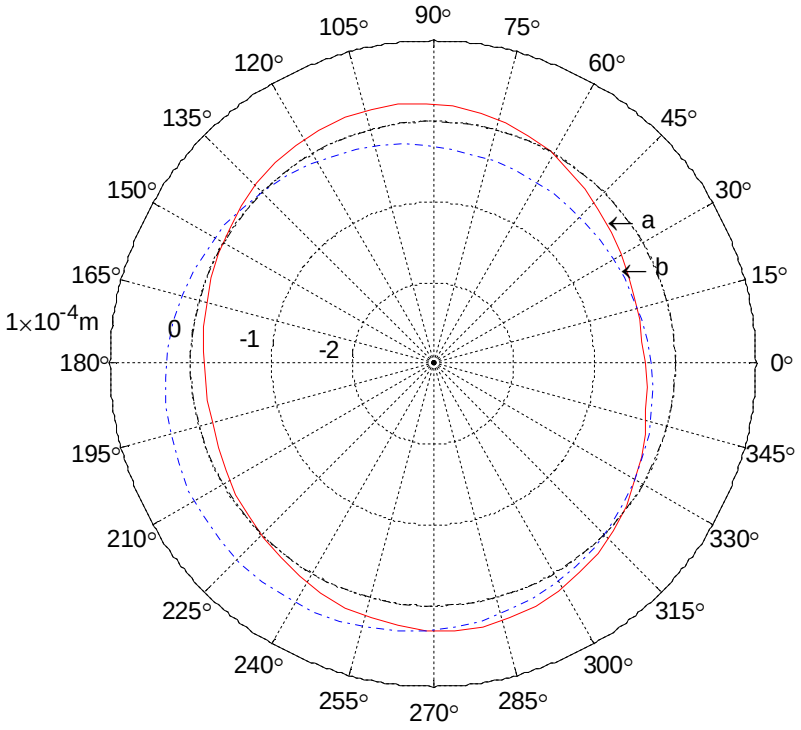

Figure 6.23: Shape and position of the cross-section of the roll at time *t = 15 s*;
a: Love's equations, b: beam theory

Figure 6.23 depicts the difference in the shape and position of the cross-section in the contact plane between the shell and the beam model. As expected the beam model yields a circular shape of the cross-section moving diagonally while the shell model shows the circumferential flexibility of the roll. When concentrating on the leftmost and uppermost points of the two different cross-sections, one can observe that in each pair the points move in the opposite directions. This is again the consequence of the circumferential flexibility of the shell.

The comparisons of the drive angular positions and velocities are left out in this case as they do not contribute with any additional information to those results presented in Figures 6.14 through 6.17.

As a conclusion for Case 2 it can be stated that the wall thickness of *5 mm* has intermediate effect on the dynamic behaviour of the studied system. Due to the fact that the beam theory cannot handle the tangential force properly and does not take into account the circumferential flexibility of the thin-walled roll, this theory does not yield an accurate result. Nevertheless, the beam model could still be useful in certain rough estimations of such a grinding system.

CASE 3: h = 2.5 mm

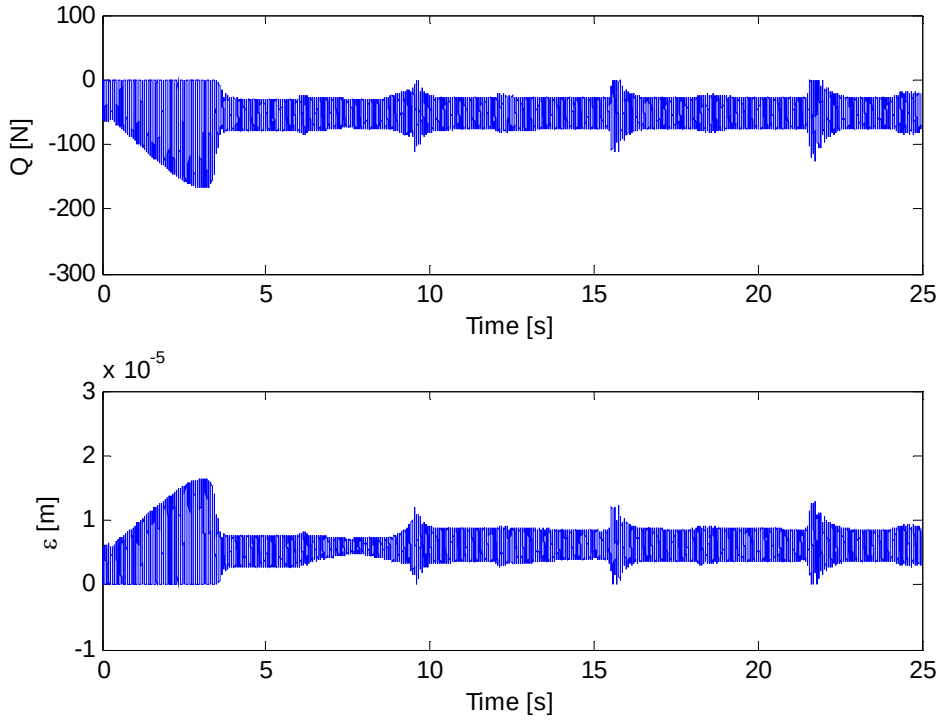

Figure 6.24: Tangential grinding force Q and chip thickness ε, Love's equations

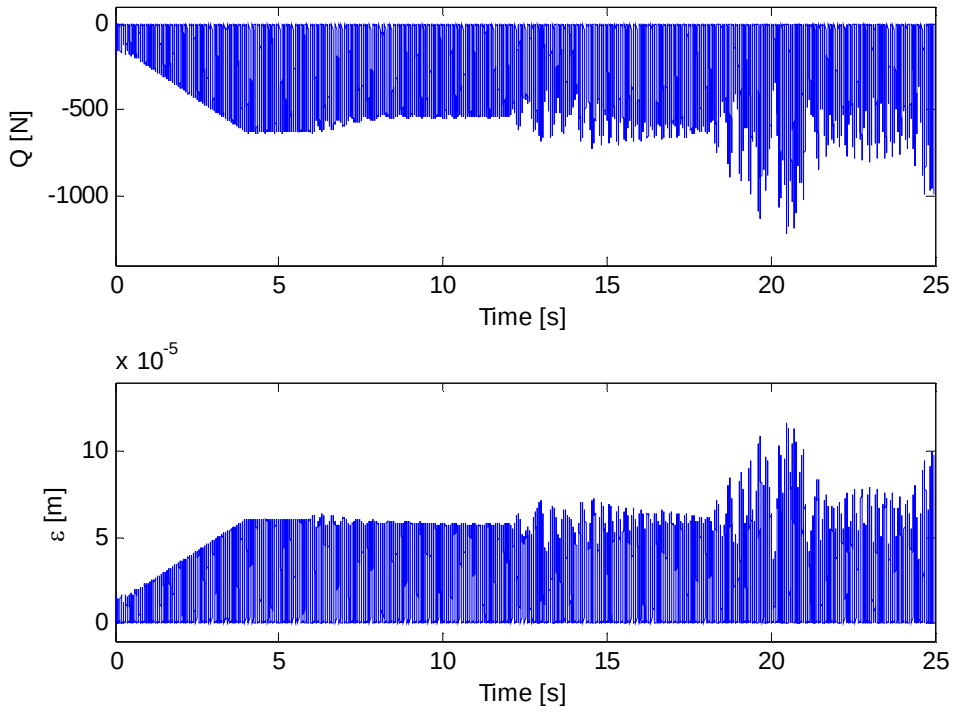

Figure 6.25: Tangential grinding force Q and chip thickness ε, beam theory

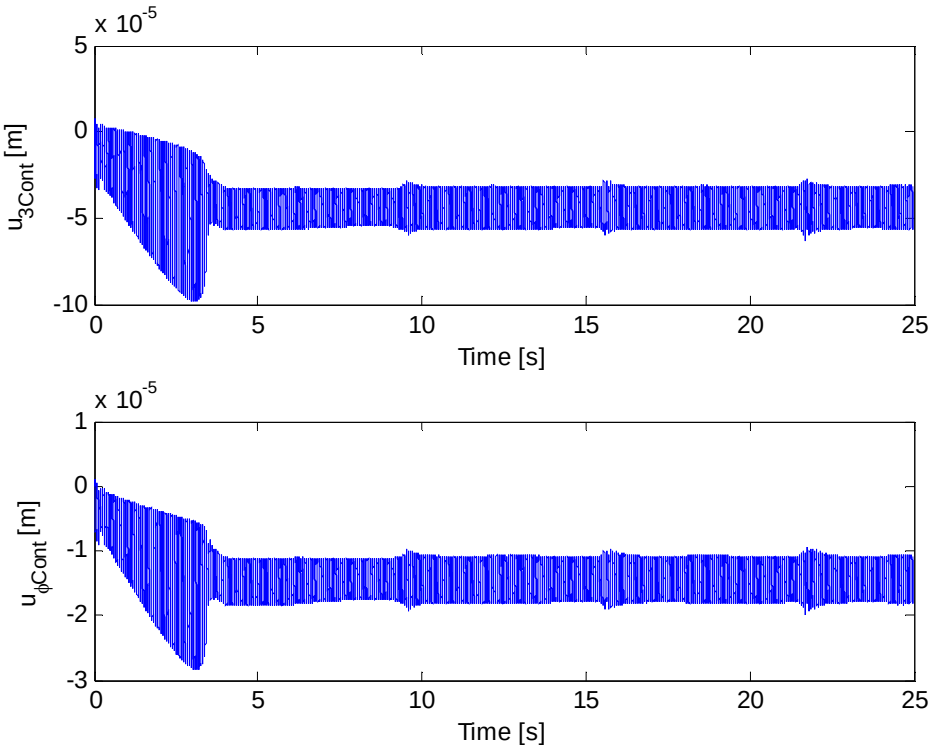

Figure 6.26: Radial and tangential displacement of the contact point, Love's equations

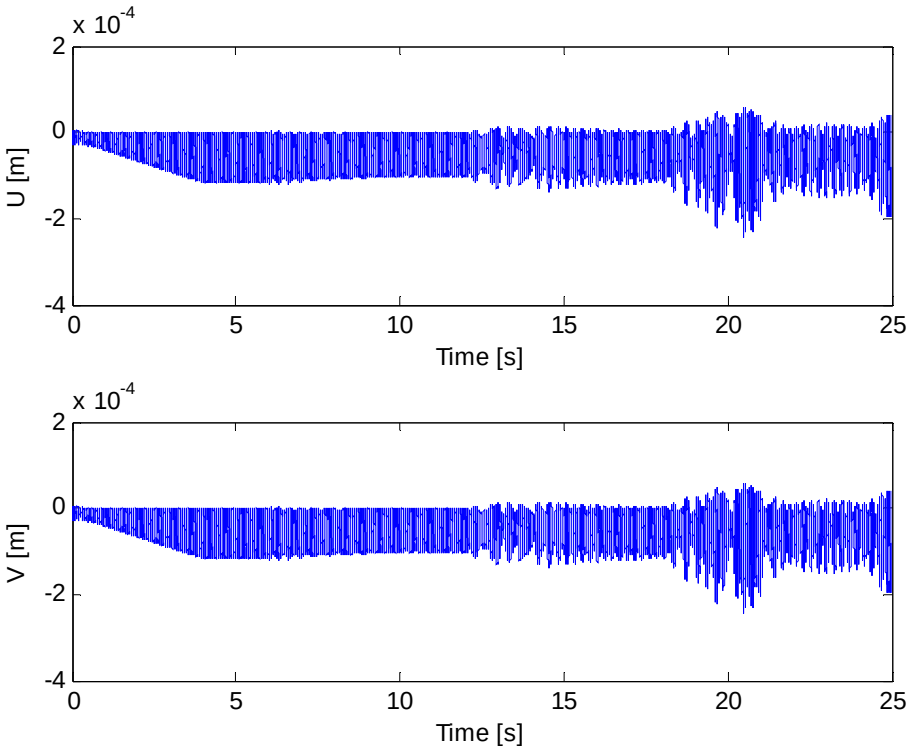

Figure 6.27: Horizontal and vertical displacement of the roll, beam theory

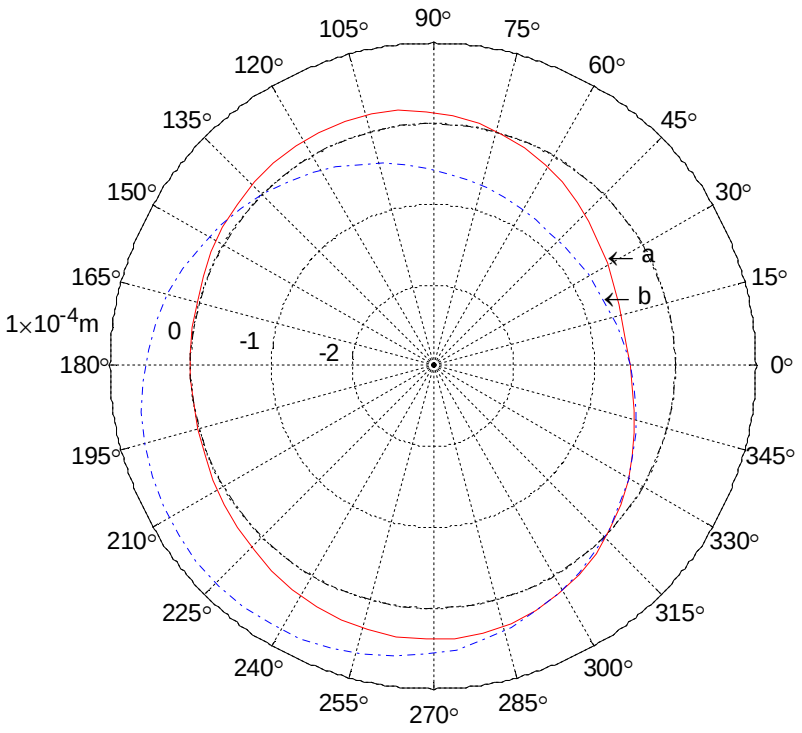

Figure 6.28: Shape and position of the cross-section of the roll at time *t = 15 s*;
a: Love's equations, b: beam theory

Plots showing the tangential grinding force Q and the chip thickness ε for the two models, depicted in Figures 6.24 and 6.25, experience significant distinction in this case. In the shell model, during the starting phase the amplitude of the vibration increases, but after reaching the nominal depth of cut the amplitude drops. This creates a sudden change in the surface profile and it is repeated with the delay period similarly as the initial surface mark caused by the first contact between the grindstone and the roll. The response appears to be rather stable. The roll flexibility is so large that the grindstone almost does not remove any material from the roll. Also the chip thickness rarely reaches the zero level, which indicates that the stone reaches the nominal depth of cut, but due to the large circumferential flexibility of the roll the contact is very soft and the amplitude of the vibration is low and stable. As a consequence the absolute value of the grinding force oscillates only about a value of *50 N*, which is about one order lower than in the beam model. In contrast to the shell model, the significance of the errors in the beam model grows with the decreasing wall thickness. The grinding forces grow enormously and the process becomes quickly unstable.

Same tendency is apparent from Figures 6.26 and 6.27 that present the radial and tangential displacements of the contact point and the horizontal and vertical displacement of the roll for the shell and the beam model, respectively. Finally, Figure 6.28 again compares the shape and position

of the cross-section of the roll in the contact plane for the two models. As expected, in the shell model the bending stiffness is dominated by the membrane stiffness, which is even more apparent than in the previous case. On the other hand the beam model behaves also as expected, yet not in agreement with reality.

As a conclusion for Case 3, it can be stated that for the wall thickness $h = 2.5\ mm$ the beam model yields significantly incorrect results. It is caused by adopting assumptions in the Euler-Bernoulli beam theory and thereby the result of this study supports the opinion that the Euler-Bernoulli beam theory is not suitable for analyzing thin-walled rolls or, based on an inductive extension, thin-walled beams in general. On the contrary, the shell model yields plausible results, which supports the conclusion that Love's equations are suitable for analyzing thin-walled rolls.

6.4 Grinding response on the whole span of the roll

The two models introduced in chapter 4 describing the grinding system provide also a comparison of the dynamic behaviour on the whole span of the roll; i.e., not only in the plane of the excitation. The behaviour of the beam model is easily predictable whereas in case of the shell model the effect of the membrane stiffness with respect to the distance away from the contact point is of higher interest. In this section the shape of cross-sections in various planes of the roll using both models is investigated. The difference in amplitudes between the two models is left aside as this issue was discussed earlier.

Figures 6.29 and 6.30 show instantaneous position and shape of cross-sections in 5 different planes perpendicular to the centre line of the roll at time $t = 10\ s$ of the time domain response of Case 3 (section 6.3), for the shell and the beam model, respectively. The planes correspond to axial positions $z = 3.105\ m$, which is the plane of contact, $z = 5.105\ m$, $z = 6.105\ m$, $z = 6.605\ m$ and $z = 7.150\ m$, which is the end of the roll. The beam model (Figure 6.30) shows a typical behaviour; the cross-section must be circular by definition and the amplitude of the vibration decreases when approaching the boundary. The cross-sections move exactly on the diagonal ($45°$ straight line) as the forces N and Q were set to be of the same magnitude. The deflected centre line follows exactly the first mode shape for a simply supported beam. The shell model (Figure 6.29) presents clearly a different result, although it uses the first beam mode shape as well. Of course, the difference is caused by the additional circumferential modes. From this figure one can see that the effect of the membrane stiffness clearly dominates the bending stiffness in the region $z = 1 - 6\ m$.

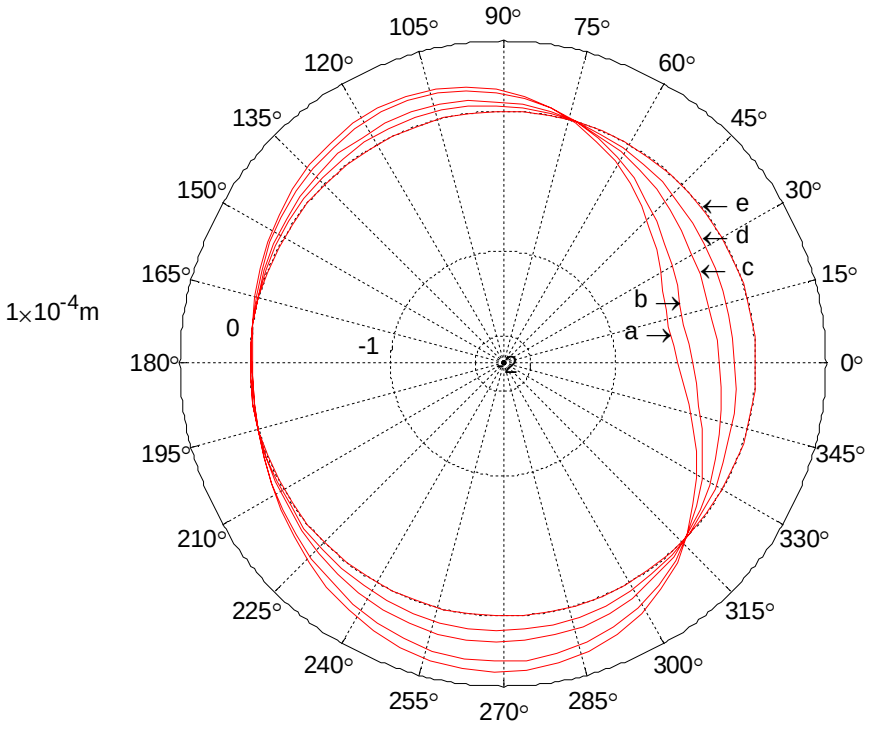

Figure 6.29: Cross-section of the roll at various axial positions at time *t = 10 s*; a: *z = 3.105 m*, b: *z = 5.105 m*, c: *z = 6.105 m*, d: *z = 6.605 m*, e: *z = 7.150 m*, Love's equations, *h = 2.5 mm*

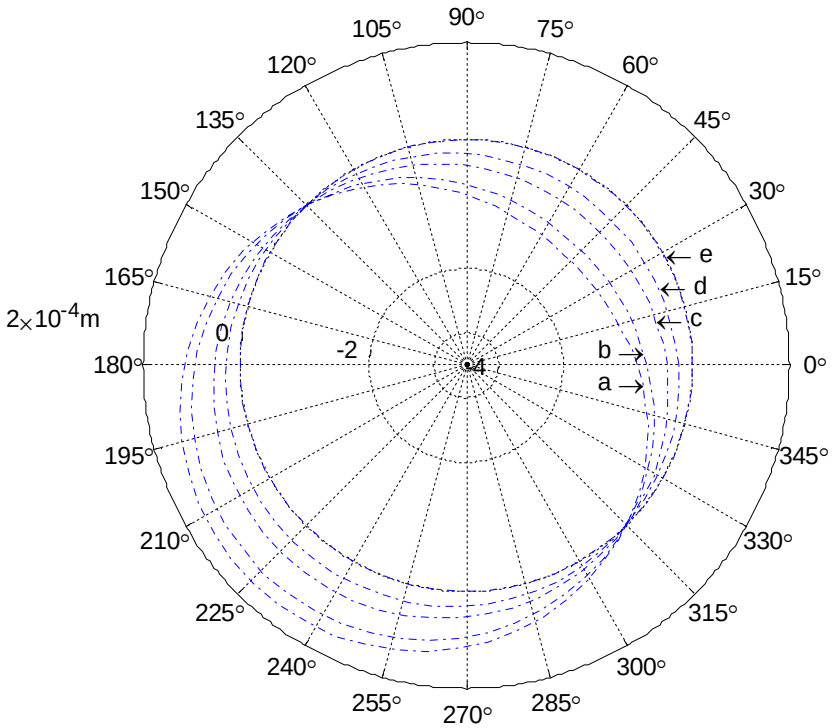

Figure 6.30: Cross-section of the roll at various axial positions at time *t = 10 s*; a: *z = 3.105 m*, b: *z = 5.105 m*, c: *z = 6.105 m*, d: *z = 6.605 m*, e: *z = 7.150 m*, beam theory, *h = 2.5 mm*

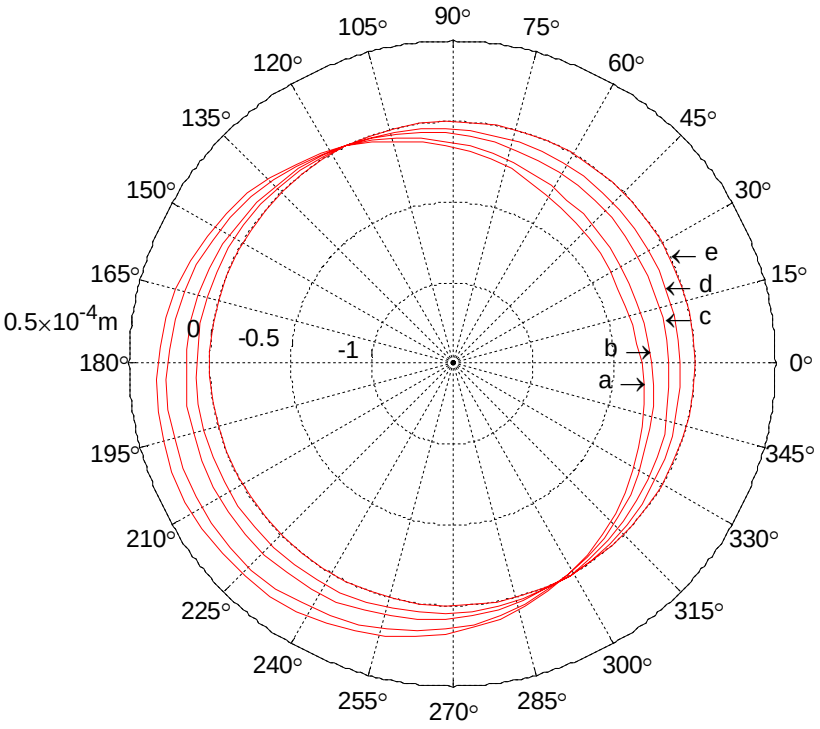

Figure 6.31: Cross-section of the roll at various axial positions at time *t = 10 s*; a: *z = 3.105 m*, b: *z = 5.105 m*, c: *z = 6.105 m*, d: *z = 6.605 m*, e: *z = 7.150 m*; Love's equations, *h = 10 mm*

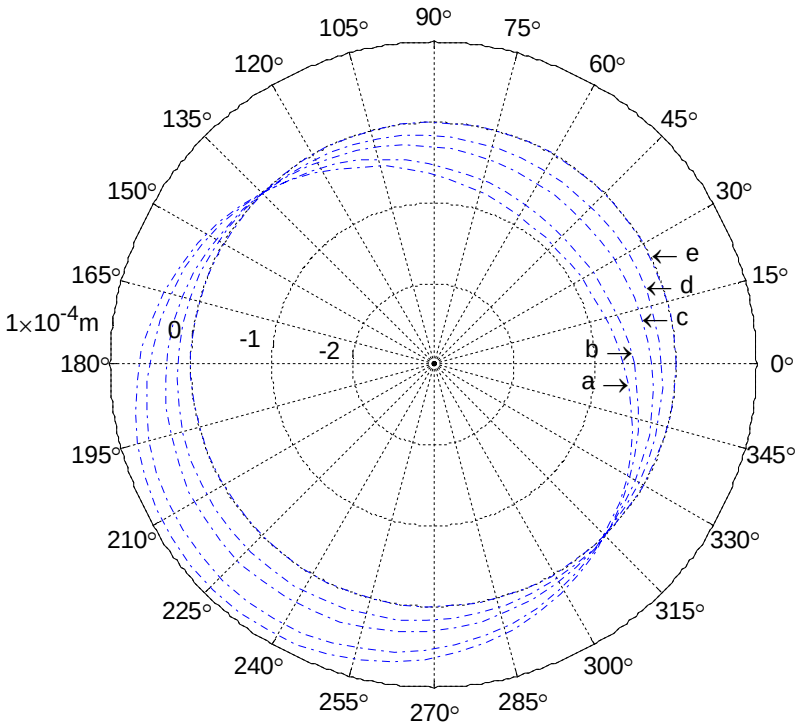

Figure 6.32: Cross-section of the roll at various axial positions at time *t = 10 s*; a: *z = 3.105 m*, b: *z = 5.105 m*, c: *z = 6.105 m*, d: *z = 6.605 m*, e: *z = 7.150 m*, beam theory, *h = 10 mm*

If similar plots are extracted from the Case 1 of the section 6.3, one can see that the two models yield similar results (see Figures 6.31 and 6.32). The shape of the cross-section in all planes is circular in both models. This indicates that the effect of the membrane stiffness, in the shell model, is overwhelmed by the effect of the bending stiffness. The only difference is the direction and the amplitude of the vibrational movement of the roll. While the roll movement in the beam model follows the antidiagonal, the roll movement in the shell model is slightly deflected with respect to the antidiagonal by about *20*°. The reason can be seen in the handling the tangential grinding force as discussed in section 6.3. It also implies that for applications with purely radial loading, nearly identical results of the two theories for a certain ratio (outer radius to the wall thickness) are to be expected. Let us call the ratio a specific coefficient. According to this study this statement holds true for the ratio interval *(10, 30),* where the lower boundary is restricted by the definition of the shell theory that says that the theory is applicable for shells whose wall thickness is less than *10%* of the radius of the shell [Blevins, 1979]. For the radius of the roll given in this study it means a wall thickness from $h = 8\ mm$ to $h = 23\ mm$.

7. Effect of the additional roll support

In industrial practice the problems with chatter vibrations are very well known. In the workshops for paper machine roll grinding, several practical means how to lower the roll vibrations during grinding have been in use. One of the simplest and widely used methods has been an application of a supporting frame acting against the grindstone. Therefore, from the industrial point of view an analysis dealing with grinding of thin-walled rolls supported by an additional support is interesting. From the scientific point of view it is interesting to investigate the dynamic behaviour of the shell under these conditions and to study the effect of the membrane stiffness on the local deformations over the roll span. A comparison with the beam model is also beneficial. This type of analysis is carried out in this chapter.

7.1 Model including additional roll support

The model presented in chapter 4 can be adjusted for this purpose. The additional support is modelled as an additional spring acting against the roll as shown in Figure 7.1. This additional spring could be handled as a third, elastic support in addition to the simply supported shell/beam situation. That would lead to change in the natural frequencies and the mode shapes of the roll. On the other hand the support is not attached to the roll, which means that it acts as a spring only when the roll presses against it.

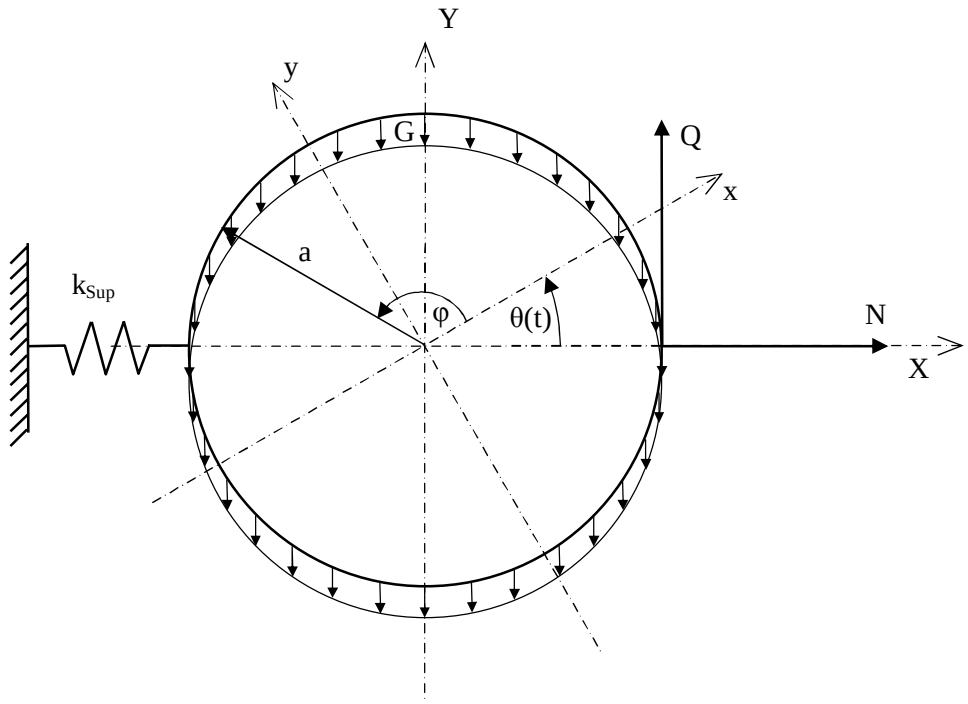

Figure 7.1: Load acting on the roll including the additional stiffness k_{Sup}

Therefore, it is advantageous to simulate the additional support as a point force F_{Sup} acting against the roll when the spring is being compressed and producing zero load when there is no contact between the roll and the support.

Thus, F_{Sup} for the shell model can be defined as:

$$F_{Sup} = \begin{cases} -k_{Sup} u_{3,stationar}(\pi, z^*, t), & u_{3,stationar}(\pi, z^*, t) > 0 \\ 0, & otherwise \end{cases} \tag{7.1}$$

Then eq. (4.115) can be completed by a forcing term $F_{k,mn,Sup}$, which is the modal force caused by the support reaction force F_{Sup}. Eq. (4.115) takes now the form:

$$m_{k,mn}\ddot{\eta}_{k,mn} + c_{k,mn}\dot{\eta}_{k,mn} + k_{k,mn}\eta_{k,mn} = F_{k,mn,C} + F_{k,mn,G} + F_{k,mn,Sup} \tag{7.2}$$

where

$$F_{k,mn,Sup} = F_{Sup} U_{3,kmn}(\varphi^* - \pi, z^*) \tag{7.3}$$

In the case of the beam model F_{Sup} can be defined as follows:

$$F_{Sup} = \begin{cases} -k_{Sub} U(z^*, t), & U(z^*, t) < 0 \\ 0, & otherwise \end{cases} \tag{7.4}$$

And similarly one can complete eq. (4.162) and (4.163) by a forcing term $F_{m,Sup}$, the modal force caused by the support reaction force F_{Sup}. Eqs. (4.162) and (4.163) become

$$m_m\ddot{\eta}_m^u + c_m\dot{\eta}_m^u + k_m\eta_m^u = \left(-F_{m,G} + F_{m,Q}\right) sin\,\theta + \left(F_{m,N} + F_{m,Sup}\right) cos\,\theta \tag{7.5}$$

$$m_m\ddot{\eta}_m^v + c_m\dot{\eta}_m^v + k_m\eta_m^v = \left(-F_{m,G} + F_{m,Q}\right) cos\,\theta - \left(F_{m,N} + F_{m,Sup}\right) sin\,\theta \tag{7.6}$$

The rest of the equations in chapter 4 remains unchanged.

7.2 Grinding response affected by additional roll support

This analysis uses system parameters of Case 3, which means that the roll wall thickness is $h = 2.5$ *mm*. The stiffness of the additional support is computed as a bending stiffness of a cantilever beam. Depending on the geometry, the stiffness of the support was estimated to be in range $(1 \cdot 10^7, 2 \cdot 10^7)$ Nm^{-1}. For this particular simulation the mean value has been chosen, which is $k_{Sup} = 1.5 \cdot 10^7$ Nm^{-1}. Other conditions of the simulation are the same as in chapter 6. The first set of results is presented in Figures 7.2 and 7.3 for the shell and the beam model, respectively.

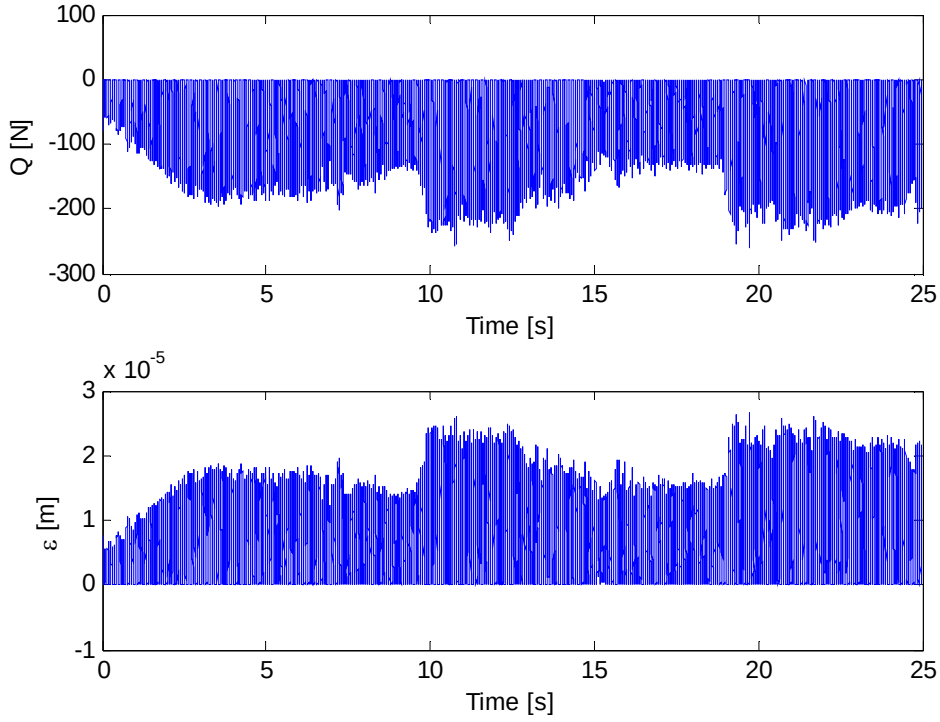

Figure 7.2: Tangential grinding force Q and chip thickness ε, Love's equations

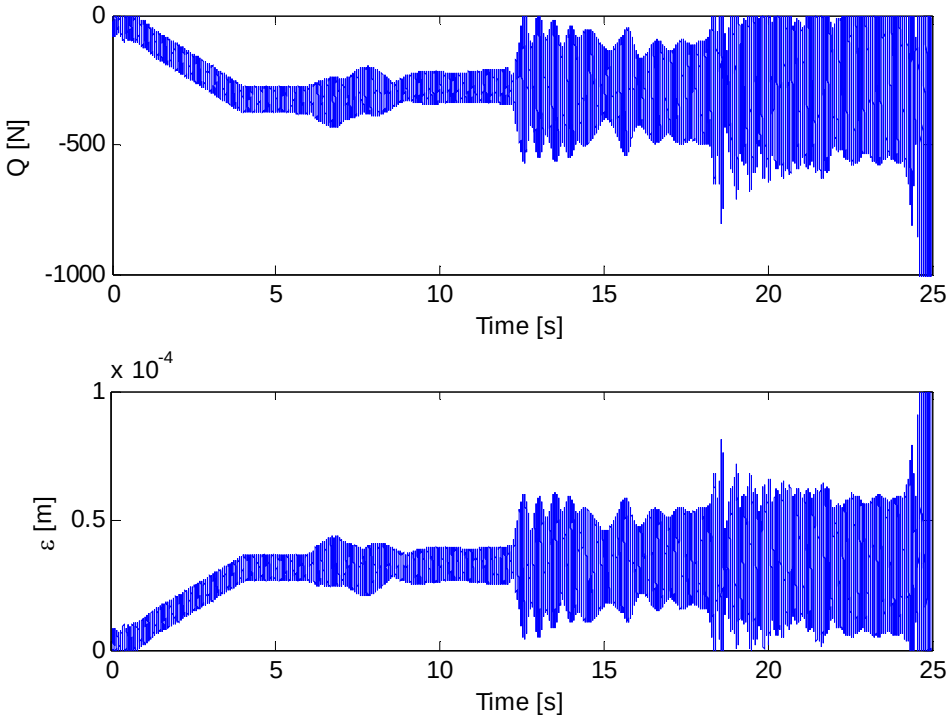

Figure 7.3: Tangential grinding force Q and chip thickness ε, beam theory

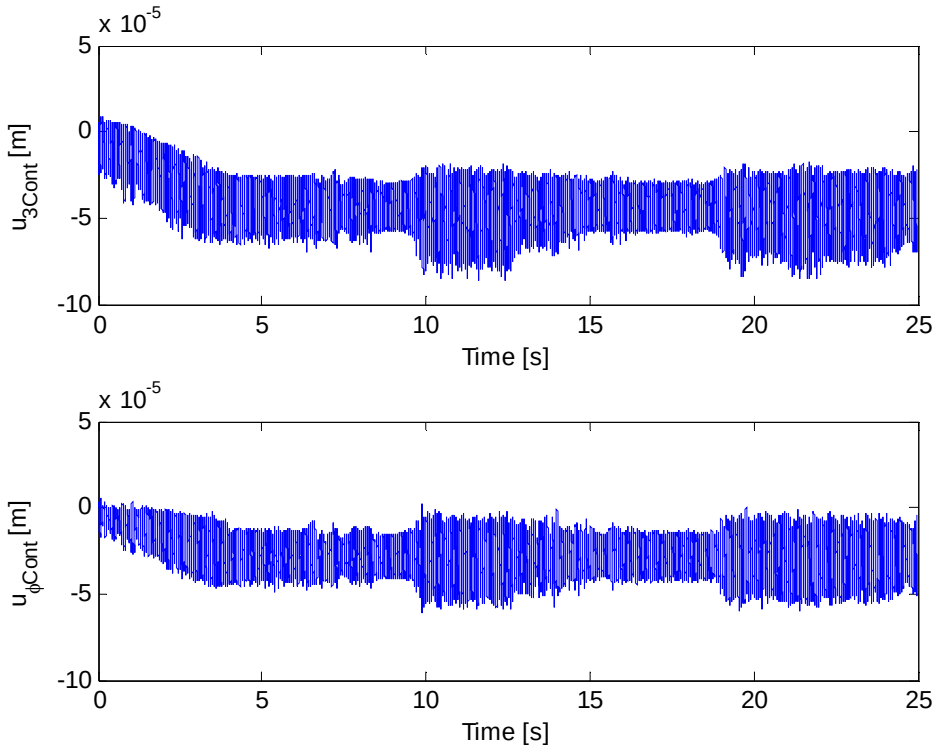

Figure 7.4: Radial and tangential displacement of the contact point, Love's equations

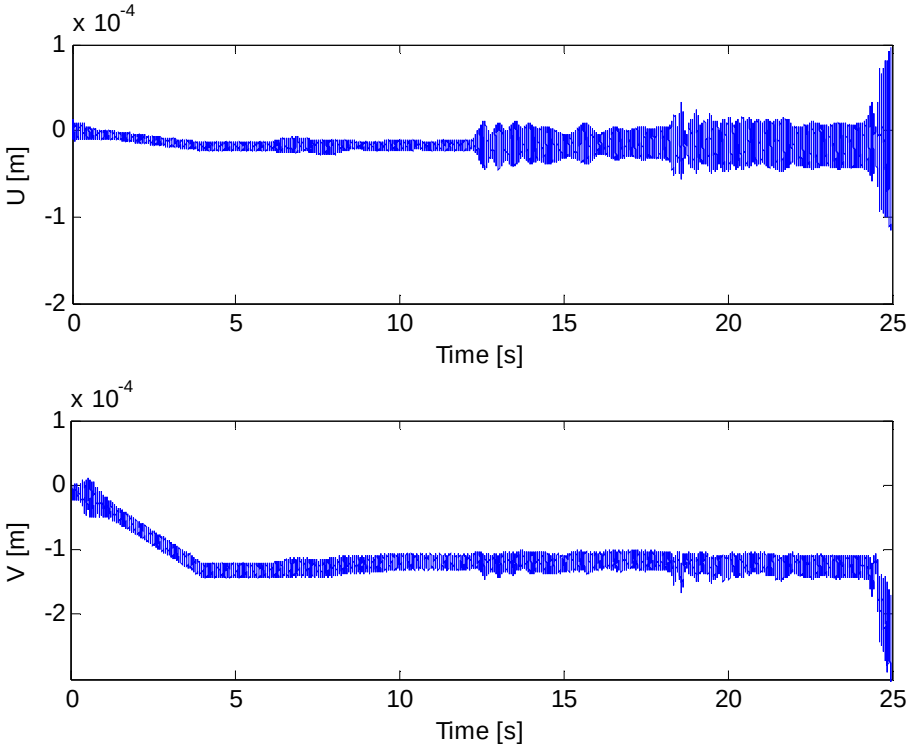

Figure 7.5: Horizontal and vertical displacement of the roll, beam theory

Let us first compare the responses of models including and having absent the additional support. Figures 7.2 and 6.22 present the tangential grinding force Q and the chip thickness ε for the shell model with and without the additional support, respectively. One can observe that the initial behaviour is in both cases very similar. Even later on, the peaks caused by the delay effect are visible. Nevertheless, the support force increases the roll stiffness, which produces a grinding force of higher values and unlike the original model, the grinding force amplitude increases. However, the higher stiffness itself would not be sufficient as the only factor. The deformation of the cross-section caused by the additional force brings an additional effect to the original situation without the support. Analogous comparison is given by Figures 7.4 and 6.24, the radial and tangential displacements of the contact point of the roll with and without the additional support, respectively. The observation result is the same – the additional stiffness and the circumferential deformation of the shell increase the amplitude of the vibrations. The mean values of the radial and tangential displacements of the contact point however remain unchanged.

On the other hand a different conclusion can be drawn by carrying out the same comparison with the beam model. Figures 7.3 and 6.23 show the tangential grinding force Q and the chip thickness ε for the beam model with and without the additional support, respectively. In the later case it is apparent that the amplitude of the grinding force is lower and no loss of contact between the roll and the grindstone is present in the first half of the simulation. This is also expected, because of the higher stiffness. It resembles a situation with a roll of higher roll thickness. This can be confirmed by utilizing results of analysis of grinding response of standard paper machine rolls presented e.g., in [Yuan 2002]. In both cases the behaviour is highly unstable. More significant change in the response is apparent from comparison of Figures 7.5 and 6.25, the horizontal and vertical displacement of the roll with and without the additional support, respectively. While the mean values of the vertical displacement V remain the same, the mean values of the horizontal displacement U are far lower in the case of the model including the additional support. Again this was to be expected, because the movement in the horizontal direction is reduced by the additional support and the cross-section does not deform.

Now, if one concentrates on the different behaviour of the shell and beam models including the additional support, following observations can be highlighted. In the case of the beam model, the application of the additional support seems to work rather well. The amplitude of the horizontal vibration decreases, also the chip thickness becomes more stable and there is no loss of contact between the roll and the grindstone, which together promises an improvement in the ground surface quality. Nevertheless, it does not solve the stability problem.

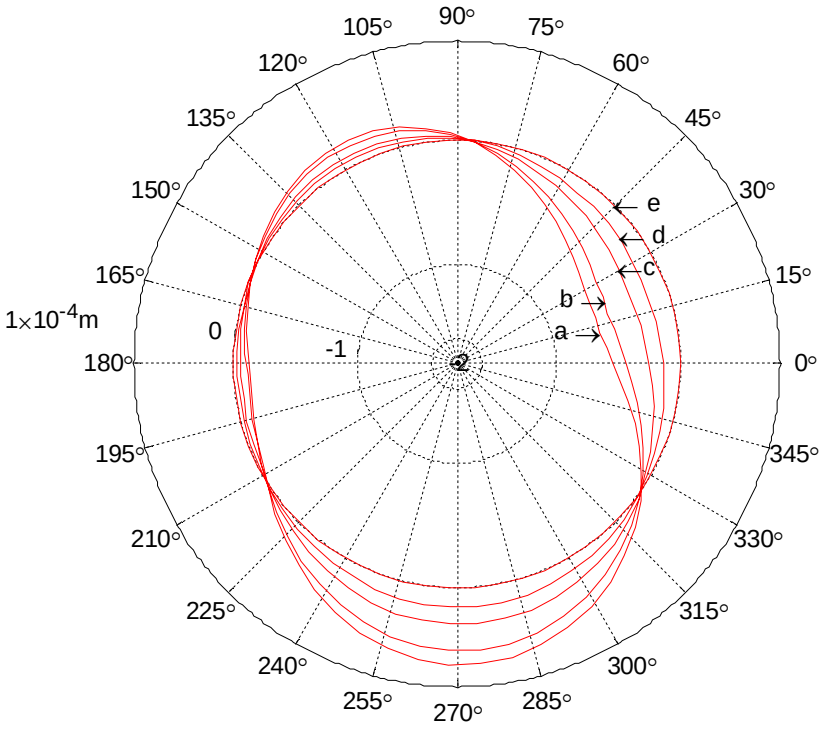

Figure 7.6: Cross-section of the roll at various axial positions at time *t = 9.5 s*; a: *z = 3.100 m*, b: *z = 5.100 m*, c: *z = 6.100 m*, d: *z = 6.600 m*, e: *z = 7.150 m*, Love's equations, *h = 2.5 mm*

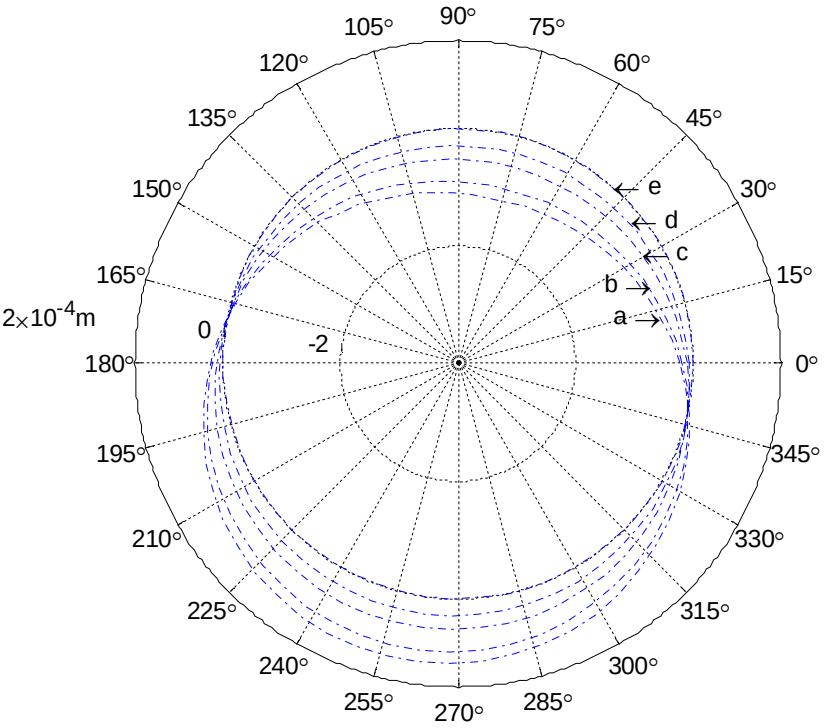

Figure 7.7: Cross-section of the roll at various axial positions at time *t = 9.5 s*; a: *z = 3.100 m*, b: *z = 5.100 m*, c: *z = 6.100 m*, d: *z = 6.600 m*, e: *z = 7.150 m*, beam theory, *h = 2.5 mm*

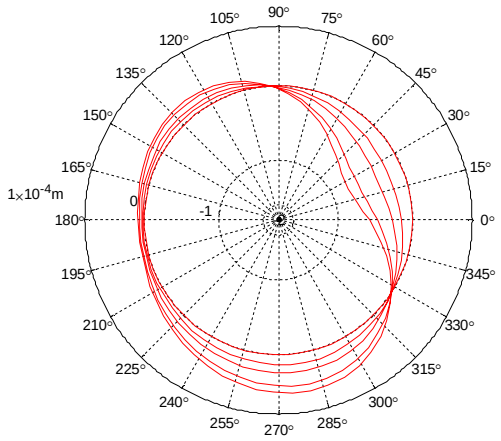

a) *t = 9.504 s*

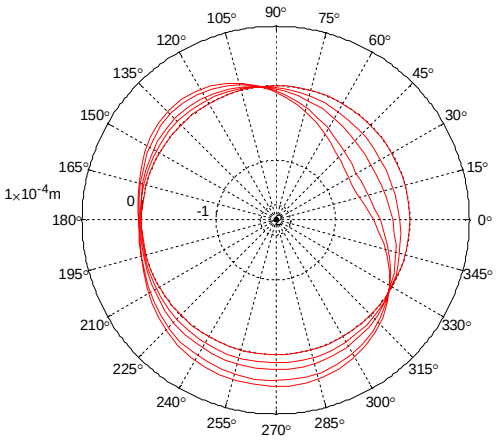

b) *t = 9.506 s*

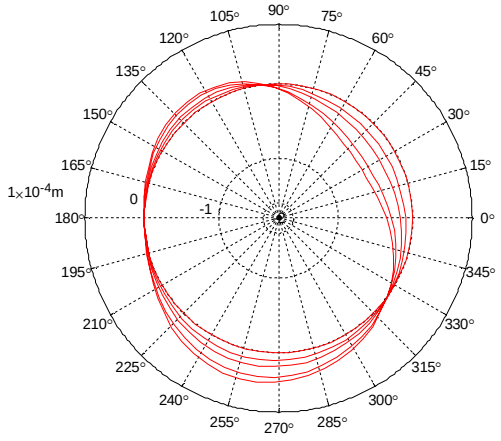

c) *t = 9.508 s*

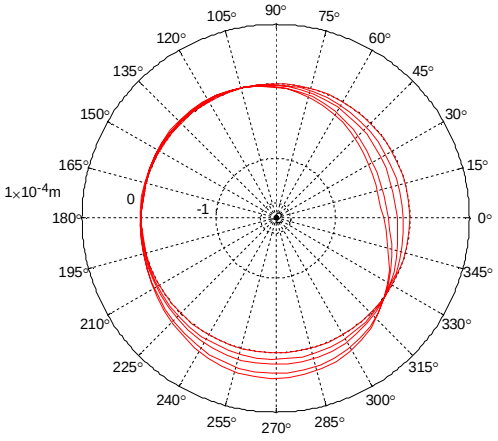

d) *t = 9.510 s*

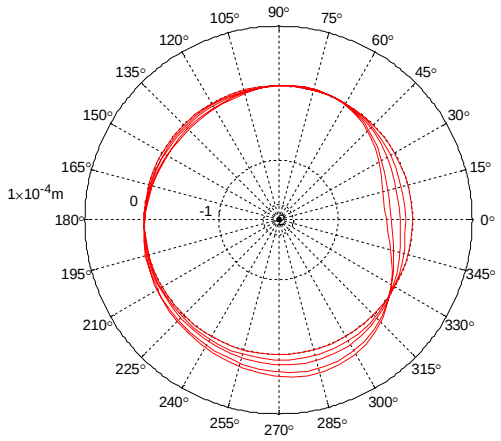

e) *t = 9.512 s*

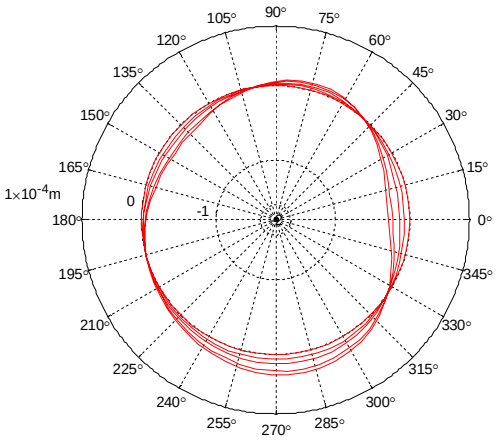

f) *t = 9.514 s*

Figure 7.8: Cross-section of the roll at various axial positions in a time sequence, Love's equations

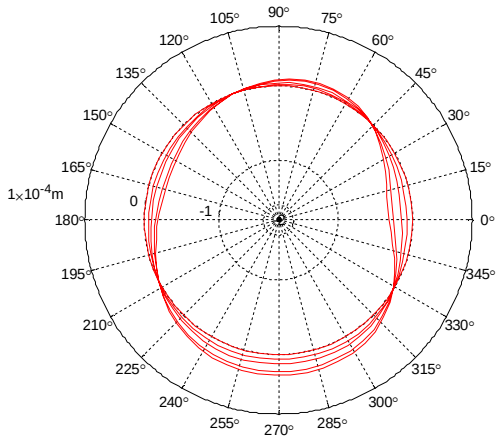

g) *t = 9.516 s*

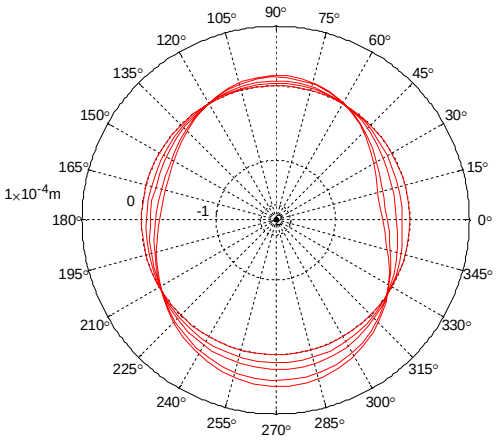

h) *t = 9.518 s*

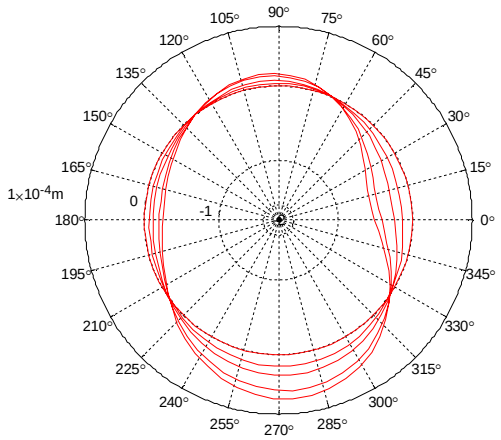

i) *t = 9.520 s*

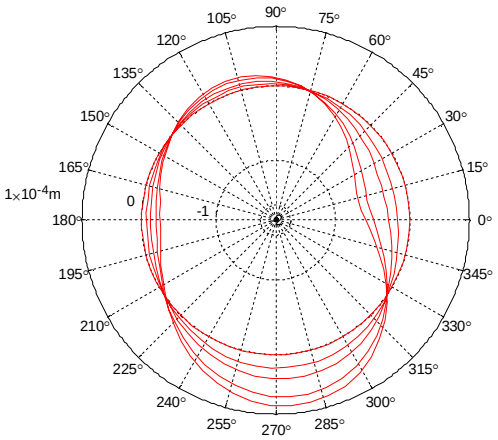

j) *t = 9.522 s*

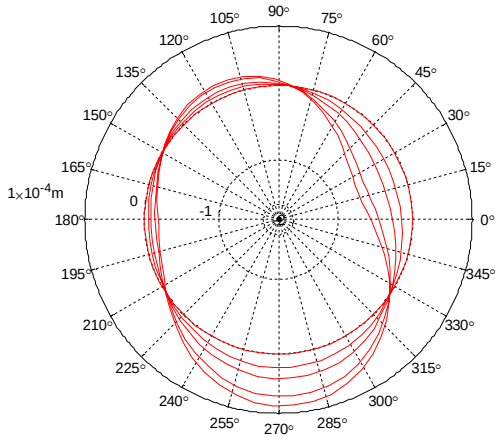

k) *t = 9.524 s*

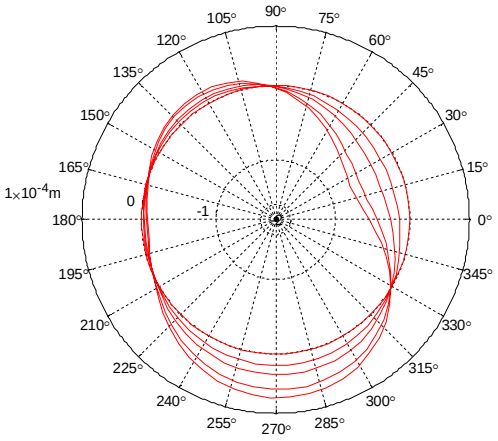

l) *t = 9.526 s*

Figure 7.8: Cross-section of the roll at various axial positions in a time sequence, Love's equations

This behaviour is naturally expected due to the fact that the normal grinding force N and the support force F_{Sup} act in the opposite directions, which leads to a lower total excitation force as it is defined in the beam theory. As was said earlier, this behaviour is expected, but at the same time it does not seem to be a reflection of the reality.

On the other hand, in the case of the shell model the tangential displacement of the contact point increases in the mean value whereas the radial displacement of the contact point remains the same. This is a consequence of the higher stiffness caused by the additional support that leads to higher grinding forces. That explains the higher tangential displacement due to the fact that the tangential force increased while the tangential stiffness is the same. The radial displacement of the contact point seems to be unchanged, because the normal grinding force is higher but also the stiffness in this direction has increased. This goes in line with a very simple explanation based on life experience, i.e. if one presses radially on a thin tube from two sides, its cross-section shape will become elliptic. This explanation is supported by another set of plots depicted in Figures 7.6 and 7.7. These Figures show instantaneous position and shape of cross-sections in 5 different planes perpendicular to the centre line of the roll at time $t = 9.5\ s$ of the time domain response presented above, for the shell and the beam model, respectively. The planes correspond to axial positions $z = 3.100\ m$, which is the plane of contact, $z = 5.100\ m$, $z = 6.100\ m$, $z = 6.600\ m$ and $z = 7.150\ m$, which is the end of the roll. These figures can again be compared with analogous plots of chapter 6, i.e. without the additional support (see Figures 6.29 and 6.30). These plots only support the evaluation of the results given in the previous paragraphs by providing perhaps a better visual effect. In addition, Figures 7.6 and 7.7 emphasize the major difference in the exploitation of the shell theory and the Euler-Bernoulli beam theory in application on thin-walled rolls, i.e., the ability of the shell theory to predict the cross-sectional deformations. This is possible due to the fact that the shell theory takes account of membrane stiffness that the beam theory does not.

To be able to study the change of the local displacements in different planes of the roll, a sequence of twelve steps that was taken from the time domain response, representing one period of the excitation function, has been recorded. The sequence is depicted in Figure 7.8. The period has a value of $0.024\ s$ in this case, which gives a printing interval $0.002\ s$. The sequence starts at time $t = 9.504\ s$, where the normal grinding force N is near its maximum absolute value, which causes the movement of the roll to the left (see Figure 7.8 a)) and compression of the support spring (or elastic deformation of the additional support). In Figures 7.8 b), c) and d) the effect of the reaction support force F_{Sup} starts to affect the left side of the roll by pressing the left side of the roll back to the initial position. At this point the normal force starts to reach its absolute minimum (see Figure 7.8 e) and

f)) and the state of the cross-section is near to the original, circular shape. After that the normal force N starts to increase in the value while the left side of the roll is still moving to the centre of the roll due to the velocity given by the support spring and the wall inertia. This trend continues through Figures 7.8 f), g) and h) until the cross-section experiences its largest deformation (see Figure 7.8 i) and j)). After that the normal force N still grows towards its maximum while the velocity of the left side of the roll reaches zero and starts to move backwards (see Figures 7.8 k) and l)). Then the normal force N finally reaches its maximum whereas the left side of the roll starts to press against the additional support and the cycle repeats. Of course, the development of the cross-sectional vibration varies in each cycle with respect to the instantaneous state of the system; however, the main character of the behaviour of the shell during each excitation period remains the same.

To summarize main results of this chapter dealing with the effect of an additional roll support on the response of a thin-walled roll under grinding conditions, one can start with the statement of the reliability of the additional support model. The support was modelled as an additional spring force, which is not connected to the roll. This assumption appears to describe the dynamic nature of the support rather realistically. Next, it can be concluded that based on a qualitative analyses the shell model describes the dynamic behaviour of the roll in a trustworthy way in contrast to the beam model. The dynamic behaviour of the roll modelled as a shell was further studied in detail and it can be stated, despite the fact that there are no measurements on hand, that the model captures the main features of the real system. Finally, the conclusions addressed to industry are following: the additional support does not provide any significant positive effect either on the stability of the grinding process or on the roll surface quality in the case of a thin-walled roll. The main reason for this is the high flexibility of the roll. Nevertheless, based on this analysis, there are enough indications to support an opinion of the author that the positive effect on the stability of the process and the quality of the ground surface can be achieved by other means than by an external mechanical support. Recommendations for achieving this state are developed in the following chapter.

8. Technical recommendation

This chapter is devoted to the practical contribution of this work and it is addressed to the industrial sector. As it has become apparent throughout this study, the results of the main part of this work, i.e., of the dynamic analysis of a thin-walled roll – grinder system, reveal that neither the stability of the process nor the acceptable surface quality can be achieved under given conditions. Moreover, in the case of grinding thin-walled rolls even the simple additional roll support does not lead to a major improvement in the dynamic behaviour of the system. Nevertheless, certain more suitable design solutions that must take special care of the higher elasticity of the roll can be introduced.

The fundamental idea is to increase the stiffness of the system. It can be done by application of various stiffening elements acting from outside or inside the roll. A technically simpler solution can be seen in application of an additional outer support, acting not as a point contact but as a surface contact. A scheme of such a design is shown in Figure 8.1.

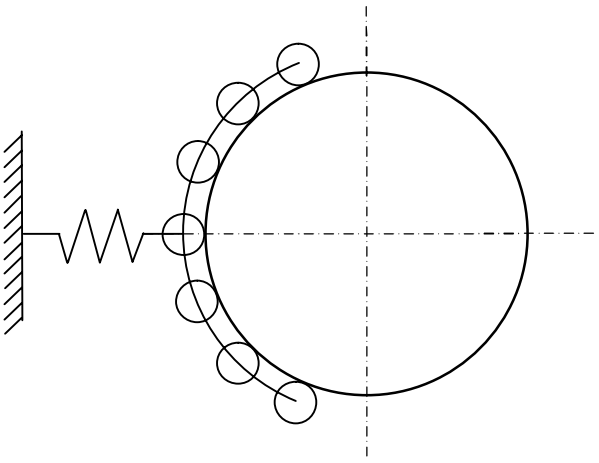

Figure 8.1: Outer support with quasi-surface contact

In practice, such a support would be a cantilever beam with a welded, shaped arc at its end, preventing the deformation of the roll on the supported side. The arc would cover less than half of the roll perimeter, let us say about *150°*, for easy installation. For low-friction contact a set of roll elements would be attached to the arc to provide a roll contact with the rotating roll. This case can be modelled similarly as in chapter 7, but with several point forces or as a distributed load similarly

as was presented in chapter 4 in case of gravity load. This solution is technically simple, but its efficiency is expected to be rather low compared to the following designs.

Higher efficiency can be reached by installing stiffening elements from inside the roll. These installations are technically more complicated though, mainly because of the necessity of partial disassembling of the roll. In this case metal structures would be placed inside the roll and would support the roll walls as illustrated in Figure 8.2.

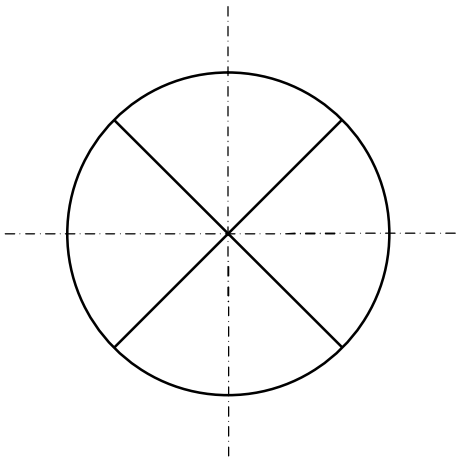

Figure 8.2: Inside stiffening by means of supporting structures

Of course, this application would increase not only the stiffness but also the mass of the roll. From the modelling point of view, this problem could be modelled as a pair of springs attached to the walls with a phase shift *90*° with respect to each other. A few scientific papers handling the problem of stiffened shells can be found. An interesting study from this field is presented in [Jafari 2006], which deals with free vibrations of ring stiffened cylindrical shells using analytical, experimental and numerical methods. For example the analytical method could be further developed and applied on the given problem.

The third proposed solution belongs to the group of inside applications. The roll stiffness would be increased by high pressure air inside the roll. Assuming that it is technically and economically possible to reach high enough pressure inside the roll for the duration of the grinding process, this method seems to be very suitable and efficient: (1) the stiffness would increase while the mass would remain almost the same, (2) the pressure would be distributed evenly on the whole inside surface of the roll, (3) no local deformation caused by e.g., the support contact would be present and

finally, (4) no dismantling of the roll would be needed. From the modelling point of view, the inside pressure could be handled as an initial stress caused by the pressure (see eqs. (4.6) to (4.8)), which would be included in the equations of motion of the shell as a non-linear term. That would increase the natural frequency of the shell. In addition, the pressure can be handled as a uniform distributed load p_0 (see Figure 8.3).

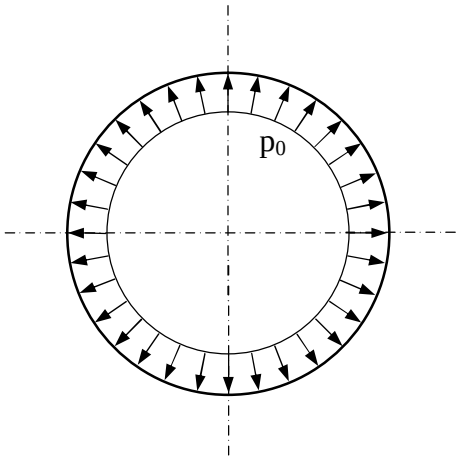

Figure 8.3: Inside stiffening by means of inside pressure

The shell model of chapter 4 could be used when adding the new loading term and with modified mass, damping and stiffness matrices due to the non-linear terms. Eq. (4.115) could be completed by a forcing term $F_{k,mn,p}$, which would be the modal force caused by the inside pressure p_0. Eq. (4.115) would become:

$$m_{k,mn}\ddot{\eta}_{k,mn} + c_{k,mn}\dot{\eta}_{k,mn} + k_{k,mn}\eta_{k,mn} = F_{k,mn,C} + F_{k,mn,G} + F_{k,mn,p} \tag{8.1}$$

where

$$F_{k,mn,p} = \int_0^{2\pi}\int_0^{L}\left[p_0 U_{3,kmn}(\varphi, z)\right] a\, dz d\varphi \tag{8.2}$$

To summarize this industrial oriented chapter, one can conclude that for improving the dynamic performance of the presented system and for increase of the ground surface quality of the roll three technical solutions have been proposed: (1) use of an outer roll support with quasi-surface contact, (2) use of inside supporting structure and (3) application of inside pressure. Of course, it would be

also possible to combine these methods. All of these concepts would need a more detailed technical design to make them work in practice. It is also suggested to carry out mathematical simulations of these modified systems before any experimental testing should begin. Such analyses could be worked out as an extension of this study as the current model has been done in a modular, parametric way. These topics can be listed among future work and challenges of the author that are related to the problem of shell vibrations.

9. Conclusions

There have been two main goals in this thesis. The first, taken from the scientific point of view, has been to present original scientific contributions in the multi-disciplinary field of machining of shell structures. The second goal, taken from the industrial point of view, has been to answer the question whether it is possible to bring the studied system to practise and to suggest potential solution leading to an improved performance of the system. The problem of grinding thin-walled rolls represents a scientifically joint problem; therefore, for establishing the mathematical model of the system existing theories of cutting mechanics, chatter vibrations and mechanics of continuum have been applied. Two models are presented here: one, which brings the original contribution, utilizes Love's equations and the other, which is used for comparison, is based on the Euler-Bernoulli beam theory.

An analytical, multi-body dynamic approach has led to derivation of governing equations that are represented by a set of second order delay differential equations with constant coefficients and constant delay. For solving these equations, several numerical methods as well as predefined commercial solvers have been tested. All of them yielded the same solution and differed only in their efficiency. Euler's first improved method has been selected as the most suitable method and it has been used in this work.

The system is defined by a set of constant and variable parameters, which makes the system highly sensitive. Therefore, in the case studies only one parameter has been changed and it has been the wall thickness of the roll. Three case studies have investigated the effect of the wall thickness of the roll, whose values have been *10 mm*, *5 mm* and *2.5 mm*. The case studies have been evaluated for both models and their results have been compared.

At first, the effect of the roll gravity load or its self-weight on the shell has been studied. The simulations have revealed that under the static load of the gravity the cross-section of the shell deforms into a shape that is neither circular nor elliptic; it resembles rather a "pear-like" shape, which is caused by the uneven load distribution along circumference of the cross-section in the vertical direction. Nevertheless, the deviation from the circular shape is so small that the effect of the "non-circular" deformation has been neglected. Next, the origin of the surface waviness on the roll has been examined. It has been concluded that the surface waviness is related to the first natural frequency of the system, which does not always necessarily equal the first bending natural frequency of the roll, since the natural frequency is significantly affected by the contact between the

roll and the grinding stone that brings an additional stiffening element to the system. This effect is more pronounced in case of thin-walled cylinders.

The time domain response of the analyzed system has been carried out for all three cases. In addition, an analysis of the cross-sectional deformation in several planes along the roll span has been carried out. In all cases the delay effect has been clearly recognized. The results of Case 1 (wall thickness of *10 mm*) are very similar in both the shell and the beam model. It shows that the beam theory is suitable for the solid and thick-walled rolls but it can be applicable also for relatively thin-walled cylinders. On the other hand, for extremely thin-walled rolls, as presented, e.g. in Case 3 (wall thickness of *2.5 mm*), the results obtained with the beam model become highly unreliable. The main reasons for the better accuracy of the shell model for extremely thin-walled rolls is the effect of the membrane stiffness that is absent in the beam theories. However, it has been concluded that both theories provide reliable solutions if a specific coefficient is in the interval *(10, 30)*, where the coefficient stands for a ratio outer radius vs. the wall thickness of the roll. For higher wall thickness the beam model and for lower thickness the shell model should be used. Nevertheless, the simulation results have shown that grinding of thin-walled rolls under given conditions cannot provide satisfactory surface quality and process stability.

The two presented models have been extended by addition of a third support, acting against the grindstone as a point contact. This method has often been used in grinding workshops when grinding standard paper machine rolls. Conclusions of this additional analysis have only supported the major observations from the main analysis. Thus, the application of the beam model has appeared to be strongly unsuitable, whereas the shell model have provided very promising results. Nonetheless, the practical conclusions have been such that even this type of additional roll support does not lead to any significant improvement in the performance of the system.

Based on these two analyses conclusions and recommendations addressed to industry have been suggested. With respect to the high flexibility of the thin-walled rolls three technical solutions have been selected. The most promising of them seems to be the one where the inside of the roll is filled with pressurized air, which would increase the roll stiffness while its mass would remain almost the same. Methods for modelling of such a system have been provided too.

Near future work consists of carrying out analyses, dealing with modelling of the existing system extended by the additional elements leading to the improved performance of the system as proposed above. Both approaches, i.e., support from inside or outside the roll, are of interest. Another challenge can be seen in further development of the current model by including thermal effects

caused by heat transfer from the grinding contact to the work piece. This topic also completes the already physically multi-task problem by the scientific discipline of thermodynamics, which also brings new mathematical elements to the model. This topic is interesting both from the scientific point of view and from the practical and technical viewpoint.

References

Al-Asnary, M. D., Flexural vibrations of rotating beams considering rotary inertia, Computers and Structures, vol. **69**, pp. 321 – 328, 1998

Altintas, Y., Manufacturing automation. Metal cutting mechanics, machine tool vibrations and CNC design, Press Syndicate of the University of Cambridge, Cambridge, 2000

Altintas, Y., Weck, M., Chatter stability of metal cutting and grinding, Annals of CIRP, Key Note Paper of STC-M, vol. **53**(2), pp. 619 – 642, 2004

Ashtakhov, V. P., Metal cutting theory – missed chances or a science without history: Part1, Personal vision of Viktor P. Astakhov, http://viktorastakhov.tripod.com/mc1.pdf, 2002

Ashtakhov, V. P., Metal cutting theory – missed chances or a science without history: Part2, Personal vision of Viktor P. Astakhov, http://viktorastakhov.tripod.com/mc2.pdf, 2002

Biera, J., Viñolas, J. and Nieto, F. J., Time-domain dynamic modeling of the external plunge grinding process, International Journal of Machine Tools and Manufacture, vol. **37**(11), pp. 1555 – 1572, 1997

Black, P. H., Theory of metal cutting, McGraw-Hill, New York, 1961

Blevins, R. D., Formulas for natural frequency and mode shape, Krieger publishing company, Malabar, Florida, 1979

Calladine, C. R., Theory of shell structures, Press Syndicate of the University of Cambridge, Cambridge, 1983

Chen, C.-C. A., Liu, W.-C. and Duffie, N. A., A surface topography model for automated surface finishing, International Journal of Machine Tools and Manufacture, vol. **38**, pp. 543 – 550, 1998

Chladni, E. F. F., Entdeckungen über die Theorie des Klanges, Weidmann und Reich, Leipzig, 1787

Civalek, Ö., Kiracioglu, O., Free vibration analysis of Timoshenko beams by DSC method, Communications in Numerical Methods in Engineering, 2009

Donnell, L. H., Beams, plates and shells, McGraw-Hill, New York, 1976

Dospěl, V., Keskinen, E., Prediction of transverse vibrations of thin-wall rolls under grinding process using Timoshenko beam theory, Proceedings of Post Graduate Workshop on Intelligent Machines and Transport Systems, CERN, Switzerland, pp. 14 – 26, 2010

Dospěl, V., Keskinen, E., Thin-Shell Response to Machining Loads, Proceedings of the International Mechanical Engineering Congress and Exposition, Denver, USA, 2011

Doyle, J. F., Wave propagation in structures, Springer, New York, 1997

Dutton, K., Thompson, S. and Barraclough, B., The art of control engineering, Addison Wesley Longman Limited, Harlow, Essex, England, 1997

Ehrich, F. F., Handbook of Rotordynamics, McGraw-Hill, Inc., 1992

Eldén, L., Wittmeyer-Koch, L. and Nielsen, H. B., Introduction to numerical computation: analysis and MATLAB® illustrations, Studentlitteratur AB, 2004

Flügge, W., Stresses in Shells, Springer, Berlin, 1960

Flügge, W., Statik und Dynamik der Schalen, Springer, Berlin, 1962

Genta, G. G., Dynamics of rotating systems, Springer Science + Business Media, Inc., 2005

Giménes, J. G., Nieto, F. J., A step by step approach to the dynamic behavior of centreless grinding machines, International Journal of Machine Tools and Manufacture, vol. **35**(9), pp. 1291 – 1307, 1995

Goldberg, J. L., Matrix theory with applications, International series in pure and applied mathematics, The McGraw-Hill Companies, Inc., New York, 1991

Gurney, J. P., An analysis of surface wave instability in grinding, Journal of Mechanical Engineering Science, vol. **7**, pp. 198 – 209, 1965

Han, S. M., Benaroya, H. and Wei, T., Dynamics of transversely vibrating beams using four engineering theories, Journal of Sound and Vibration, pp. 935 – 988, 1999

Hirsch, M. W., Smale, S. and Devaney, R. L., Differential equations, dynamical systems and an introduction to chaos, Second Edition, Elsevier Academic Press, USA, 2004

Horr, A. M., Schmidt, L. C., Closed-form solution for the Timoshenko beam theory using a computer-based mathematical package, Computers and Structures, vol. **55**(3), pp. 405 – 412, 1995

Huang, S. C., Soedel, W., Response of rotating rings to harmonic and periodic loading and comparison with the inverted problem, Journal of Sound and Vibration, vol. **118**(2), pp. 253 – 270, 1987

Huang, S. C., Soedel, W., On the forced vibration of simply supported rotating cylindrical shells, Journal Acoustical Society of America, **84**(1), pp. 275 – 285, 1988

Hung, V. V., Ramin, S. E, Dynamic systems: Modeling and analysis, The McGraw-Hill Companies, Inc., 1997

Inasaki, I., Selbsterregte Ratterschwingungen beim Schleifen, Methoden zu ihrer Unterdrückung, Werkstatt und Betrieb **110** (8), pp. 521 – 524, 1977

Inasaki, I., Karpuschewski, B. and Lee, H.-S., Grinding chatter – origin and suppression, CIRP Annals - Manufacturing Technology, vol. **50**(2), pp. 515 – 534, 2001

Jafari, A. A., Bagheri, M., Free vibration of non-uniformly ring stiffened cylindrical shells using analytical, experimental and numerical methods, Thin-Walled Structures, vol. **44**(1), pp. 82 – 90, 2006

Järvenpää, V.-M., Yuan L., Numerical modeling of paper machine roll contact with regenerative out-of-roundness excitation, Multiscale problems in multibody system contact, Springer, pp. 55 – 64, 2007

Järvinen, V., Polymeeripinnoitettujen telojen dynamiikka ja käynninvalvonta, Telaston värähtelydynamiikka, Internal report, Tampere University of Technology, (in Finnish), 1998

Kaliszer, H., Singhal, P. D., Analysis of the rigidity of the grinding wheel-workpiece-grinding machine system, Proceedings of the Institutions of Mechanical Engineers, vol. **181**, pp. 89 – 104, 1966

Keskinen, E., Kivinen J. M. and Launis, S., Telahionnan dynamiikka, Internal Report, Lab of Machine Dynamics, Tampere University of Technology (in Finnish), 1999

Kim, Y.-J., Bolton, J. S., Effects of rotation on the dynamics of a circular cylindrical shell with application to tire vibration, Journal of Sound and Vibration, vol. **275**, pp. 605 – 621, 2004

Kirchhoff, G. R., Über das Gleichgewicht und die Bewegung einer elastischen Scheibe, J. Mathematik, Crelle's Journal, vol. **40**, pp. 51 – 88, 1850

Kopchenova, N. V., Maron, I. A., Computational mathematics, Worked examples and problems with elements of theory, Mir Publisher, Moscow, 1981

Kraus, H., Thin elastic shells, An introduction to the theoretical foundations and the analysis of their static and dynamic behavior, John Wiley and Sons, Inc., New York, 1967

Larsson, S., Thomee, V., Partial differential equations with numerical methods, Springer-Verlag Berlin, Berlin, 2003

Laura, P. A. A., Gutierres, R. H., Analysis of vibrating Timoshenko beams using the method of differential quadrature, Shock and Vibration, vol. **1**(1), pp. 89 – 93, 1993

Leissa, A. W., Vibration of shells, National Aeronautics and Space Administration, Washington DC, 1973

Li, H., Shin, Y. C., A time-domain dynamic model for chatter prediction of cylindrical plunge grinding process, ASME Journal of Manufacturing Science and Engineering, vol. **128**(2), pp. 404 – 415, 2006

Li, H., Shin, Y. C., A study on chatter boundaries of cylindrical plunge grinding with process condition-dependent dynamics, International Journal of Machine Tools and Manufacture, vol. **47**, pp. 1563 – 1472, 2007

Lin, S. C., Hsiao, K. M., Vibration analysis of a rotating Timoshenko beam, Journal of Sound and Vibration, vol. **240**(2), pp. 303 – 322, 2001

Lin, G. C. I., Mathew, P., Oxley, P. L. B. and Watson, A. R., Predicting cutting forces for oblique machining conditions, Proceedings of the Institutions of Mechanical Engineers, vol. **196**, pp. 141 – 148, 1982

Liu, Z., Payre G., Stability analysis of doubly regenerative cylindrical grinding process, Journal of Sound and Vibration**,** vol. **301**(3-5), pp. 950 – 962, 2007

Love, A. E. H., A treatise on the mathematical theory of elasticity, General Publishing Company, Toronto, Canada, 1927

Mannan, M. A., Drew, S. J., Stone, B. J. and Wager, J. G., Torsional vibration effects in grinding? Annals of the CIRP, vol. **49**(1), pp. 249 – 252, 2000

Meirovitch, L., Elements of vibration analysis, Second Edition, McGraw-Hill Book Company, New York, USA, 1986

Merchant, M. E., Mechanics of the metal cutting process I. Orthogonal cutting and a type 2 chip, Journal of Applied Physics, vol. **16**, pp. 267 – 275, 1945

Merchant, M. E., Mechanics of the metal cutting process II. Plasticity conditions in orthogonal cutting, Journal of Applied Physics, vol. **16**, pp. 318 – 324, 1945

Merritt, H. E., Theory of self-excited machine-tool chatter - contribution to machine-tool chatter - Research - 1, Journal of engineering for industry, vol. **87**, pp. 447 – 454, 1965

Miller, P. R., Free Vibrations of a stiffened cylindrical shell, Aeronautical research council reports and memoranda, Her majesty's stationery office, London, 1960

Moon, F. C., Dynamics and chaos in manufacturing processes, John Wiley and Sons, Inc., New York, 1998

Mushtari, Kh. M., Non-linear theory of thin elastic shells, The Israel program for scientific translations, Jerusalem, 1961

Ng, T. Y., Lam, K. Y., Vibration and critical speed of a rotating cylindrical shell subjected to axial loading, Applied Acoustics, vol. **56**, pp. 273 – 282, 1999

Novozhilov, V. V., Thin shell theory, Noordhoff, Groningen, 1964

Ong, L. S., Tooth, A. S., Analysis of a cylindrical shell supported by two longitudinal beams, Proceedings of the Institutions of Mechanical Engineers, Part E, Journal of Process Mechanical Engineering, vol. **210***(2)*, pp. 109 – 119, 1996

Ouyang, H., Wang, M., A dynamic model for a rotating beam subjected to axially moving forces, Journal of Sound and Vibration, vol. **308**, pp. 674 – 682, 2007

Palmer, W. B., Oxley, P. L. B., Mechanics of orthogonal machining, Proceedings of the Institutions of Mechanical Engineers, vol. **173**(24), pp. 623 – 654, 1959

Paulapuro, H., Papermaking Part 1: Stock Preparation and Wet End, Finnish Paper Engineers' Association and TAPPI, 2000

Przemieniecki, J. S., Theory of matrix structural analysis, Dover publications, Inc., New York, 1968

Ramos, J. C., Viñolas, J. and Nieto, F. J., A simplified methodology to determine the cutting stiffness and the contact stiffness in the plunge grinding process, International Journal of Machine Tools and Manufacture, vol. **41**, pp. 33 – 49, 2001

Saito, T., Endo, M., Vibration analysis of rotating cylindrical shells based on the Timoshenko beam theory, Bulletin of Japan Society of Mechanical Engineers, vol. **29**, pp. 1239 – 1245, 1986

Salisbury, E. J., Domala, K. V., Moon, K. S., Miller, M. H. and Sutherland, J. W., A three-dimensional model for the surface texture in surface grinding, Part 1: Surface generation model, Journal of Manufacturing Science and Engineering, vol. **123**(4)**,** pp. 576 – 581, 2001

Salisbury, E. J., Domala, K. V., Moon, K. S., Miller, M. H. and Sutherland, J. W., A three-dimensional model for the surface texture in surface grinding, Part 2: Grinding wheel surface texture model, Journal of Manufacturing Science and Engineering, vol. **123**(4), pp. 582 – 590, 2001

Shampine, L. F., Gladwell, I. and Thompson, S., Solving ODEs with Matlab, Press Syndicate of the University of Cambridge, Cambridge, 2003

Sharma, I. R., Troubleshooting handbook: machining, Tata McGraw-Hill, New Delhi, 1986

Shaw, M. C., Metal cutting principles, Clarendon, Oxford, 1984

Snoeys, R., Brown D., Dominating parameters in grinding wheel and workpiece regenerative chatter, Proceedings of the 10th International Conference on Machine Tool Design and Research, University of Birmingham, pp. 325 – 348, 1969

Soedel, W., Vibrations of shells and plates, Marcel Denker, Inc., New York and Basel, 1981

Stabler, G. V., The Fundamental geometry of cutting tools, Proceedings of the Institutions of Mechanical Engineers, pp. 14 – 26, 1951

Strutt, J. W., Theory of sound, Macmillan Publications Co. Inc., London, 1877

Thompson, R. A., On the doubly regenerative stability of a grinder: The theory of chatter growth, ASME Journal of Engineering for Industry, Series B, **108** (2), pp. 75 – 82, 1986

Timoshenko, S. P., On the correction for shear of the differential equation for transverse vibrations of bars of uniform cross-section, Philosophical Magazine, vol. **41**, pp. 744 – 746, 1921

Timoshenko, S. P., On the transverse vibrations of bars of uniform cross-section, Philosophical Magazine, vol. **43**, pp. 125 – 131, 1922

Tlustý, J., Poláček, M., The stability of the machine-tool against self-excited vibration in machining, Proceedings of the International Research in Production Engineering Conference, Pittsburgh, PA, ASME: New York, 1963

Tlustý, J., Technology of machine tools, A survey of the state of the art by the Machine Tool Task Force, Volume 3: Machine tool mechanics, Lawrence Livermore Laboratory, California, 1980

Tobias, S. A., Fishwick, W., Theory of regenerative machine tool chatter, The Engineer, London, 1958

Todhunter, I., A history of the theory of elasticity, vol. I, Cambridge university Press, New York, 1886

Trent, E. M., Metal cutting, Butterworths, London, 1977

Tse, F. S., Morse, I. E. and Hinkle, R. T., Mechanical vibrations, Theory and applications, Prentice Hall, Inc., New Jersey, 1978

Vlasov, V. Z., General theory of shells and its applications in engineering, U.S. Department of Commerce, Washington DC, 1964

Wang, S., A unified Timoshenko beam B-spline Rayleigh-Ritz method for vibration and buckling analysis of thick and thin beams and plates, International Journal for Numerical Methods in Engineering, vol. **40**, pp. 473 – 491, 1997

Weck, M., Klotz, N., Schwingungsphänomene beim Abricht- und Schleifprozeß, Industrie-Anzeiger **105**(30), pp. 50 – 54, 1983

Yuan, L., Analysis of delay phenomena in roll dynamics, doctoral thesis, TUT, Tampere, 2002

Yuan, L., Järvenpää, V.-M., Keskinen, E. and Cotsaftis, M., Response and analysis of multi-digree-of-freedom cylindrical roll grinding system, Proceedings of the Institution of Mechanical Engineers, vol. **216**, Part K, pp. 315 – 325, 2002

Yuan, L., Järvenpää, V.-M., Keskinen, E. and Cotsaftis, M., Simulation of roll grinding system dynamics with rotor equations and speed control, Communications in Nonlinear Science and Numerical Simulation, vol. **7**, pp. 95 – 106, 2002

Yuan, L., Keskinen, E. and Järvenpää, V.-M., Stability analysis of roll grinding system with double time delay effects, In: Ulbrich, H., Günthner, W. (eds.), Proceedings of IUTAM Symposium on Vibration Control of Nonlinear Mechanisms and Structures, Munich, Germany, pp. 375 – 387, 2005

Tampereen teknillinen yliopisto
PL 527
33101 Tampere

Tampere University of Technology
P.O.B. 527
FI-33101 Tampere, Finland

ISBN 978-952-15-2723-4
ISSN 1459-2045